



FATIGUE MODULE

Module Coordinator: Jean-Jacques Janosch
CATERPILLAR, FRANCE

7 Fatigue Module

7	Fatigue Module	7-1
7.1	Introduction	7-3
7.2	Definitions and Input Parameters	7-5
7.2.1	Definition of Fatigue Service Conditions	7-5
7.2.1.1	Description of Variable Loads	7-5
7.2.1.2	Partial Safety Factors	7-6
7.2.1.3	Fatigue Actions	7-6
7.2.1.4	Cumulative Fatigue Assessment	7-6
7.2.1.5	Fatigue Limit Assessment	7-8
7.2.2	Environmental Issues	7-8
7.2.3	Exemption from Fatigue Assessment	7-8
7.3	Fatigue Assessment Routes	7-9
7.3.1	Route 1 - Fatigue Damage Assessment using Nominal Stresses	7-9
7.3.1.1	Route 1 (Welded Structures)	7-9
7.3.1.1.1	Step 1: No Postulated or Detected Flaw is Present in the Structure	7-10
7.3.1.1.2	Step 2: Service Condition	7-10
7.3.1.1.3	Step 3: Environmental Issues	7-10
7.3.1.1.4	Step 4: Thresholds for Fatigue Assessment	7-10
7.3.1.1.5	Step 5: Fatigue Resistance Data Specification	7-10
7.3.1.1.6	Step 6: R-Ratio effects	7-12
7.3.1.1.7	Step 7: Thickness Reduction Factor Effects	7-12
7.3.1.1.8	Step 8: Fatigue Assessment using S-N Curves	7-13
7.3.1.2	Route 1 for Non-Welded Locations	7-13
7.3.1.2.1	Step 1: No Postulated or Detected Flaw is Present in Component	7-14
7.3.1.2.2	Step 2: Service Conditions	7-14
7.3.1.2.3	Step 3: Environmental Issues	7-14
7.3.1.2.4	Step 4: Influence of geometric parameters	7-14
7.3.1.2.5	Step 5: Permissible stress σ_a and mean stress effects	7-19
7.3.1.2.6	Step 6: Results	7-20
7.3.2	Route 2 - Fatigue Damage Assessment using Structural or Notch Stresses	7-21
7.3.2.1	Route 2 for Welded Structures	7-21
7.3.2.1.1	Step 1: No Postulated or Detected Flaw is Present in the Structure	7-22
7.3.2.1.2	Step 2: Service Conditions	7-22
7.3.2.1.3	Step 3: Environmental issues	7-26
7.3.2.1.4	Step 4: Thresholds for fatigue assessment	7-26
7.3.2.1.5	Step 5: Fatigue Data Specifications	7-26
7.3.2.1.6	Step 6: Fatigue assessment using S-N Curves	7-28
7.3.2.2	Route 2 for Non-Welded Parts	7-28
7.3.2.2.1	Step 1: No Postulated or Detected Flaw is Present in the Component or Structure	7-29
7.3.2.2.2	Step 2: Service Conditions	7-29
7.3.2.2.3	Step 3: Issues, Corrosion and High Temperatures	7-29
7.3.2.2.4	Step 4: Thresholds for Fatigue Assessment	7-29
7.3.2.2.5	Step 5: Fatigue Resistance Data	7-29
7.3.2.2.6	Step 6: Fatigue Assessment using $\Delta\sigma_e$ -N Curves	7-35
7.3.3	Route 3 - Fatigue Damage Assessment using Local Stress-Strain Approach	7-36
7.3.3.1	Step 1: No Postulated or Detected Flaw is Present in the Component or Structure	7-37
7.3.3.2	Step 2: Service Condition	7-37
7.3.3.2.1	Constant amplitude loading	7-37
7.3.3.2.2	Variable amplitude loading	7-37
7.3.3.3	Step 3: Environmental issues chapter	7-38
7.3.3.4	Step 4: Thresholds for fatigue assessment	7-38
7.3.3.5	Step 5: Fatigue resistance data for elasto-plastic loading	7-38
7.3.3.5.1	Material elasto-plastic behaviour	7-38
7.3.3.6	Step 5: Cumulative Fatigue life calculation	7-39
7.3.4	Route 4 - Fatigue Crack Growth Assessment	7-40
7.3.4.1	Step 1: Detected or Postulated Planar Flaw	7-40

7.3.4.2	Step 2: Establish Service Conditions and Cause of Cracking.....	7-40
7.3.4.3	Step 3: Exclude Environmental or Creep Effects.....	7-41
7.3.4.4	Step 4: Collect Materials Data and Perform Stress Analysis.....	7-41
7.3.4.5	Step 5: Pre-Checks.....	7-41
7.3.4.6	Step 6: Calculate Crack Growth.....	7-42
7.3.4.6.1	Paris Equation	7-42
7.3.4.6.2	Forman-Mettu Approach.....	7-44
7.3.4.7	Crack Growth under Variable Amplitude Loading	7-45
7.3.5	Route 5 - Non-Planar Flaw Assessment	7-46
7.3.5.1	Step 1: Postulated or Detected Non Planar Flaw is Present in the Component or Structure.....	7-46
7.3.5.2	Step 2: Service Condition	7-46
7.3.5.3	Step 3: Environmental Issues	7-46
7.3.5.4	Step 4: Types of Imperfections	7-46
7.3.5.5	Step 5: Effects and Assessment of Imperfections.....	7-47
7.3.5.5.1	Undercut.....	7-47
7.3.5.5.2	Porosity and Inclusions	7-48
7.3.5.5.3	Crack-like Imperfections (Route 4)	7-49
7.4	Life Improvement [7.22].....	7-50
7.4.1	Introduction	7-50
7.4.2	Applicability of Improvement Methods.....	7-51
7.4.3	Procedures for some improvement techniques	7-51
7.4.3.1	Burr Grinding	7-51
7.4.3.2	TIG dressing	7-54
7.4.3.3	Hammer Peening	7-55
7.4.3.4	Needle Peening	7-57
7.4.4	Fatigue design data for improved welds	7-58
7.4.4.1	Fatigue strength of joints improved by weld toe grinding or TIG dressing	7-58
7.4.4.2	Fatigue strength of joints improved by hammer peening or needle peening.....	7-59
7.5	Special Options	7-60
7.5.1	Dang Van criterion	7-60
7.5.1.1	The macroscopic-microscopic approach	7-60
7.5.1.2	Link between macroscopic and mesoscopic scales	7-60
7.5.1.3	Failure criterion	7-61
7.5.2	Multiaxial analysis.....	7-62
7.5.2.1	Local effective equivalent stress	7-63
7.5.2.1.1	Local stress for fatigue assessment	7-63
7.5.2.1.2	Effective equivalent stress	7-63
7.5.2.2	Failure Criteria	7-65
7.5.3	Rolling contact fatigue	7-65
7.5.3.1	Introduction.....	7-65
7.5.3.2	Analytic determination of the limit thermo-mechanical state for fatigue assessment	7-65
7.5.3.3	Numerical methods for treatment of fatigue.....	7-66
7.5.3.4	Example of application to analysis of rail damage	7-66
7.5.4	Fatigue – creep.....	7-67
7.5.5	Fatigue – corrosion.....	7-67
7.5.6	Growth of Short Cracks.....	7-67
7.6	Additional information.....	7-70
7.6.1	Variable amplitude loading	7-70
7.6.1.1	Loading description	7-70
7.6.1.1.1	Time history sequences description	7-70
7.6.1.1.2	Histogram description	7-70
7.6.1.1.3	Power or energy density spectrum description.....	7-71
7.6.1.2	Data reduction	7-71
7.6.1.3	Presentation of results.....	7-71
7.6.1.3.1	Miner sum.....	7-71
7.6.1.3.2	Equivalent stress range.....	7-72
7.6.1.3.3	Gassner curve.....	7-73
7.7	Bibliography	7-73

7.1 Introduction

The FITNET fatigue module provides a series of assessment routes for evaluating the fatigue damage due to cyclic or fluctuating loads. Two basic scenarios are foreseen:

- a) There is no pre-existing flaw, and the goal of the analysis is to determine the accumulation of fatigue damage at a critical location. In this case the basic approach is to determine the fluctuating stress range at the location in question and to relate this to appropriate fatigue life curves. Three different routes are proposed (Routes 1, 2 and 3), depending on the choice of stress or strain to be used in the assessment. Any of the routes can be used to determine the accumulation of fatigue damage during the specified operational life (referred to later as 'cumulative fatigue assessment') or to ensure that no significant fatigue damage will be introduced, so that the life can be regarded as being infinite (a 'fatigue limit assessment'). The second approach may be required if there is a risk of unstable fracture from a small fatigue crack or the number of fluctuating stress cycles to be endured in service is very large, typically greater than 10^9 .
- b) A real or postulated flaw is present, and the goal of the analysis is to determine its fatigue life. Two different routes are considered, fatigue crack growth analysis in Route 4 and the use of S-N curves in Route 5. Route 4 is required if the flaw is planar or if it is necessary to quantify the progress of the crack propagating from a planar or non-planar flaw (e.g. to establish inspection intervals or to allow for possible fracture at a particular critical crack size). Route 5 is used only to assess non-planar flaws.

The overall scheme is shown in Figure 7.1. The scope and background of the five assessment routes are briefly described in the following, while Figure 7.2 shows the basic steps used in applying them.

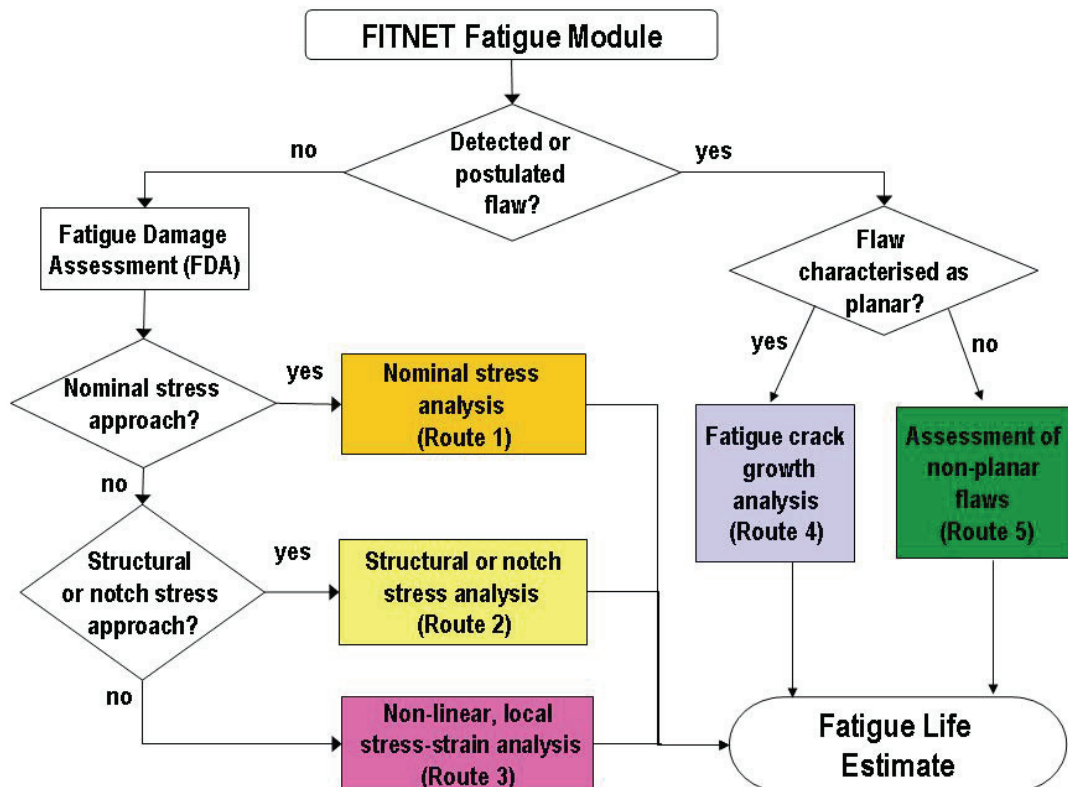


Figure 7.1 - Selection of a fatigue assessment route.

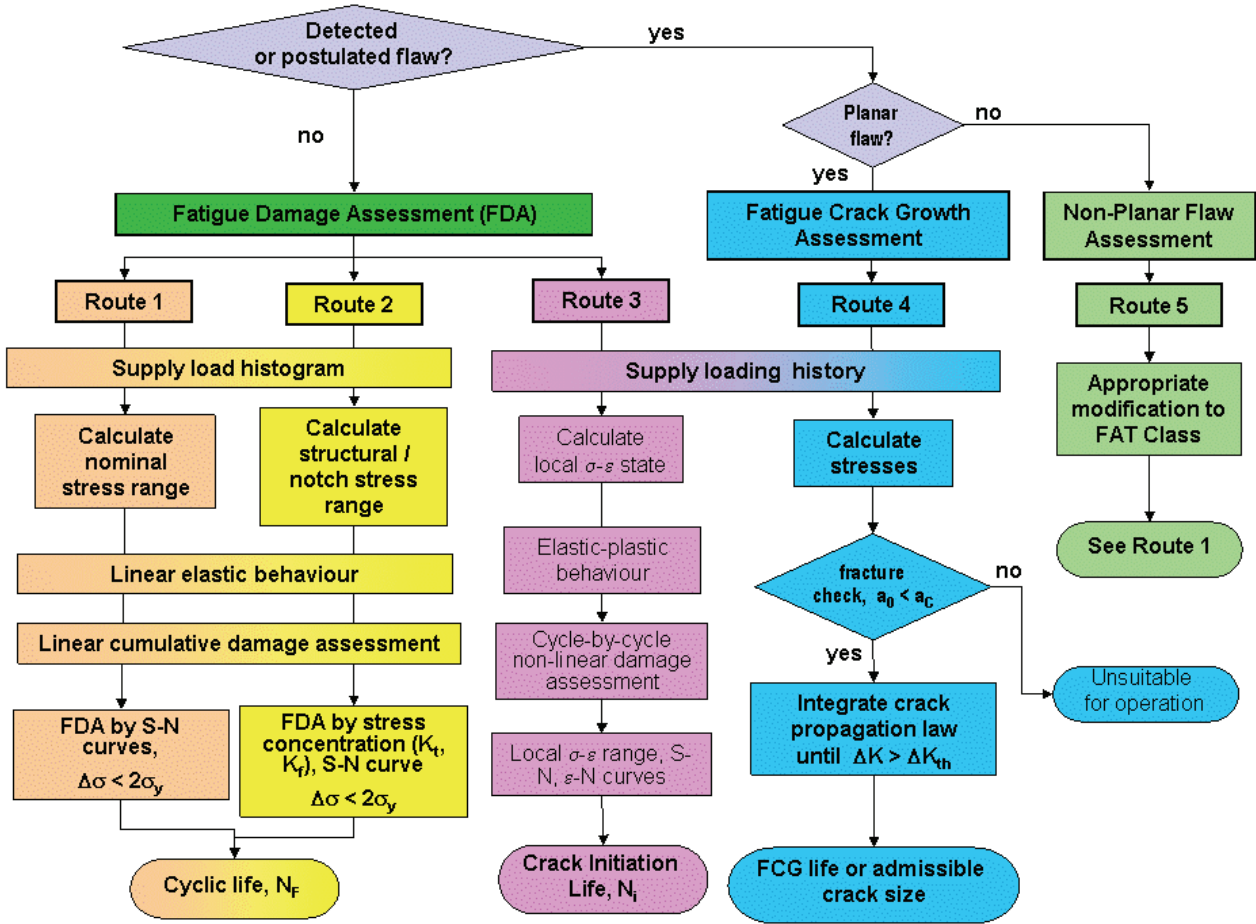


Figure 7.2 - Basic steps in the FITNET fatigue assessment routes

Route 1 – Fatigue damage assessment using nominal stresses

This route considers nominal elastic stress values at the location of interest. For welded features, the fatigue life is determined from a set of S-N curves classified according to different levels of fatigue resistance. The effects of local geometric, weld or microstructural details and, if relevant, residual stress are accounted for in the S-N curve itself. It is based on currently used procedures, in particular the International Institute of Welding guidelines [7.1]. For variable loads, the Palmgren-Miner linear cumulative damage rule is used. For non-welded features the “intrinsic” endurance is modified to account for factors such as geometric discontinuities, section size, surface roughness and mean stress. A permissible nominal stress is derived and compared to the value arising at the component as a result of the operational loading.

Route 2 – Fatigue damage assessment using either structural hot spot stress or notch stress

This route considers that the appropriate structural stress in a critical area of a component can be calculated by formula (in some cases it can be measured using specific methods). Two approaches are possible:

- (a) calculate the structural stress (hot spot stress) [7.2] and apply with appropriate S-N curves
- (b) calculate a notch stress via stress concentration factors such as K_t or K_f [7.3] and apply with appropriate S-N curves

The Palmgren-Miner linear cumulative damage rule is used to deal with variable loads.

Route 3 – Fatigue damage assessment using a local stress-strain approach

This route is mainly directed at non-welded applications and foresees direct calculation of strains at a critical location using an appropriate elastic or elasto-plastic description of the material behaviour. The fatigue life is then determined from a strain range vs. cycles to initiation curve or relation such as the Manson-Coffin law. It is also noted that the analysis can be taken further by considering subsequent crack growth using fracture mechanics, as described in Route 4. The damage accumulation is calculated cycle-by-cycle, allowing for consideration of non-linear effects if necessary.

Route 4 – Fatigue crack propagation

This route addresses the assessment of detected or postulated planar flaws that can be considered as macro-cracks. The initial flaw position, size and orientation can be determined in two ways: either based on the reported or detected size from non-destructive inspection results or from a postulated flaw, based on consideration of service experience, the manufacturing process, resolution limits of a non destructive technique, from the threshold stress intensity factor etc. The basic approach foreseen for calculating fatigue crack growth is via the standard Paris law. A more sophisticated approach is also provided, based on the Forman-Mettu [7.4] equation.

Route 5 – Non-planar flaw assessment

Non-planar flaws can sometimes be assessed in the same way as planar flaws using Route 4. Since they are not crack-like, this will be conservative. However, it may be the only option if it is necessary to quantify the growth of the flaw under fatigue loading and to ensure the margin against unstable fracture at a specific crack size. Otherwise, Route 1, using S-N curves for welded joints, can be applied directly in cases for which the equivalent fatigue strength has been established for the non-planar flaw under consideration. At present, this approach is only available for assessing slag inclusions less than 1 mm deep or porosity in steel or aluminium butt welds.

7.2 Definitions and Input Parameters

7.2.1 Definition of Fatigue Service Conditions

7.2.1.1 Description of Variable Loads

The accumulation of fatigue damage results from the cycle by cycle variation of stress. Therefore to be able to assess fatigue life, the stress versus time history must be known or estimated. In practice, the more commonly applied methods in design use the stress range distribution (also referred to as the histogram or spectrum) versus the number of cycles as shown in Figure 7.3. In addition to the stress range, the loading is characterised

by the mean stress or R ratio:
$$R = \frac{\sigma_{\min}}{\sigma_{\max}} \quad (7.1)$$

where σ_{\min} and σ_{\max} are the minimum and maximum values of the stress cycle respectively.

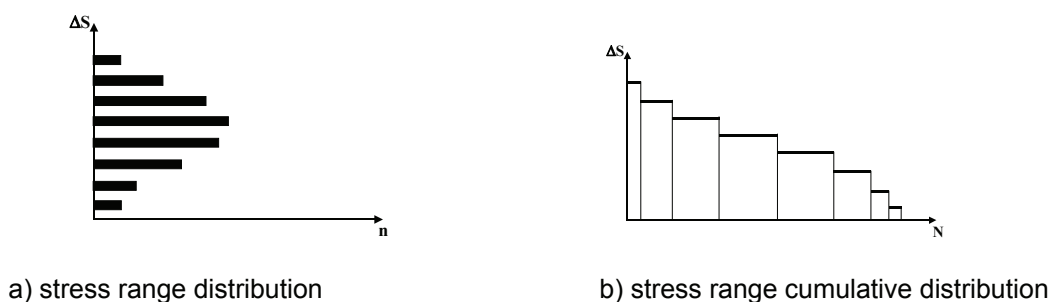


Figure 7.3 - Stress histogram

7.2.1.2 Partial Safety Factors

Depending on the level of safety built into the fatigue resistance data being used in the assessment, the confidence with which the fatigue actions can be estimated and possibly the consequences of fatigue failure, partial safety factors may need to be introduced. Those applied to the fatigue actions are termed γ_F while those applied to the resistance data are termed γ_M .

7.2.1.3 Fatigue Actions

Fatigue assessments are carried out using the design spectrum (histogram) of the fatigue actions in terms of stress ranges $\Delta\sigma_{i,s,d}$, which correspond to the stresses of the characteristic spectrum (histogram) $\Delta\sigma_{i,s,k}$ multiplied by the partial safety factor γ_F for fatigue actions.

For constant amplitude loading, the characteristic and design spectra are reduced to only one stress level $\Delta\sigma_{s,d} = \Delta\sigma_{s,k} \times \gamma_F$.

7.2.1.4 Cumulative Fatigue Assessment

A cumulative fatigue assessment is applied in situations where it is considered that fatigue crack initiation and growth can be tolerated without the risk of failure during the required lifetime. The fatigue resistance is usually derived from constant or variable amplitude tests. The fatigue resistance data given here are based on published results from constant amplitude tests.

The fatigue resistance data must be expressed in terms of the same stress (nominal, hot spot, notch) or strain as that controlled or determined during the generation of those data. In conventional endurance testing, there are different definitions of failure. In general, small specimens are tested to complete rupture, while in large components the observation of a through-wall crack is taken as a failure criterion. In practice, the former is often essentially the same as the latter. The fatigue resistance data are based on the number of cycles N to failure at given stress ranges and provided in the form of S-N curves.

$$N = \frac{C}{\Delta\sigma^m} \quad \text{or} \quad N = \frac{C}{\Delta\tau^m} \quad (7.2)$$

where:

- $\Delta\sigma$ normal stress range
- $\Delta\tau$ shear stress range
- N number of cycles to failure
- C, m constants, characteristic of the material and detail being assessed

The fatigue resistance is defined by the mean curve (50% probability of survival) and the standard deviation on Log(C).

The conventional fatigue resistance data can be given as characteristic values, $\Delta\sigma_{R,k}$ or $\Delta\tau_{R,k}$, which are assumed to have a survival probability of at least 95%, calculated from a mean value of a two-sided 75% confidence level. In practice these characteristic values may be reduced further by dividing them by a partial safety factor γ_M to give the design resistance values $\Delta\sigma_{R,d}$ and $\Delta\tau_{R,d}$ used in the fatigue assessment. The design resistance S-N curve may be modified further according to the needs of the damage calculation procedure.

For constant amplitude loading, the characteristic stress range $\Delta\sigma_{R,k}$ at the required number of stress cycles is first determined. Next, the fatigue design criterion is checked:

7.2.1.5 Fatigue Limit Assessment

A fatigue limit assessment is one that is applied to cases where no significant fatigue crack growth can be tolerated, for example because there is a risk of failure from a small crack, or a very high number of stress cycles, typically greater than 10^9 cycles, needs to be endured. The fatigue limit resistance is defined by the stress range $\Delta\sigma_{L,R}$ below which the lifetime is considered to be infinite from an engineering point of view.

Again, characteristic values $\Delta\sigma_{L,R,k}$ are reduced to design values $\Delta\sigma_{L,R,d} = \Delta\sigma_{L,R,k} / \gamma_M$.

When the fatigue limit assessment is applied for constant amplitude loading, the design verification criterion is:

$$\Delta\sigma_{M,s,d} < \Delta\sigma_{L,R,d} \quad (7.4)$$

where $\Delta\sigma_{M,s,d}$ is the maximum applied stress range and $\Delta\sigma_{L,R,d}$ is the design acceptable fatigue limit stress range.

For variable amplitude loading, if the maximum design stress range $\Delta\sigma_{M,s,d}$ of the load spectrum is lower than the design fatigue limit $\Delta\sigma_{L,R,d}$ of the design fatigue resistance S-N curve, or if it is lower than the design cut-off limit $\Delta\sigma_{cut,R,d}$ in cases where no fatigue limit is given (see sections 7.2.3 and 7.3.1.1.5), the life of the assessed detail can be assumed to be infinite and no further damage calculation is necessary [7.1].

7.2.2 Environmental Issues

The fatigue resistance data given here refer to non-corrosive environments (air) and for structures with normal protection against atmospheric corrosion. For free atmospheric corrosion, in particular a sea environment, the S-N curve to be applied can be derived from the standard curve applying the following conditions:

- the curve has no fatigue limit nor cut-off and no change of slope
- the life time is divided by 2

Concerning service temperature, unless stated otherwise the fatigue resistance data refer to temperatures lower than 100°C; a fatigue reduction factor has to be considered beyond this temperature level [7.1].

If the effect of environment cannot be excluded, then the assessment should be made using the creep or corrosion modules (see sections 8 and 9 respectively).

7.2.3 Exemption from Fatigue Assessment

In the following cases, fatigue assessment is **not** required [7.1]. N.B. This paragraph is not applicable to tubular joints.

1 - Weld Details

a) The highest nominal design stress range satisfies:

$$\text{Steel: } \Delta\sigma_{M,s,d} \leq \frac{36}{\gamma_M} \quad \text{Al: } \Delta\sigma_{M,s,d} \leq \frac{14}{\gamma_M} \quad (\text{in MPa}) \quad (7.5)$$

b) For a detail for which a constant amplitude fatigue limit $\Delta\sigma_{R,L}$ is specified and all design stress ranges are under the design resistance fatigue limit

$$\Delta\sigma_{M,s,d} \leq \Delta\sigma_{R,L} / \gamma_M \quad (7.6)$$

where the partial safety factor γ_M should be taken from an applicable design code.

2 - non-welded details

In Route 1 for non-welded applications a constant amplitude fatigue limit σ_a is defined. A fatigue assessment is not required for a detail for which the maximum stress amplitude (local stress at the reference point under consideration, calculated by linear elastic analysis) is less than $0.73 \sigma_a$.

7.3 Fatigue Assessment Routes

7.3.1 Route 1 - Fatigue Damage Assessment using Nominal Stresses

This route can be applied to both welded structures and to non-welded components.

7.3.1.1 Route 1 (Welded Structures)

The flowchart is shown in Figure 7.5.

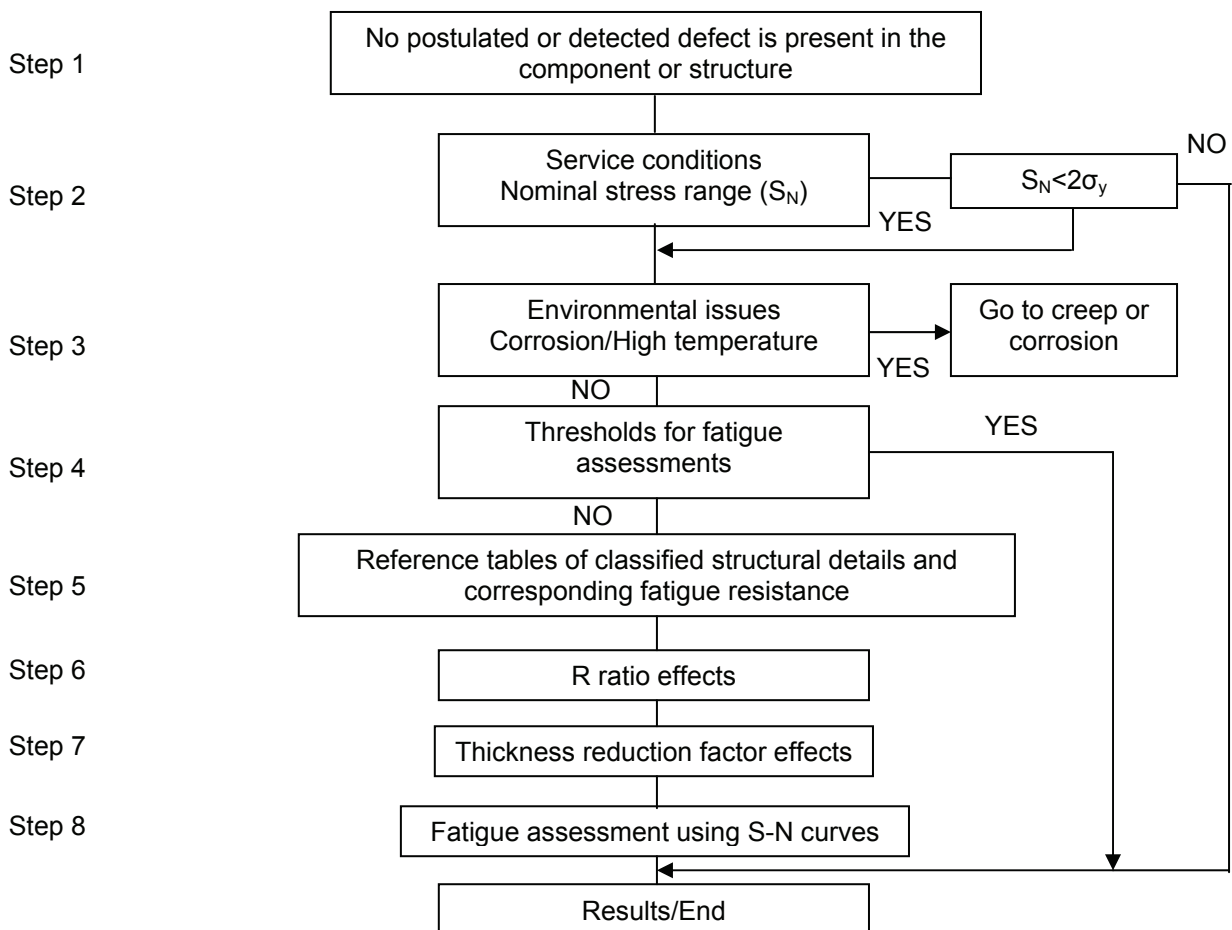


Figure 7.5 - Fatigue Assessment Route 1

7.3.1.1.1 Step 1: No Postulated or Detected Flaw is Present in the Structure

Route 1 assumes that no defect is postulated or is detected by NDE in the structure or component under consideration. The fatigue assessment is based on linear damage analysis. Annex D provides guidance on NDE techniques and detection capability.

7.3.1.1.2 Step 2: Service Condition

Fatigue resistance will be calculated in Route 1 by using the nominal stress range S_N . Nominal stress can be calculated by using elementary theories of structural mechanics based on linear-elastic behaviour. In other cases, finite element method (FEM) modelling may be used. FEM meshing can be relatively coarse. Care must be taken to ensure that all stress raising effects on the structural detail of the welded joint are excluded when calculating the "modified nominal stress". The design value of the nominal stress range S_N must be smaller than $2\sigma_y$.

7.3.1.1.3 Step 3: Environmental Issues

See section 7.2.2

7.3.1.1.4 Step 4: Thresholds for Fatigue Assessment

See section 7.2.3

7.3.1.1.5 Step 5: Fatigue Resistance Data Specification

The fatigue assessment of classified structural details (see Annex N) and welded joints is based on the nominal stress range. In most cases structural details are assessed on the basis of the maximum principal stress range in the section where potential fatigue cracking is considered. However, guidance is also given for the assessment of shear loaded details, based on the maximum shear stress range. Separate S-N curves are provided for normal or shear stress ranges, as illustrated in Figure 7.6 and Figure 7.7 respectively.

Care must be taken to ensure that the stress used for the fatigue assessment is the same as that given in the tables of the classified structural details. Guidance on the calculation of the nominal stress calculation is given in Section 5. Macro-structural hot spot stress concentrations not covered by the structural detail of the joint itself, e.g. large cut outs in the vicinity of the joint, have to be accounted for by the use of a detailed stress analysis, e.g. finite element analysis, or appropriate stress concentration factors (see Section 5).

The fatigue curves for welds are based on representative experimental investigations and thus include the effects of:

- structural hot spot stress
- concentrations due to the detail shown
- local stress concentrations due to the weld geometry
- weld imperfections consistent with normal fabrication standards
- stress direction
- welding residual stresses
- metallurgical conditions
- welding process (fusion welding, unless otherwise stated)
- inspection procedure (NDE), if specified
- post weld treatment, if specified

Furthermore, within the limits imposed by static strength considerations, the fatigue curves of welded joints are independent of the tensile strength of the material. Each fatigue strength curve is identified by the characteristic fatigue strength of the detail at 2 million cycles. This value is the fatigue class (FAT). The slope of the fatigue

strength curves for details assessed on the basis of normal stresses is $m = 3.00$. The constant amplitude fatigue limit is 5×10^6 cycles. The slope of the fatigue strength curves for details assessed on the basis of shear stresses is $m = 5.00$, but in this case the fatigue limit corresponds to an endurance of 10^8 cycles.

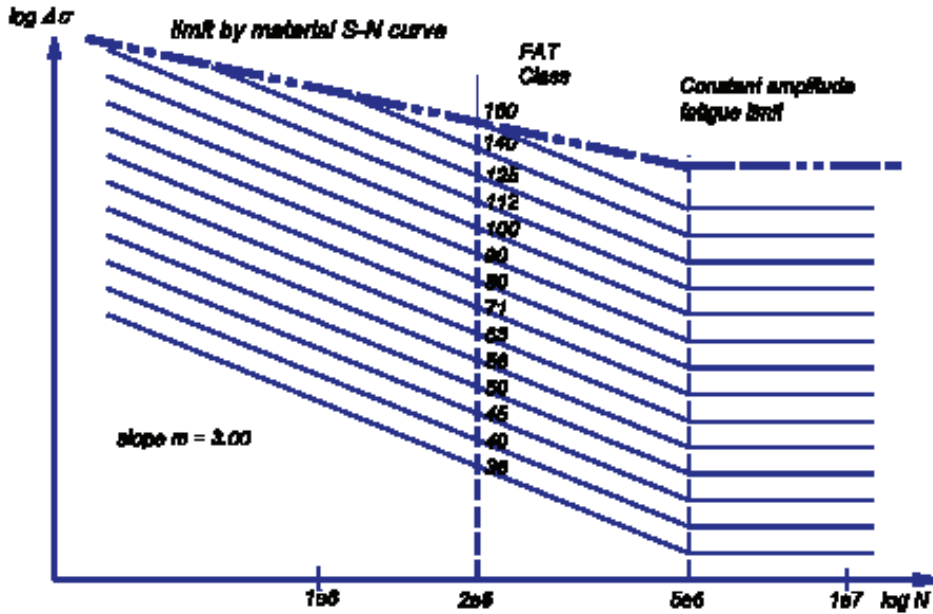


Figure 7.6 - Fatigue resistance S-N curves for $m=3.00$, normal stress (steel)

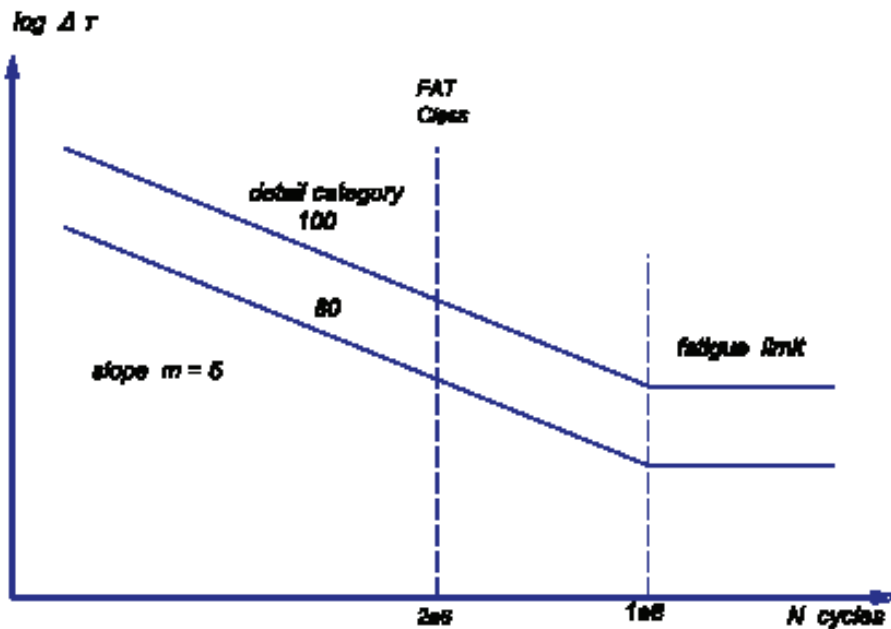


Figure 7.7 - Fatigue resistance S-N curves for shear stress (steel)

The descriptions of the structural details include information about the weld size, shape and quality only in part. The data refer to a standard quality as given in codes and standard welding procedures. For higher or lower qualities, conditions of welding may be specified and verified by tests.

The fatigue classes given in Figure 7.6 should be modified as given in Annex N, considering also the limitations imposed by weld imperfections.

All S-N curves of details are limited by the material S-N curve, which may vary due to different strengths of the materials. In the absence of major weld flaws, fatigue cracks originate from the weld toe, and then propagate through the base material, or from the weld root, and then propagate through the weld throat. For potential toe cracks, the nominal stress in the base material has to be calculated and compared with the fatigue resistance given in the tables. For potential root cracks, the nominal stress in the weld throat has to be calculated. If both failure modes are possible, e.g. at cruciform joints with fillet welds, both potential failure modes have to be assessed.

7.3.1.1.6 Step 6: R-Ratio effects

For stress ratios (R-ratios) $R < 0.5$ a fatigue enhancement factor $f(R)$ may be considered by multiplying the fatigue class of classified details by $f(R)$. The fatigue enhancement factor depends on the level and direction of residual stresses. The following cases can be distinguished:

a) Base material and wrought products with negligible residual stresses ($< 0.2 \sigma_y$), stress relieved welded components, in which the effects of constraints or secondary stresses have been considered in analysis.

$$\begin{aligned} f(R) &= 1.6 && \text{for } R < -1 \\ f(R) &= -0.4 \cdot R + 1.2 && \text{for } -1 \leq R \leq 0.5 \\ f(R) &= 1 && \text{for } R > 0.5 \end{aligned}$$

b) Small scale thin-walled simple structural elements containing short welds. Parts or components containing thermally cut edges

$$\begin{aligned} f(R) &= 1.3 && \text{for } R < -1 \\ f(R) &= -0.4 \cdot R + 0.9 && \text{for } -1 \leq R \leq -0.25 \\ f(R) &= 1 && \text{for } R > -0.25 \end{aligned}$$

c) Complex two or three-dimensional components, components with global residual stresses, thick-walled components

$$f(R) = 1 \quad \text{No enhancement}$$

7.3.1.1.7 Step 7: Thickness Reduction Factor Effects

The influence of the plate thickness on fatigue strength should be taken into account in cases where cracks start from the weld toe on plates thicker than 25 mm or thinner than 5 mm. The reduced strength is taken in consideration by multiplying the fatigue class of the structural details by the thickness reduction factor $f(t)$.

The thickness correction exponent "n" depends on the effective thickness t_{eff} and the joint category, as set out in Table 7.1 below.

$$f(t) = \left[\frac{25}{t_{eff}} \right]^n \quad \text{where } t > 25 \text{ mm}$$

If $L/t < 2$ then $t_{eff} = 0.5 \cdot L$ (see **Figure 7.8 Fehler! Verweisquelle konnte nicht gefunden werden.**) otherwise $t_{eff} = t$

7.3.1.1.8 Step 8: Fatigue Assessment using S-N Curves

The fatigue damage assessment requirements are provided in Section 7.2.1.4.

Table 7.1 - Values for the thickness correction exponent.

Joint Category	Condition	n
Cruciform joints, transverse T-joints plates with transverse attachments	As-welded	0.3
Cruciform joints, transverse T-joints plates with transverse attachments	Toe ground	0.2
Transverse butt welds	As-welded	0.2
Butt welds with ground flush, base material, longitudinal welds or attachments	Any	0.1

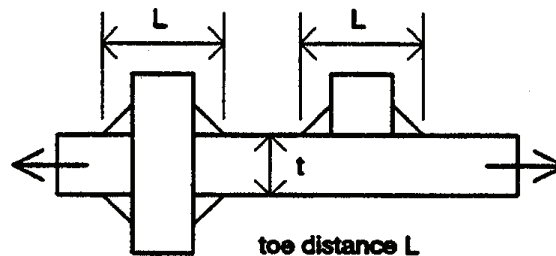


Figure 7.8 – Weld toe parameters used to define the thickness reduction factor.

7.3.1.2 Route 1 for Non-Welded Locations

This route is applicable to components with geometric discontinuities operated in the high cycle regime and subject to constant amplitude loads [7.4, 7.5]. Figure 7.9 shows the stepwise flowchart for its application.

The conventional approach starts from the knowledge of the fatigue resistance of the base material submitted to fatigue cycles. This approach leads to a modification of this “intrinsic” endurance or reliability limit, σ_w , for a mean stress equal to 0 by taking into account parameters such as:

- the geometrical discontinuities of the component (notch effect): coefficient K_t or K_f
- its size (scale effect), coefficient K_e
- the surface roughness (surface effect), coefficient K_s
- the mean stress, σ_m

Finally, the permissible nominal stress σ_a , is derived and compared to the actual (nominal) stress, σ_e , applied to the component. N.B. The method uses the stress amplitude instead of the stress range as for welded joints.

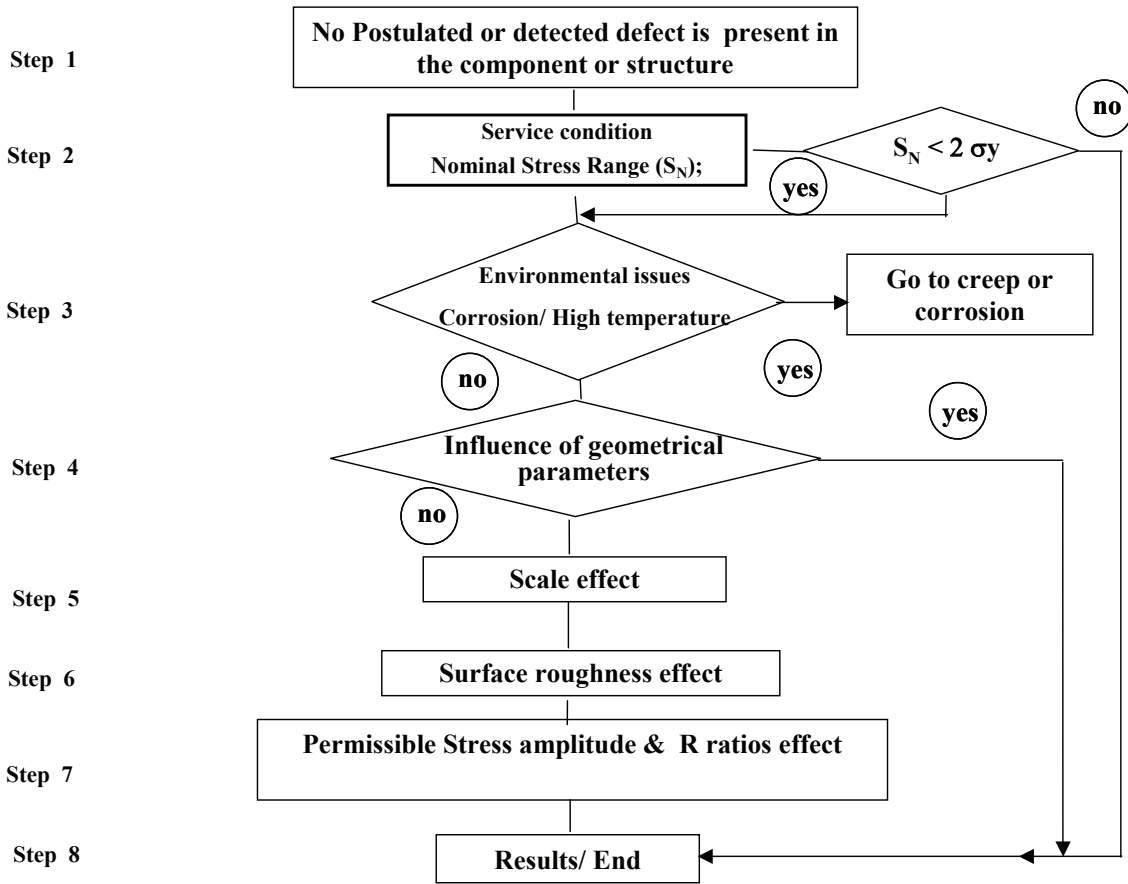


Figure 7.9 – Route 1 for Non-Welded Locations

7.3.1.2.1 Step 1: No Postulated or Detected Flaw is Present in Component

Route 1 assumes that no defect is postulated or is detected by NDE in the structure or component to be assessed. Annex D provides guidance on NDE techniques and capabilities.

7.3.1.2.2 Step 2: Service Conditions

Fatigue resistance is calculated using nominal stress range σ_N . The nominal stress can be calculated using elementary theories of structural mechanics based on linear-elastic behaviour. In other cases, finite element modelling may be used.

7.3.1.2.3 Step 3: Environmental Issues

See Section 7.2.2.

7.3.1.2.4 Step 4: Influence of geometric parameters

7.3.1.2.4.1 Notch Effect

a) Definition

The term notch is used to describe a discontinuity, either intended or unintended, in the form of the material, or it can describe a non-uniform condition. The effect of a notch on a part is to create local stress concentrations. Fehler! Verweisquelle konnte nicht gefunden werden. Figure 7.10 shows an example of locations where the notch effect must be considered.

b) Notch concentration factor K_t

The geometry of a part enables a theoretical stress concentration factor K_t to be evaluated using graphs from handbooks (an example is shown in Figure 7.10 Fehler! Verweisquelle konnte nicht gefunden werden.) or calculated using formulae or finite element methods.

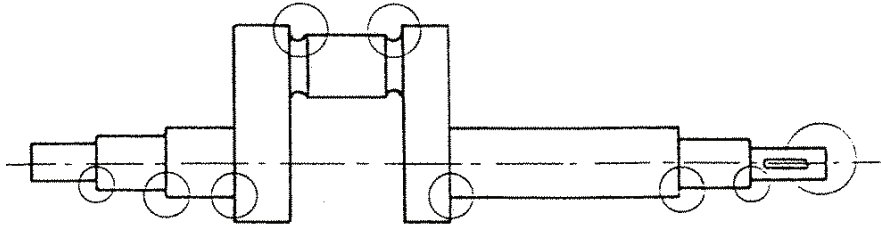


Figure 7.10 – Locations where the notch effect must be considered

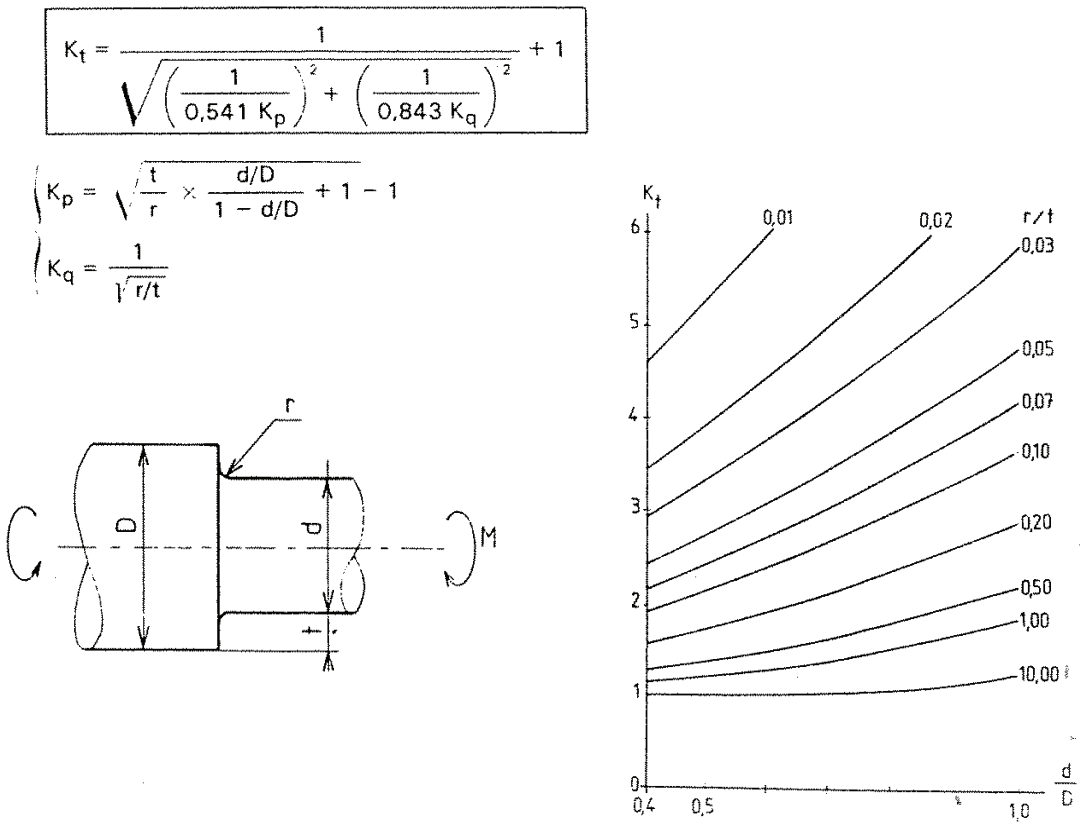


Figure 7.11 - Graph for determining K_t in bending for a shaft with a shoulder.

c) Effective notch fatigue concentration factor K_f

In practice, the reduction in the endurance level or reliability is less than may be deduced from K_t . In order to obtain the notch fatigue factor K_f , it is necessary to correct K_t using a variable parameter, δ :

$$\delta = K_t / K_f$$

The value of δ will depend on the form and shape of the part, the relative severity of the notches and on the material used. Figure 7.12 provides the relationship between $1/\delta$, the tensile strength, R_m , and K_t . From this K_f can be derived. This approach is valid for endurance levels with $N \geq 2.10^6$. For lower values of N , δ becomes a function of K_t and N ; for further guidance see ref. [7.5].

To take into consideration the form and dimensions of the component part, δ can be calculated versus a stress gradient χ , as shown in Figure 7.13. The stress gradient χ can be determined from Table 7.2. Values greater than 10 mm^{-1} are unacceptable from an industrial point of view and in such cases the design should be modified to obtain a lower value. For $\chi < 0.02 \text{ mm}^{-1}$, a lower bound value of $\chi = 0.02$ should be used for the assessment.

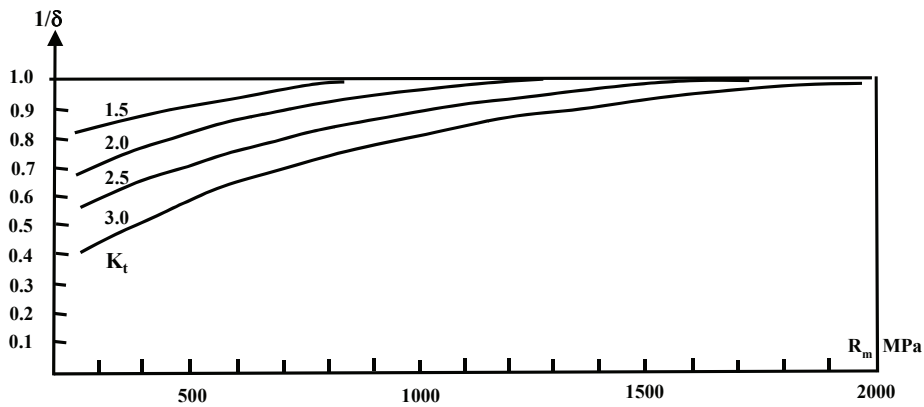


Figure 7.12 - Determination of $1/\delta$ as a function of R_m and K_t

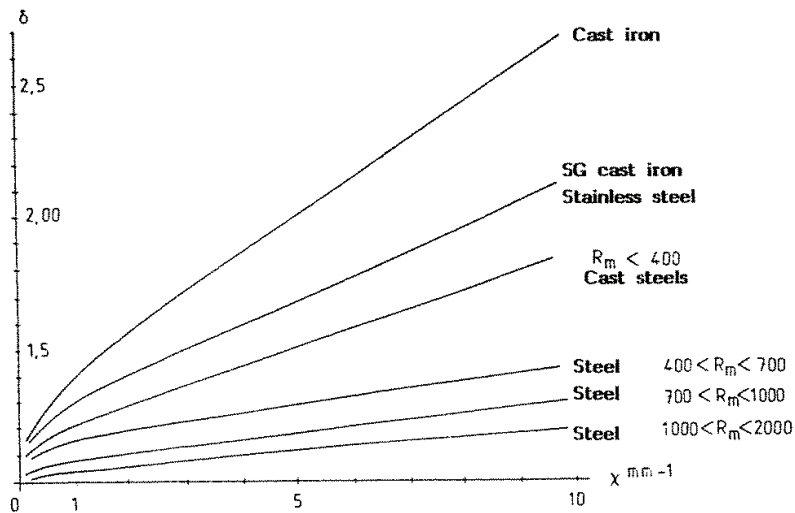
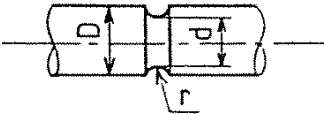
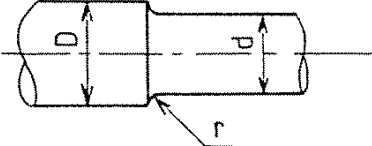
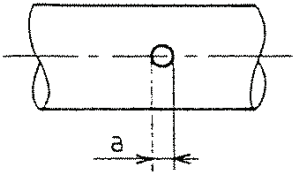
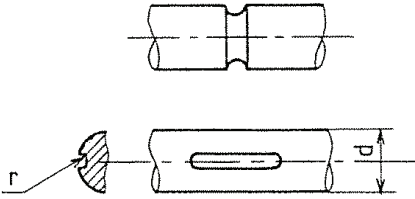

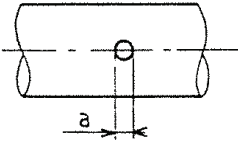


Figure 7.13 - The dynamic factor δ in terms of the stress gradient χ and material type

Table 7.2 - Simple formulae for calculating the stress gradient χ , from the geometry of the part and the type of stresses applied.

<u>Bending</u>		$\chi = \frac{2}{r} + \frac{2}{d}$
		$\chi = \frac{2}{r} + \frac{4}{d+D}$
		$\chi = \frac{6}{a}$
<u>Torsion</u>		$\chi = \frac{1}{r} + \frac{2}{d}$
		$\chi = \frac{1}{r} + \frac{4}{d+D}$
		$\chi = \frac{6}{a}$

d) Alternative effective notch fatigue concentration factor K_f

In certain cases, it is possible to use K_t directly, as this should provide a higher safety factor. The designer may then, by calculation, pass directly from K_t to the corrected endurance limit σ'_a , using the following formulae :

In bending :

$$\sigma_{a/N} = \frac{1}{K_t} (a \log \chi + b) \quad (7.7)$$

In torsion :

$$\sigma_{a/N} = \frac{1}{K_t} \frac{\sqrt{3}}{3} (a \log \chi + b) \quad (7.8)$$

where the coefficients a and b vary in accordance with the material as given in Table 7.3. It is noted that K_f can be obtained by:

$$K_f = \frac{\sigma_w}{\sigma_{a/N}} \tag{7.9}$$

Table 7.3 - Value of coefficients a and b in terms of the material

R_m for steel	a	b
1400 < R _m	100/3	655
1200 < R _m < 1400	110/3	585
1000 < R _m < 1200	120/3	520
900 < R _m < 1000	130/3	465
800 < R _m < 900	130/3	430
700 < R _m < 800	135/3	390
600 < R _m < 700	135/3	335
500 < R _m < 600	140/3	295
400 < R _m < 500	140/3	245
R _m < 400		195
R_m for cast steels		
350 < R _m < 500	140/3	180
R _m < 350	140/3	135

7.3.1.2.4.2 Section Size Effect

The endurance or reliability limits given in the literature are typically established using test pieces of small dimensions (in general 6 mm diameter). However it has been observed experimentally that, if all other values remain the same, the endurance limit is reduced as the size of the test piece increases. A factor K_e can be used to account for this effect. The relationship between K_e and section diameter is given in Figure 7.14.

7.3.1.2.4.3 Surface Roughness Effect

The endurance limit of the base material is measured using test pieces which have been fully polished and it is therefore necessary to allow for any reduction due to surface roughness of the component under consideration. For this a coefficient K_s is used, which is a function of the ultimate tensile strength, R_m , of the material and its surface roughness, defined by the factor R_t (total distance between the highest point of the peaks and the lowest point of the valleys in the surface profile after filtering). The relationship between K_s , R_m and R_t is shown in Figure 7.15.

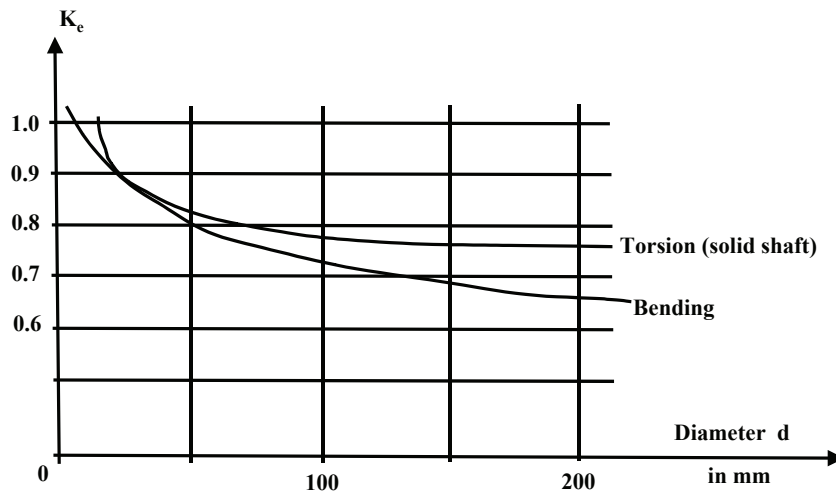


Figure 7.14 - Graph for obtaining K_e in terms of the diameter

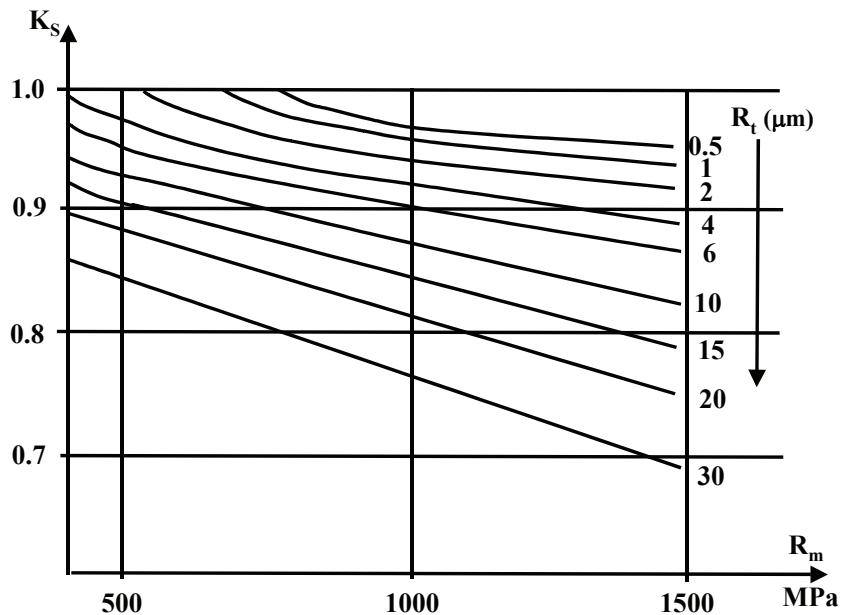


Figure 7.15 - Mean values of the surface roughness factor K_s in terms of the tensile strength R_m and the total surface roughness R_t

7.3.1.2.5 Step 5: Permissible stress σ_a and mean stress effects

The permissible stress for a mean stress equal to 0, $\sigma_{a/0}$, is given by:

$$\sigma_{a/0} = \frac{\sigma_w}{K_f} K_S K_e \quad \text{or} \quad \sigma_{a/0} = \sigma_{a/N} K_S K_e \tag{7.10}$$

where σ_w is the endurance limit for the loading type considered.

The fatigue resistance of metallic components subjected to axial loading is influenced by the mean stress of the load cycle; this influence is absent under torsion. To account for the mean stress effect, the permissible stress amplitude can be evaluated using the Haigh or generalized Haigh diagrams ($\sigma_a - \sigma_m$).

a) Haigh diagram

The Haigh diagram (Figure 7.16) is obtained from the Goodman equation:

$$\sigma_a = \sigma_{a/0} \left(1 - \frac{\sigma_m}{\sigma_{m/M}} \right) \tag{7.11}$$

where $\sigma_{m/M} = \frac{R_m}{K_t}$ and R_m is the tensile strength for the material.

b) Generalized Haigh diagram

The generalized Haigh diagram is shown in Figure 7.17, where the equations of the curve are the following:

$$\text{for } 0 < \sigma_m < (\sigma_{m/M} - 0.5 \sigma_{a/0}) \quad \sigma_a = \sigma_{a/0} \left(1 + \frac{\sigma_m}{\sigma_{a/0} - 2 \sigma_{m/M}} \right) \tag{7.12}$$

$$\text{for } (\sigma_{m/M} - 0.5 \sigma_{a/0}) < \sigma_m < \sigma_{m/M} \quad \sigma_a = \sigma_{m/M} - \sigma_m \tag{7.13}$$

Equation 7.11 provides a higher safety factor than equations 7.12 and 7.13, which can be applied to ductile steels.

7.3.1.2.6 Step 6: Results

The design is acceptable when the (σ_m, σ_e) point is located in the safe region of the Haigh or modified Haigh diagram as shown in Figure 7.18.

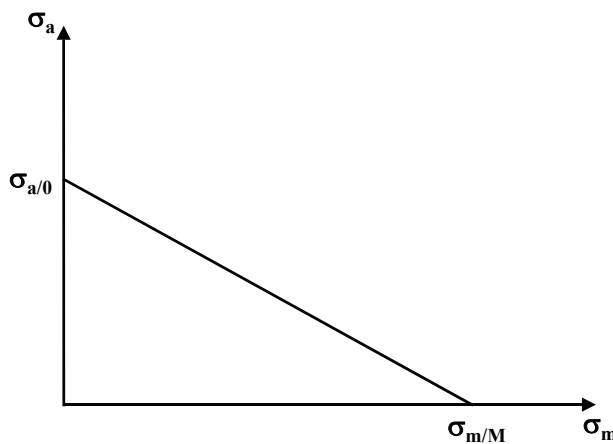


Figure 7.16 – The Haigh diagram

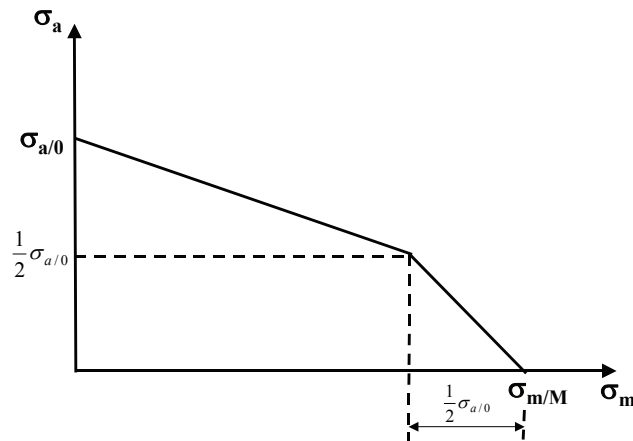


Figure 7.17 - The modified Haigh diagram ([after 7.7])

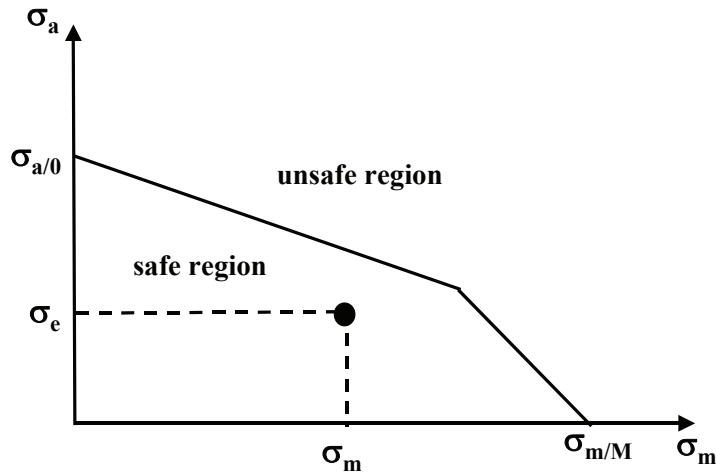


Figure 7.18 – Illustration of acceptance criteria verification for the modified Haigh diagram.

7.3.2 Route 2 - Fatigue Damage Assessment using Structural or Notch Stresses

Route 2 is designed to be applied to welded structures and also non-welded components. This route uses cumulative linear damage assessment and is applicable to components under random loads.

7.3.2.1 Route 2 for Welded Structures

For welded structures, Route 2 is applied according to the flowchart shown in Figure 7.19.

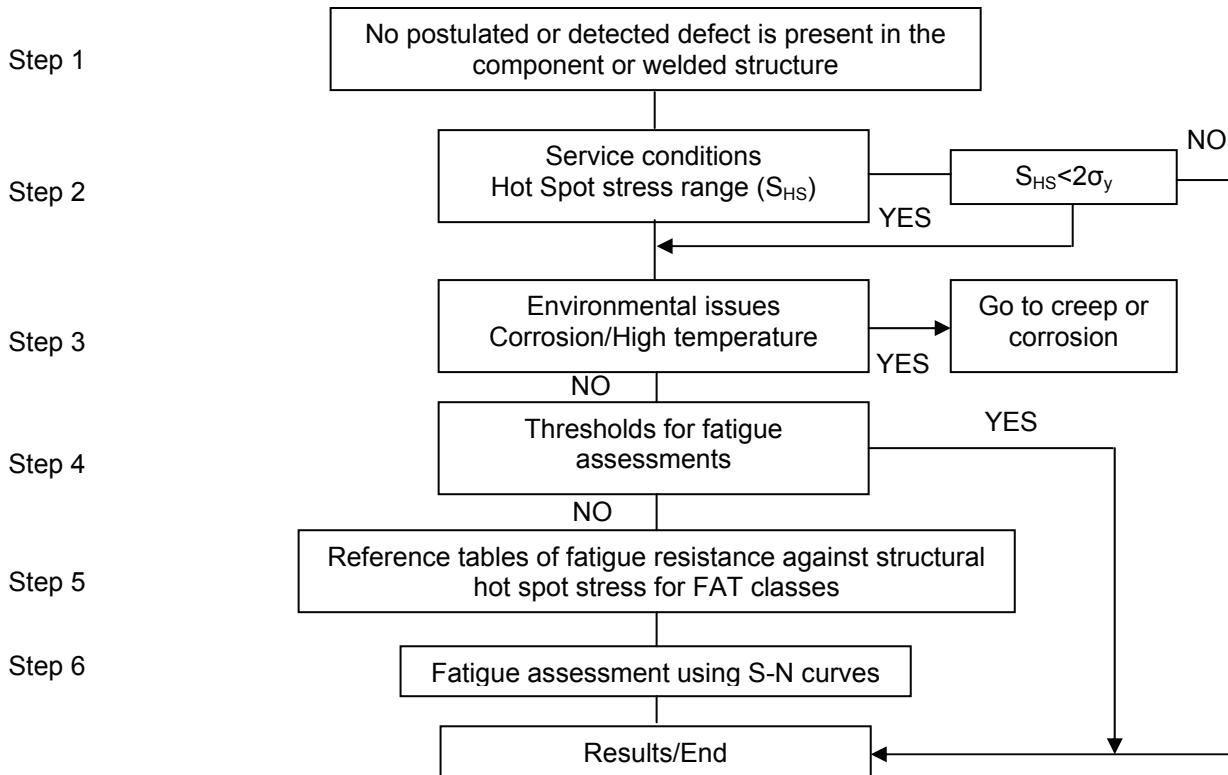


Figure 7.19 The Route 2 flowchart for welded components.

7.3.2.1.1 Step 1: No Postulated or Detected Flaw is Present in the Structure

Route 2 assumes that no defect is postulated or is detected by NDE in the structure or component to be assessed. Annex D provides guidance on NDE techniques.

7.3.2.1.2 Step 2: Service Conditions

Fatigue resistance is calculated using the hot spot stress range $\Delta\sigma_{HS}$ or the notch stress range ($\Delta\sigma_{notch}$). When using spectral analysis, the stress range $\Delta\sigma$ can be determined directly.

When using finite element models with conventional loads or time step analysis, the maximum σ_{max} and minimum σ_{min} stress levels are calculated. Then, the stress range is given by:

$$\Delta\sigma = \sigma_{max} - \sigma_{min}$$

The design value of the stress range $\Delta\sigma_{HS}$ or $\Delta\sigma_{notch}$ must be smaller than $2\sigma_y$

7.3.2.1.2.1 Definition of hot spot stress and effective notch stress at welds

The structural hot spot stress and effective notch stress (Figure 7.20) are defined versus the nominal stress by means of two stress concentration factors: structural hot spot stress SCF_{HS} and notch effect SCF_{Notch} .

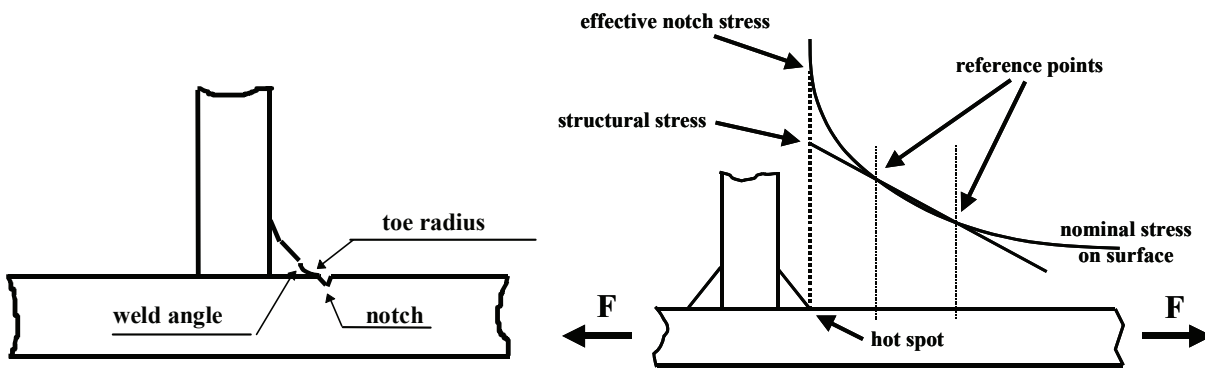


Figure 7.20 - Hot spot and notch stress in a welded joint

7.3.2.1.2.2 Calculation of the structural hot spot stress

The hot spot is defined as an area of the structure where a stress concentration is observed and where the stress field gradient is important. The hot spot is the critical location at a weld toe or at a discontinuity where a fatigue crack can be expected to initiate. Hot spots can be classified into two types, "a" and "b" as shown in Figure 7.21.

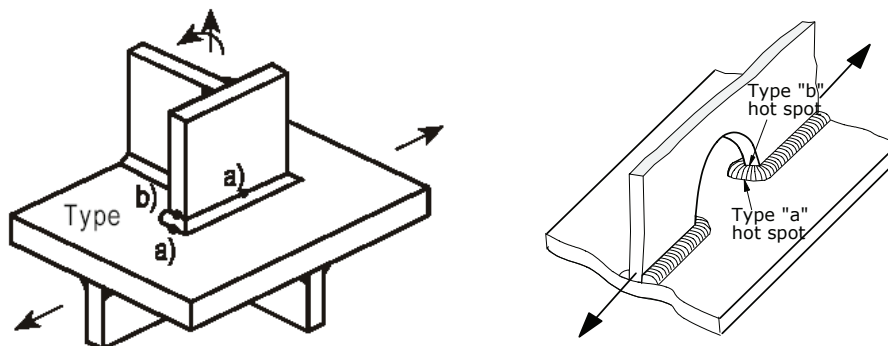


Figure 7.21 - Hot spot types

For the hot spot type "a", the weld is located on a plate surface and for the hot spot type "b", the weld is located on a plate edge. The hot spot stress for fatigue calculation is an extrapolated value following the standard method as illustrated on Figure 7.20. For non welded areas, the hot spot stress range is simply the range of the structural stress at the hot spot. For a plate, the structural stress, S_s , is the sum of membrane stress, S_m , and shell bending stress, S_b , on the surface of the plate, as shown in Figure 7.22.

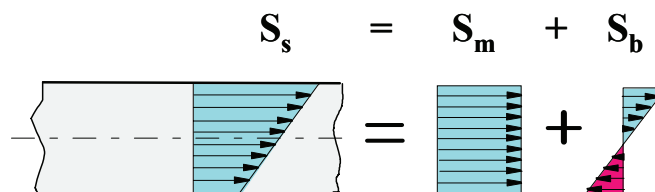


Figure 7.22 - Structural stress for a plate subject to membrane and bending loads

In the design phase, finite element analysis (FEA) is an ideal tool for determining the structural hot-spot stress. It is also useful in production of stress concentration factor formulae for various types of structural detail. Analysis of large structures with several potential hot-spots can be performed in two phases. First, a coarse model is solved in order to identify the hot-spot areas. Second, sub-models are created from these areas one at a time, using the nodal displacements or nodal forces from the original model as loading at the boundaries of the submodel. Another possibility is to refine the original element mesh in the hot-spot regions. Care is needed to avoid misinterpreting the finite element results. In general, post-processor programs do not show valid structural stress results at the weld toe directly. Therefore, in this method, extrapolation techniques are used. The stresses are obtained at the integration points of adjacent elements, or at the nodal points some distance away from the weld toe. The element mesh must be refined near the hot-spot such that the stress, and the stress gradient, can be determined accurately.

For welded joints, when the stress gradient is not too high, the hot spot stress or structural stress can be defined by a fine mesh modelling and a linear extrapolation to the weld toe from the computed stress values at two reference points located at 0.4t and 1.0t from the weld toe as shown in Figure 7.20 as recommended by the IIW [7.2]. In such cases, the hot spot stress coefficient factor is given by:

$$SCF_{HS} = \frac{1.67S_{0.4t} - 0.67S_{1.0t}}{S_{nom}} \quad (7.14)$$

When the stress gradient is high, the hot spot stress or structural stress can be defined from three reference points located at 0.4t, 0.9t and 1.4t from the weld toe and a parabolic extrapolation [7.2]. The formula for SCF_{HS} therefore becomes:

$$SCF_{HS} = \frac{2.52 S_{0.4t} - 2.24 S_{0.9t} + 0.72 S_{1.4t}}{S_{nom}} \quad (7.15)$$

When the hot spot is on a non-welded edge, the hot spot stress or structural stress can be better defined from a fine mesh modelling and thrust elements on the free edge. So the hot spot stress is directly given by the stress as shown in Figure 7.23.

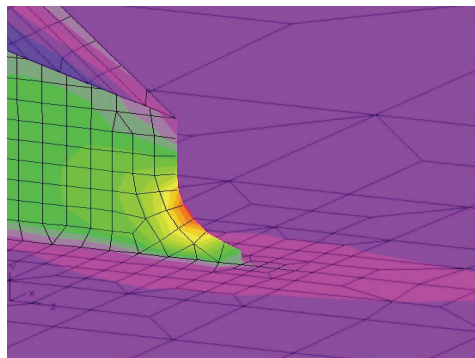


Figure 7.23 - Hot spot at the end of a bracket

The definition of the hot spot stress at a weld toe is not yet totally standardised and other definitions and formulae can be found in existing standards. When the structure is subject to certification or classification the calculation method should conform to the corresponding rules and regulations.

7.3.2.1.2.3 Calculation of effective notch stress

a) Direct approach

The effective notch stress is the total stress at the root of a notch, obtained assuming linear-elastic material behaviour. To take into account the statistical nature and scatter of weld shape parameters, as well as of non-linear material behaviour at the notch root, the real weld contour is replaced by an effective one. For structural steels and aluminium an effective notch root radius of $r=1$ mm has been shown to give consistent results (Figure

7.24). For fatigue assessment, the effective notch stress is compared with common fatigue resistance curves. This approach is restricted to welded joints which are expected to fail from the weld toe or weld root only. Also it is not applicable to cases where significant stress components exist parallel to the weld or parallel to the root gap. It is limited to section thickness values $t \geq 5$ mm.

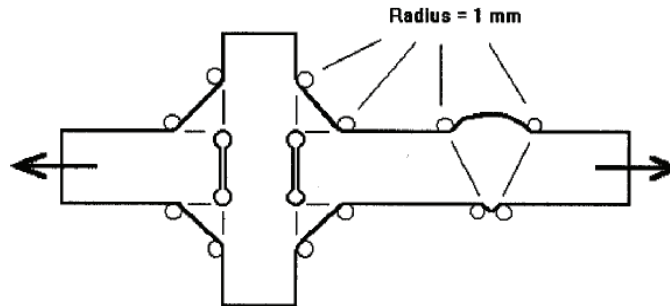


Figure 7.24 - Possible effective notch stress locations

b) Analytical approach

At the weld toe, as shown in Figure 7.20, the hot spot stress does not represent the real stress level at the point where the fatigue crack will initiate, i.e. the root of the notch.

The notch stress can be determined from the hot spot stress by:

$$S_{\text{notch}} = SCF_{\text{notch}} \cdot S_{\text{HS}} \quad \text{with} \quad SCF_{\text{notch}} = f(\lambda, \theta, r) \quad (7.16)$$

where:

- λ coefficient depending on the weld configuration and post weld treatment
- θ mean weld toe angle
- r weld toe radius

In the case of ship building applications the value of $f(\lambda, \theta, r)$ is given as:

$$SCF_{\text{notch}} = \lambda \sqrt{\frac{\theta}{30}} \quad (7.17)$$

where θ is not less than 30° and if not specified is set equal to 30° for butt welds or 45° for fillet weld or cruciform joints. Values of λ are given in Table 7.4.

For non-welded areas, such as a plate edge, there is no notch and the only stress to be considered is the hot spot stress ($SCF_{\text{notch}} = 1$).

Table 7.4 – Parameters used to define the notch stress concentration factor (ship building applications)

Type	Weld configuration		Coefficient λ	
	Description	Stress direction	As welded	Ground
Butt weld		Parallel	2.10	1.85
		Perpendicular	2.40	2.10
Fillet weld	Continuous	Parallel	1.80	1.60
		Perpendicular	2.15	1.90
	Well contoured end	Perpendicular	2.15	1.90
	Discontinuous	Parallel	2.90	2.55
	Overlapped	Perpendicular	4.50	3.95
Cruciform joint	Full/partial penetration Toe cracking	Perpendicular	2.10	1.85
	Partial penetration Root cracking	Perpendicular	4.5	not applicable

7.3.2.1.3 Step 3: Environmental issues

See Section 7.2.2.

7.3.2.1.4 Step 4: Thresholds for fatigue assessment

See section 7.2.3.


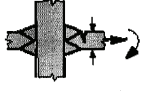
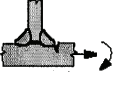
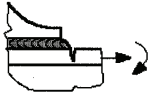

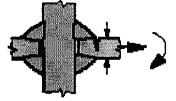
7.3.2.1.5 Step 5: Fatigue Data Specifications

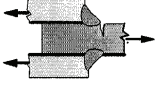
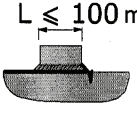
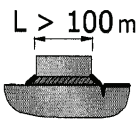
Before defining the relevant S-N curves, it must be noted that: a) The design value of the structural hot spot stress $\Delta\sigma_{HS}$ or the effective notch stress $\Delta\sigma_{notch}$ must be smaller than $2\cdot\sigma_y$, and b) root failure is outside the scope of this Route. In such cases, Route 1 or Route 4 should be applied.

7.3.2.1.5.1 S-N curves for the structural hot spot stress approach

The S-N curves for fatigue resistance with respect to the structural hot spot stress $\Delta\sigma_{HS}$ are defined in Table 7.5 for steel and aluminium, in relation to the FAT class i.e. the S-N curve stress range at $2\cdot 10^6$ cycles. The resistance values taken from these curves refer to the as-welded condition unless stated otherwise. The effects of welding residual stress are included. When the structure is subjected to certification or classification, the S-N curves must conform with the relevant rules and regulations.

Table 7.5 - Fatigue resistance against structural hot spot stress range

No	Structural detail	Description	Requirements	FAT Steel	FAT Alu.
1		Butt joint	As welded, NDT	100	40
2		Cruciform or T-joint with full penetration K-butt welds	K-butt welds, no lamellar tearing	100	40
3		Non load-carrying fillet welds	Transverse non-load carrying attachment, not thicker than main plate, as welded	100	40
4		Bracket ends, ends of longitudinal stiffeners	Fillet welds welded around or not, as welded	100	40
5		Cover plate ends and similar joints	As welded	100	40
6		Cruciform joints with load-carrying fillet welds	Fillet welds, as welded	90	36

No	Structural detail	Description	Requirements	FAT Steel	FAT Alu.
7		Lap joint with load carrying fillet welds	Fillet welds, as welded	90	36
8		Type "b" joint with short attachment	Fillet or full penetration weld, as welded	100	40
9		Type "b" joint with long attachment	Fillet or full penetration weld, as welded	90	36

7.3.2.1.5.2 Effective notch stress

a) Direct calculation

The S-N curves for fatigue resistance against effective notch stress $\Delta\sigma_{\text{notch}}$ are specified for steel and aluminium in Table 7.6 in relation to the FAT class i.e. the S-N curve stress range at $2 \cdot 10^6$ cycles.

Table 7.6 - Fatigue resistance against notch stress range

Material	Quality of weld notch	Description	FAT
Steel:	Effective notch radius equalling 1mm replacing the weld toe and weld root notch	Notch as-welded, normal welding quality m=3	225
Aluminium	Effective notch radius equalling 1mm replacing weld toe and weld root notch	Notch as-welded, normal welding quality m=3	75

b) Analytical calculation:

When the effective notch stress range has been determined by the analytical method, the S-N curve to be used is given by the equation:

$$\left((\Delta\sigma_{notch})^m \right) N = C \tag{7.18}$$

where the mean curve is given by m=3 and C=3.913 10¹³ and the standard deviation of log(C) is 0.1821. This curve is a fictitious base material S-N curve, taking into account the notch effect (m=3), derived from flame cut and machined butt weld sample results and adjusted by theoretical considerations and practical experience.

7.3.2.1.6 Step 6: Fatigue assessment using S-N Curves

Requirements for fatigue assessment using linear damage accumulation are provided in section **Fehler!**
Verweisquelle konnte nicht gefunden werden..

7.3.2.2 Route 2 for Non-Welded Parts

The procedure for applying Route 2 to non-welded parts is shown in Figure 7.25.

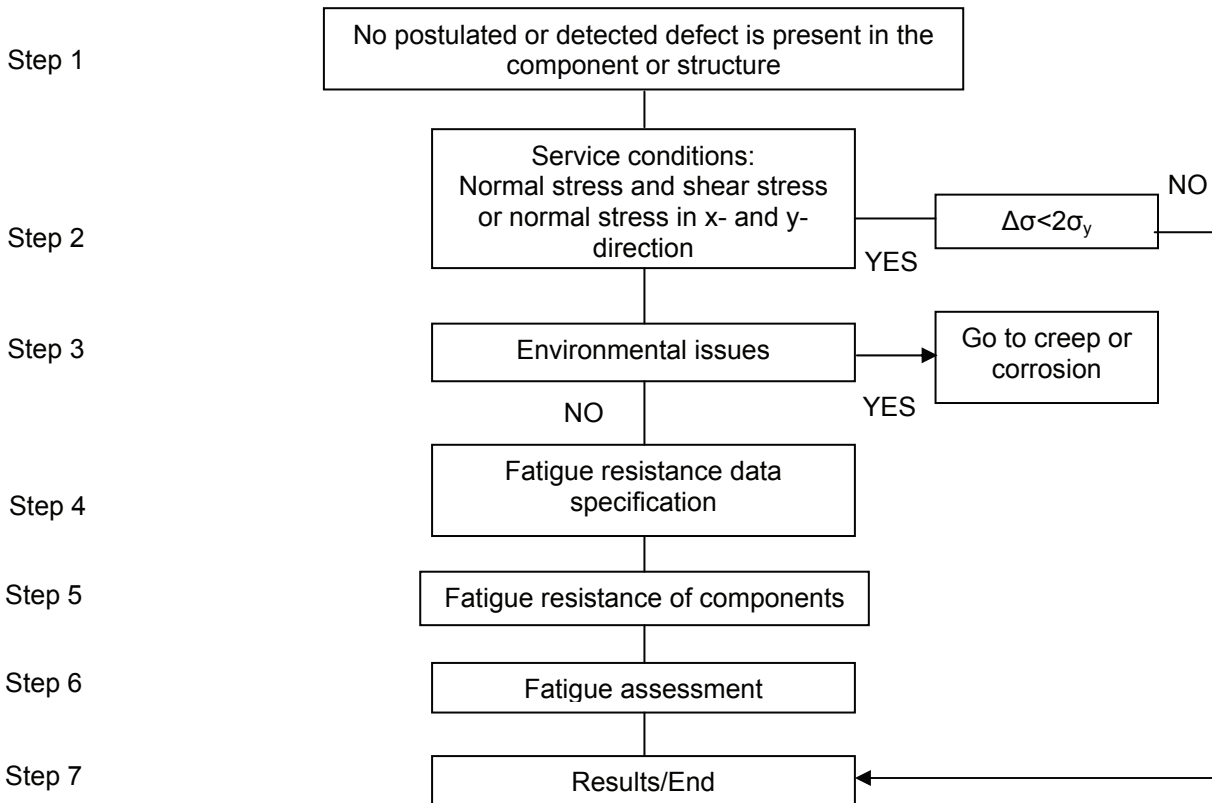


Figure 7.25 – Route 2 for non-welded applications

7.3.2.2.1 Step 1: No Postulated or Detected Flaw is Present in the Component or Structure

Route 2 assumes that no flaw is postulated or is detected by NDE in the component which is assessed in fatigue. This procedure has to be applied to all potential points of failure. These may be defined by relevant codes and standards, the design procedure or practical experience. The fatigue assessment is based on linear fatigue damage analysis. Annex D provides guidance on NDE techniques and capabilities.

7.3.2.2.2 Step 2: Service Conditions

To apply this procedure the stresses resulting from the service loadings have to be determined for each so-called reference point, that is a potential point of fatigue crack initiation on the section or component under consideration. In case of doubt, several reference points are to be considered. If several stress components act simultaneously at the reference point they are to be overlaid. For the same type of stress (for example unidirectional normal stresses) the superposition of contributions from several loading sequences is to be carried out at this stage, so that in the following a single stress sequence exists for each type of stress ($\sigma_x, \sigma_y, \tau_{xy}$ and so on). For different types of stress (normal stress and shear stress or normal stress in x- and y-direction) the superposition to arrive at their combined effect on the fatigue strength is to be carried out at the assessment stage. As a result, the histograms of local stress components are obtained according to the theory of elasticity.

7.3.2.2.3 Step 3: Issues, Corrosion and High Temperatures

The limits for applying this procedure are given as follows:

- for fine grain structural steel from -40°C to 60°C ,
- for other kinds of steel from -40°C to $+100^\circ\text{C}$,
- for cast iron materials from -25°C to $+100^\circ\text{C}$,
- for age-hardening aluminium alloys from -25°C to 50°C ,
- for non-age-hardening aluminium alloys from -25°C to 100°C

For low and elevated temperatures, and for the case of superimposed corrosion, see Section 7.2.2.

7.3.2.2.4 Step 4: Thresholds for Fatigue Assessment

See section 7.2.3.

7.3.2.2.5 Step 5: Fatigue Resistance Data

The constant amplitude resistance curves in terms of amplitudes of local elastic stresses, σ_a , are given as specified in Figure 7.26. The knee point of all resistance curves is fixed at 10^6 cycles to failure. The amplitudes at the knee point are termed σ_{AK} and τ_{AK} for normal and shear stresses, respectively. For a number of cycles to failure smaller than 10^6 , the slope is given as $k_{D,\sigma}=5$ for normal and $k_{D,\tau}=8$ for shear stresses, respectively. Two models for describing the resistance curves for a number of cycles to failure larger than 10^6 are specified:

- For steel and cast iron material, except austenitic steel, model I applies: A horizontal resistance curve is defined.
- For aluminium alloys, austenitic steel and other metallic materials, model II applies: The slopes are defined as $k_{D,\sigma}=15$ for normal and $k_{D,\tau}=25$ for shear stresses, respectively. For a number of cycles to failure larger than 10^8 , a horizontal resistance curve is defined.

The constant amplitude resistance curves are completely determined as soon as the values for σ_{AK} and τ_{AK} are specified. The characteristic values for σ_{AK} and τ_{AK} are to be calculated using the fatigue limit of the material for completely reversed (no mean stress, $R=-1$) normal stress, σ_W , and shear stress, τ_W . The following influencing factors are taken into account:

- the size (scale) effect

- geometrical discontinuities of the component (notch effect)
- surface roughness (surface effect)
- mean stress

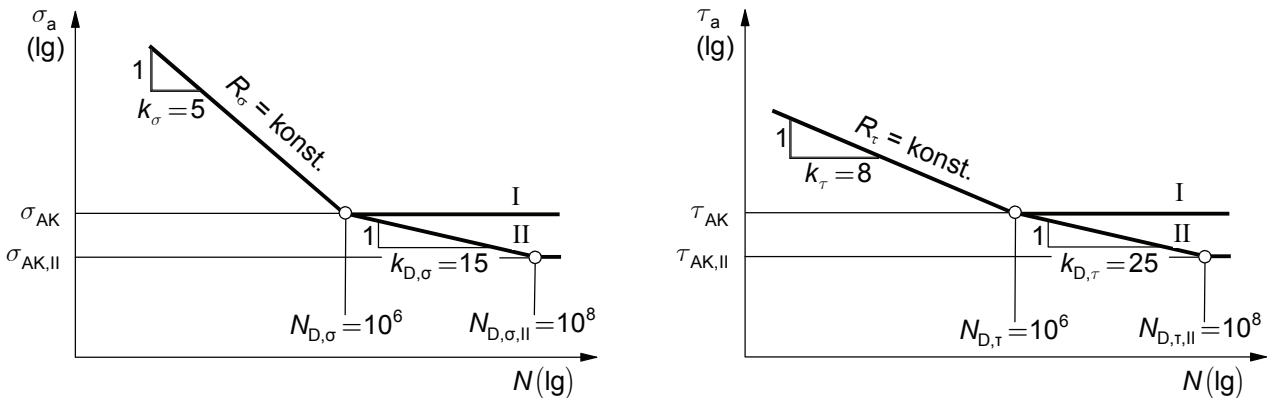


Figure 7.26 - Component S-N curves for constant amplitude loads.

The fatigue limit of the material, σ_W , and τ_W , is to be taken either from the material data base (see Annex L) or from an estimate based on the ultimate tensile strength R_m according to the following equations

$$\begin{aligned} \sigma_W &= f_{W,\sigma} \cdot R_m \\ \tau_W &= f_{W,\tau} \cdot \sigma_W \end{aligned} \tag{7.19}$$

The fatigue strength factors $f_{W,\sigma}$ and $f_{W,\tau}$ are given in Table 7.7.

Table 7.7 - Fatigue strength factors, $f_{W,\sigma}$ and $f_{W,\tau}$

Types of material	$f_{W,\sigma}$	$f_{W,\tau}$
Case hardening steel	0.40	0.577
Stainless steel	0.40	0.577
Forging steel	0.40	0.577
Cast steel	0.34	0.577
Steel other than the above	0.45	0.577
Nodular cast iron	0.34	0.65
Malleable cast iron	0.30	0.75
Grey cast iron	0.30	0.85
Wrought aluminium alloys	0.30	0.577
Cast aluminium alloys	0.30	0.75

a) Size factor K_d

The size factor accounts for the decrease of the material fatigue strength values that is usually observed with increasing dimensions of the component. It is specified as a function of the effective diameter. For components

with a simple cross section, the effective diameter is given according to the cross section. In general, the upper limit of the effective diameter is specified in the material standards. For the determination of the effective diameter d_{eff} two cases can be distinguished, depending on the type of material.

- Case 1: Components (including forgings) made of heat treatable steel, of case hardening steel, of nitriding steel, both nitrided or quenched and tempered, of heat treatable cast steel of GGG, GT or GG. In general: $d_{\text{eff}} = 4 \times V/A$, with V and A as volume and surface area of the section of the component considered.
- Case 2: Components (including forgings) made of non-alloyed structural steel, of fine grained structural steel, of normalized quenched and tempered steel, of cast steel, or of aluminium materials: The effective diameter d_{eff} is equal to the diameter or wall thickness of the component.

The effective diameter is the diameter existing while the heat treatment is performed.

In case of machining subsequent to the heat treatment the effective diameter d_{eff} is the largest diameter of the rod. In case of machining prior to the heat treatment the effective diameter d_{eff} according to the first sequence of machining is an estimate on the safe side.

The dependency of the size factor, K_d , on the effective diameter is specified as:

- For grey cast iron:

$$K_d = \begin{cases} 1.207 & \text{for } d_{\text{eff}} \leq 7.5 \text{ mm} \\ 1.207 \cdot \left(\frac{d_{\text{eff}}}{7.5 \text{ mm}} \right)^{-0.1922} & \text{for } d_{\text{eff}} > 7.5 \text{ mm} \end{cases} \quad (7.20)$$

- For stainless steel within the dimensions given in material standards:

$$K_d = 1 \quad (7.21)$$

- For all other types of steel and cast iron materials the technological size factor is:

$$K_d = \begin{cases} 1 & \text{for } d_{\text{eff}} \leq d_{\text{eff,min}} \\ \frac{1 - 0,7686 \cdot a_d \cdot \lg(d_{\text{eff}} / 7.5 \text{ mm})}{1 - 0,7686 \cdot a_d \cdot \lg(d_{\text{eff,min}} / 7.5 \text{ mm})} & \text{for } d_{\text{eff,min}} < d_{\text{eff}} \leq d_{\text{eff,max}} \\ \frac{1 - 0,7686 \cdot a_d \cdot \lg(d_{\text{eff,max}} / 7.5 \text{ mm})}{1 - 0,7686 \cdot a_d \cdot \lg(d_{\text{eff,min}} / 7.5 \text{ mm})} & \text{for } d_{\text{eff}} \geq d_{\text{eff,max}} \end{cases} \quad (7.22)$$

The constants a_d and $d_{\text{eff,min}}$ are to be taken from Table 7.8.

- For wrought aluminium alloys the component values of the tensile strength, R_m , depend on the thickness or diameter of the semi-finished product. The size factor $K_d = 1$ applies to these cases.
- For cast aluminium alloys the size factors are as follows:

$$K_d = \begin{cases} 1 & \text{for } d_{\text{eff}} \leq 12\text{mm} \\ 1.1 \cdot (d_{\text{eff}} / 7,5\text{mm})^{-0.2} & \text{for } 12\text{mm} < d_{\text{eff}} \leq 150\text{mm} \\ 0.6 & \text{for } d_{\text{eff}} \geq 150\text{mm} \end{cases} \quad (7.23)$$

Table 7.8 - Constants a_d and $d_{\text{eff,min}}$

Type of material	$d_{\text{eff,min}}$ in mm	a_d
Non-alloyed structural steel	40	0.15
Fine grain structural steel	70	0.2
Fine grain structural steel	100	0.25
Heat treatable steel, Q&T	16	0.3
Heat treatable steel, n	16	0.1
Case hardening steel, bh	16	0.5
Nitriding steel, Q&T	40	0.25
Steel for large forgings, Q&T	250	0.2
Steel for large forgings	250	0
Cast steel	100	0.15
Heat treatable steel casting	300	0.15
Heat treatable steel casting Q&T, types 1, 3, 4	100	0.3
as above, type 2	200	0.15
as above, types 5, 6, 8	200	0.15
as above, types 7, 9	500	0.15
Nodular cast iron	60	0.15
Malleable cast iron	15	0.15

b) Notch effect support factors n_σ and n_τ

To take into account a component's shape and the dimensions, a normalised stress gradient χ has to be determined. Values of c are determined from the stress amplitudes for normal stress σ_a and for shear stress, τ_a , at the reference point. The direction X is to be chosen in such a way that maximum values of χ are calculated.

$$\chi_\sigma = - \left. \frac{d\sigma_a}{dx} \right|_{x=0} \cdot \frac{1}{\sigma_{a,(x=0)}} \quad (7.24)$$

$$\chi_\tau = - \left. \frac{d\tau_a}{dx} \right|_{x=0} \cdot \frac{1}{\tau_{a,x=0}} \quad (7.25)$$

The support factor for normal stress, n_σ , is computed from χ_σ :

$$n_{\sigma} = \begin{cases} 1 + \chi_{\sigma} \cdot \text{mm} \cdot 10^{-\left(a_G - 0.5 + \frac{R_m}{b_G \cdot \text{MPa}}\right)} & \text{for } \chi_{\sigma} < 0.1 \text{mm}^{-1} \\ 1 + \chi_{\sigma} \cdot \text{mm} \cdot 10^{-\left(a_G + \frac{R_m}{b_G \cdot \text{MPa}}\right)} & \text{for } 0.1 \text{mm}^{-1} < \chi_{\sigma} < 1 \text{mm}^{-1} \\ 1 + 4\sqrt{\chi_{\sigma} \cdot \text{mm}} \cdot 10^{-\left(a_G + \frac{R_m}{b_G \cdot \text{MPa}}\right)} & \text{for } \chi_{\sigma} > 1 \text{mm}^{-1} \end{cases} \quad (7.26)$$

with constants a_G and b_G according to Table 7.9.

Table 7.9 - Constants a_G and b_G

Material	Stainless steel	Other steels	Cast Steel	Nodular cast iron	Malleable cast iron	Grey cast iron	Wrought aluminium alloys	Cast aluminium alloys
a_G	0.40	0.50	0.25	0.05	-0.05	-0.05	0.05	-0.05
b_G	2400	2700	2000	3200	3200	3200	850	3200

The support factor for shear stress, n_{τ} , is computed from the normalised stress gradient χ_{τ} according to Eq.7.26, after having replaced σ by τ and the tensile strength R_m by $(f_{W,\tau} \cdot R_m)$, where $f_{W,\tau}$ is taken from Table 7.7.

c) Surface roughness factor K_S

The endurance limit of the base material is measured using test pieces which have been fully polished and it is therefore necessary to consider a reduction in endurance by using a coefficient K_S which is a function of the ultimate tensile strength of the material and its surface roughness. For the latter the parameter R_Z is used, which is the average roughness of the surface of the component in μm , according to DIN 4768 [7.8]. Normal stress and shear stress related roughness factors are distinguished, $K_{S,\sigma}$ and $K_{S,\tau}$,

$$\begin{aligned} K_{S,\sigma} &= 1 - a_{R,\sigma} \cdot \lg(R_Z / \mu\text{m}) \cdot \lg(2R_m / R_{m,N,\min}) \\ K_{S,\tau} &= 1 - f_{W,\tau} \cdot a_{R,\sigma} \cdot \lg(R_Z / \mu\text{m}) \cdot \lg(2R_m / R_{m,N,\min}) \end{aligned} \quad (7.27)$$

where the constants $a_{R,\sigma}$ and $R_{m,N,\min}$ are as defined in Table 7.10.

Table 7.10 - Constant $a_{R,\sigma}$ and minimum tensile strength, $R_{m,N,\min}$

Material	Steel	Cast steel	Nodular cast iron	Malleable cast iron	Grey cast iron	Wrought aluminium alloys	Cast aluminium alloys
$a_{R,\sigma}$	0.22	0.20	0.16	0.12	0.06	0.22	0.20
$R_{m,N,\min}$ [MPa]	400	400	400	350	100	133	133

d) Combination of scale, notch and roughness effects

Combining these three influencing factors defines a constant amplitude fatigue limit relevant to the material at a given reference point of the component, σ_{WK} and τ_{WK} :

$$\sigma_{WK} = \sigma_W \cdot K_d \cdot n_\sigma \cdot K_{S,\sigma} \tag{7.28}$$

$$\tau_{WK} = \tau_W \cdot K_d \cdot n_\tau \cdot K_{S,\tau} \tag{7.29}$$

For steel with high normalised stress gradients $\chi_\sigma > 1\text{mm}^{-1}$ a reduced surface roughness factor $K_{S,\sigma,\text{red}}$ may be applied according to:

$$K_{S,\sigma,\text{red}} = \frac{2}{1 + \frac{1}{K_{S,\sigma}}} \tag{7.30}$$

e) Mean stress effects

The mean stress effect for normal stresses can be evaluated using the Haigh diagram in Figure 7.27.

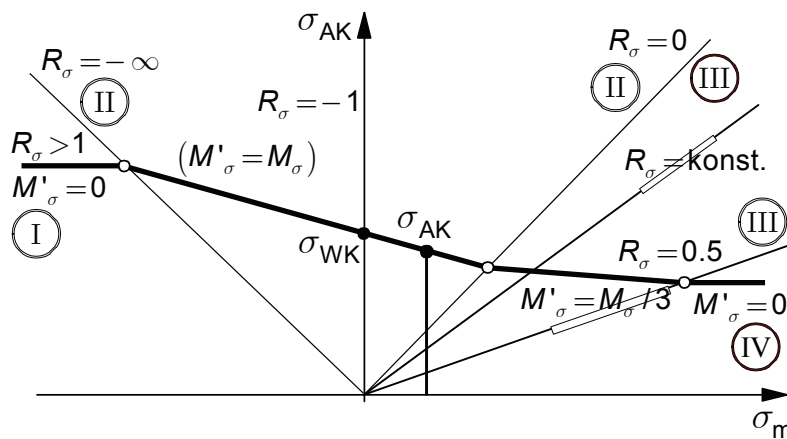


Figure 7.27 - Amplitude of the component fatigue strength as a function of mean stress or stress ratio (Haigh diagram) for four fields of mean stress

The mean stress sensitivity M_σ is the absolute value of the slope in field II of Figure 7.27 ($-\infty < R < 0$). It describes to what extent the mean stress affects the amplitude of the component fatigue strength. For shear stresses the line of the first quadrant in Figure 7.27 ($-1 < R < 0$) is mirrored to the second quadrant using the axis $\sigma_m = 0$ as the axis of symmetry. Values for M_σ and M_τ are given as

$$M_\sigma = a_M \cdot 10^{-3} \cdot R_m / \text{MPa} + b_M \tag{7.31}$$

$$M_\tau = f_{W,\tau} \cdot M_\sigma$$

with constants a_M and b_M according to Table 7.11.

The mean stress dependent amplitudes of the component fatigue limit for normal stress and for shear stress to be used for describing the resistance curve (Figure 7.26) can be calculated via:

$$\begin{aligned}\sigma_{AK} &= K_{AK,\sigma} \cdot \sigma_{WK} \\ \tau_{AK} &= K_{AK,\tau} \cdot \tau_{WK}\end{aligned}\quad (7.32)$$

with the mean stress factors $K_{AK,\sigma}$ and $K_{AK,\tau}$, which follow from the definitions in Figure 7.27.

Table 7.11 - Constants a_M and b_M used to account for mean stress effects.

Material	Steel	Cast steel	Nodular cast iron	Malleable cast iron	Grey cast iron	Wrought aluminium alloys	Cast aluminium alloys
a_M	0.35	0.35	0.35	0.35	0	1.0	1.0
b_M	-0.1	0.05	0.08	0.13	0.5	-0.04	0.2

7.3.2.2.6 Step 6: Fatigue Assessment using $\Delta\sigma_e$ - N Curves

Fatigue assessment specifications are provided in section 7.2.1.4. The results of such an assessment may be presented as

$$\begin{aligned}\sigma_{BK} &= K_{BK,\sigma} \cdot \sigma_{AK} \\ \tau_{BK} &= K_{BK,\tau} \cdot \tau_{AK}\end{aligned}\quad (7.33)$$

The amplitudes σ_{BK} and τ_{BK} are the component's variable amplitude fatigue strengths for normal stress and for shear stress. $K_{BK,\sigma}$ and $K_{BK,\tau}$ are the variable amplitude fatigue strength factors, as illustrated in Figure 7.28.

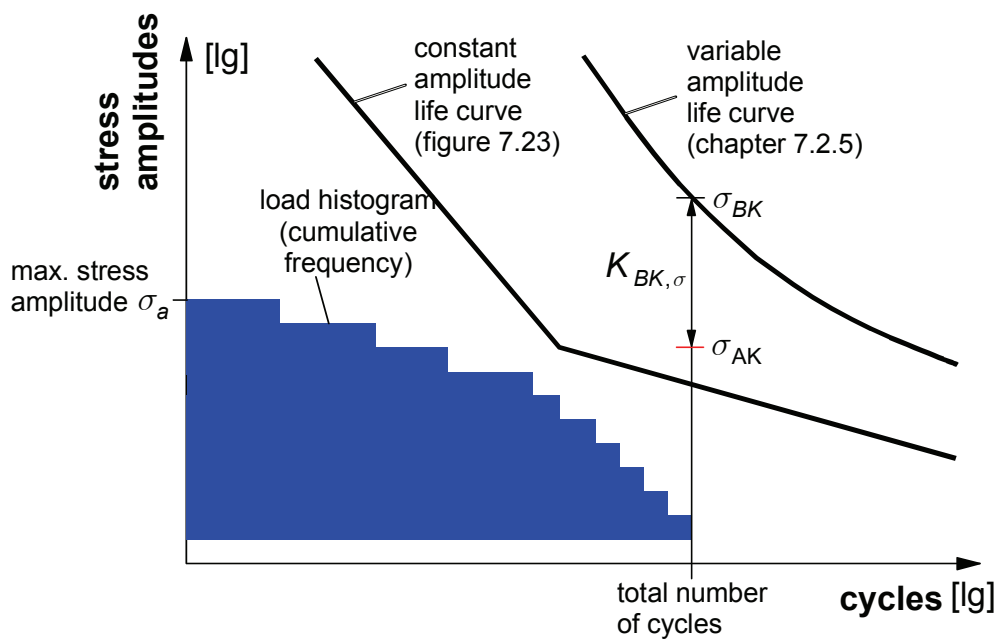


Figure 7.28 - Variable amplitude fatigue life curve, definition of factors $K_{BK,\sigma}$ and $K_{BK,\tau}$

The static strength of the component must not be exceeded at any time during fatigue loading.

The assessment is to be carried out by determining the degree of utilisation of the component fatigue strength. The degree of utilisation $a_{BK,\sigma}$ and $a_{BK,\tau}$ is the quotient of the local characteristic stress amplitude σ_a and τ_a (highest amplitudes in stress histogram) divided by the allowable local stress amplitude of the component fatigue strength at the total number of cycles during the life of the component (for the reference point under consideration) σ_{BK} and τ_{BK} , respectively, divided by the total safety factor γ .

$$a_{BK,\sigma} = \frac{\sigma_a}{\sigma_{BK} / \gamma} \leq 1$$

$$a_{BK,\tau} = \frac{\tau_a}{\tau_{BK} / \gamma} \leq 1 \tag{7.34}$$

The safety factor γ is determined in accordance with principles outlined in section 11.

Under the combined action of the different loadings and a multiaxial state of stress at the reference point, the degrees of utilisation are obtained for each of the stress components. These particular degrees of utilisation are added linearly to obtain the overall degree of utilisation which again must not reach or exceed the value of 1. In case of doubt an experimental assessment should be carried out. Additional information is provided in [7.9].

7.3.3 Route 3 - Fatigue Damage Assessment using Local Stress-Strain Approach

The flowchart for Route 3 is shown in Figure 7.29.

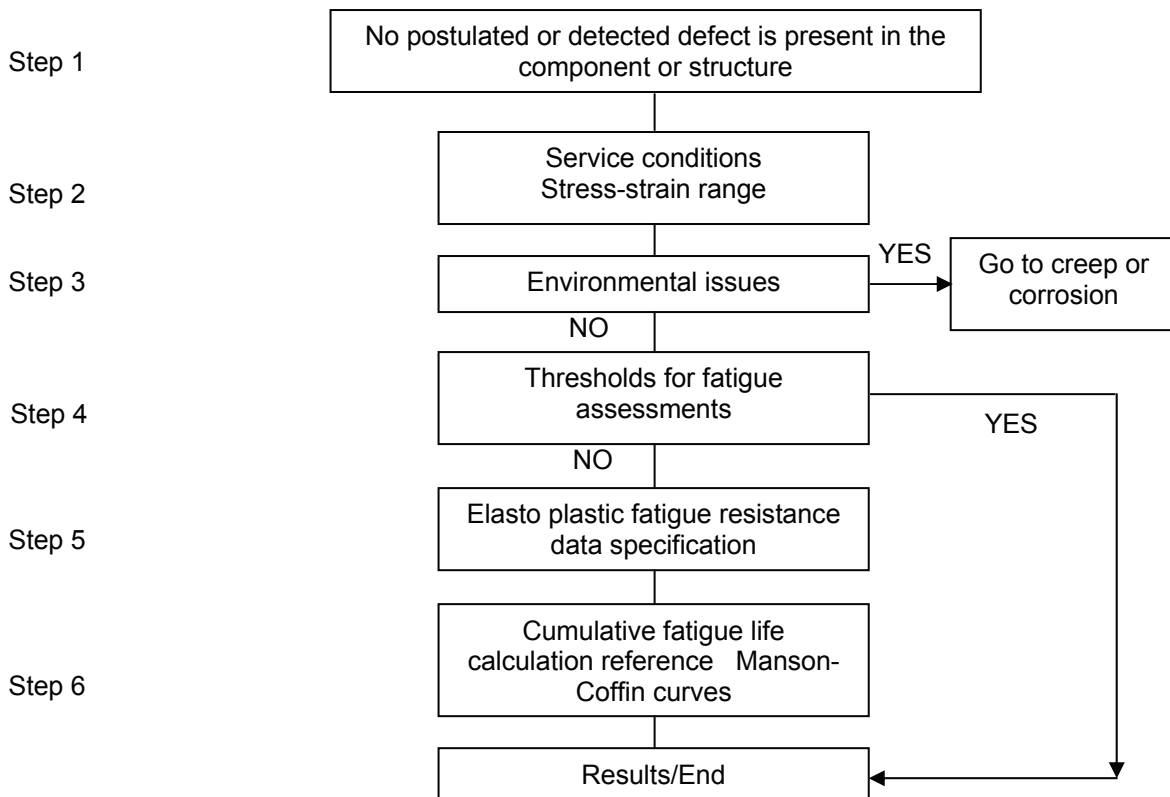


Figure 7.29 - Route 3 flowchart

7.3.3.1 Step 1: No Postulated or Detected Flaw is Present in the Component or Structure

Route 3 assumes that no flaw is postulated or is detected by NDE in the structure or component which is assessed in fatigue. Annex D provides guidance on NDE techniques and capabilities.

7.3.3.2 Step 2: Service Condition

The approach concerns fatigue life assessment made on the basis of the cyclic plastic strain at a high local stress concentration such as a groove or a notch, where the local surface roughness at the bottom of such features cannot be measured. For moderate local stress concentrations such as shaft shoulders and grooves with medium to large radii (for which the local surface roughness can be measured), Route 1 can be applied. These analyses can be performed cycle-by-cycle, allowing for non-linear damage accumulation effects if necessary.

7.3.3.2.1 Constant amplitude loading

When a notch exists, under cyclic loading, the stress concentration (characterised by the factor K_t) leads the material to exceed the yield strength (σ_y), as soon as $K_t \sigma_{nom} > \sigma_y$, when σ_{nom} represents the calculated nominal stress in the component section. It is then necessary to determine the local stress (σ_{loc}) and strain (ε_{loc}) state to calculate the notched component strength or life time correctly.

The unknown σ_{loc} and ε_{loc} values can be easily related to known parameters, σ_{nom} and K_t , using the Neuber rule [7.10]. This rule is expressed by the following relationship:

$$\sigma_{loc} \cdot \varepsilon_{loc} = \frac{K_t^2 \sigma_{nom}^2}{E} = \text{constant for a given loading} \quad (7.35)$$

The graphical representation of this rule is illustrated in Figure 7.30 where:

- point A represents the elastic stress state for a stress value equal to σ_{nom}
- point B represents the virtual elastic stress state for a stress $\sigma^* = K_t \cdot \sigma_{nom}$,
- point C represents the stabilised stress state at the notch tip for a cyclic loading of amplitude σ_{nom}

When the loading is purely alternate ($\sigma_{min} = -\sigma_{max}$), the method described is sufficient. When the loading is more complex, for example with a mean stress, the Neuber rule should be applied separately to the maximum and minimum loads (curves B and B' of Figure 7.30).

7.3.3.2.2 Variable amplitude loading

When the loading is of variable amplitude, the Neuber rule has to be applied cycle by cycle to determine for each extreme (i) the stress and strain deformation state σ_i and ε_i , as described in 7.3.3.2.1.

Other analytic approaches are available to determine the local stress and strain state, such the Glinka [7.11] method, which is similar to Neuber's rule. For components which are analysed with finite elements, the cyclic hardening curve can be used directly for elasto-plastic modelling. The stationary method [7.12] provides an efficient means of performing such analyses.

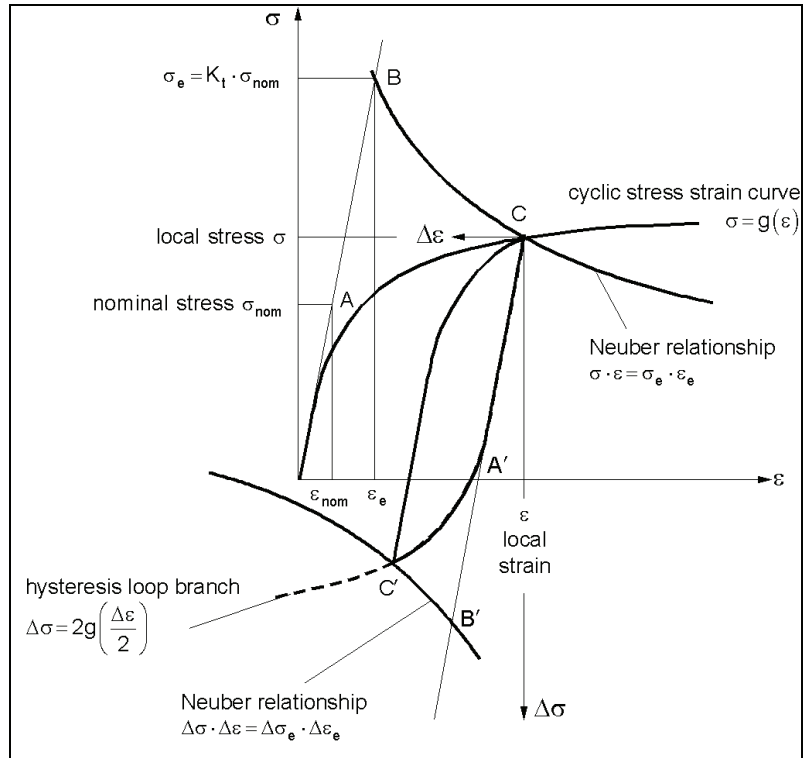


Figure 7.30 - Graphical representation of the Neuber rule

7.3.3.3 Step 3: Environmental issues chapter

See section 7.2.2.

7.3.3.4 Step 4: Thresholds for fatigue assessment

See section 7.2.3.

7.3.3.5 Step 5: Fatigue resistance data for elasto-plastic loading

7.3.3.5.1 Material elasto-plastic behaviour

The local elasto-plastic approach, detailed in [7.13], has been developed from the observation that the majority of cracks initiate at a geometric discontinuity (notch, groove, slot, fillet, hole) and that the material local stress at this point exceeds the yield strength at each cycle or during the initial cycles before shaking down to elastic behaviour. In such cases it is necessary to take into account cyclic plastic deformation and to determine the resulting local stresses and strains. A further consideration is that the material behaviour may change over time due to cyclic deformation at the notch tip, by becoming more resistant (hardening) or less resistant (softening). To model the cyclic material behaviour at the notch tip, the following hardening law can be used:

$$\epsilon_a = \frac{\sigma_a}{E} + \left(\frac{\sigma_a}{K'} \right)^{1/n'} \tag{7.36}$$

where:

- ε_a : total strain amplitude = ε_a elastic + ε_a plastic
- K' : plastic strength coefficient
- n' : cyclic hardening exponent
- E : Young modulus

σ_a : measured stress amplitude for sample mid life time submitted to the total deformation ε_a

These parameters can be calibrated from appropriate tests e.g. following the NF A03-403 standard.

When a material is submitted to cyclic plastic deformation, the life time N (cycles) is given by the Manson-Coffin curve equation:

$$\varepsilon_a = \varepsilon_e + \varepsilon_p = \frac{\sigma_f'}{E} (2N)^b + \varepsilon_f' (2N)^c \quad (7.37)$$

where

ε_f' : fatigue ductility coefficient

σ_f' : fatigue strength coefficient

b, c : material constants

E : Young modulus

7.3.3.6 Step 5: Cumulative Fatigue life calculation

When the local stress state σ_{loc} and ε_{loc} is known, the component life time can be determined applying the classical Palmgren-Miner damage accumulation rule (see paragraph 7.2.1.4), with a mean stress Goodman correction when the material is "adapted" at the notch tip (elastic behaviour after the first applied elasto-plastic cycles), a mean stress Morrow or Smith-Watson-Topper (SWT) [7.14] correction when the material is "accommodated" at the notch end (closed elasto-plastic loop in a stress-stain plot). The life time calculation procedure is represented in Figure 7.31. For constant amplitude loading, the cycle counting step is not necessary. For variable amplitude loading it is necessary to apply to the local stress distribution obtained via the Neuber rule and a cycle counting method (peak or rainflow counting method).

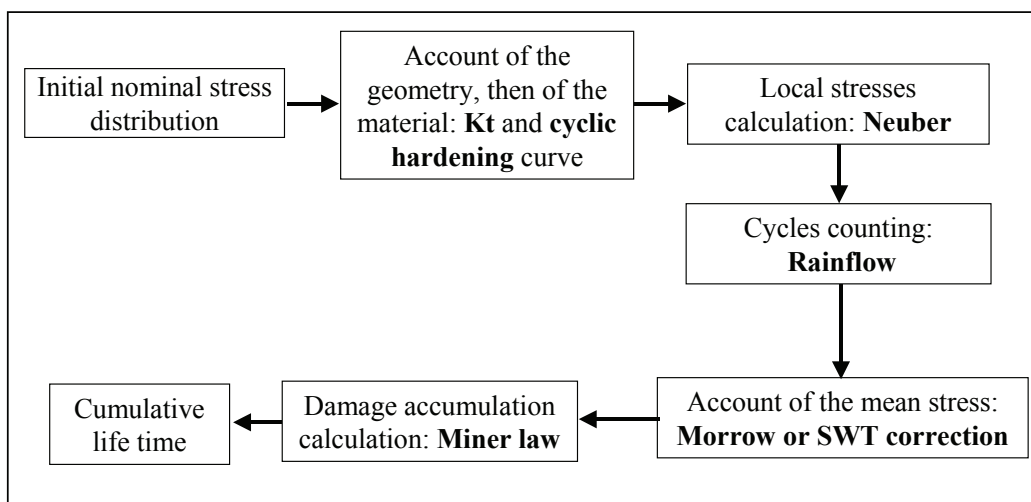


Figure 7.31 - Notched component life time calculation procedure

7.3.4 Route 4 - Fatigue Crack Growth Assessment

This section sets out the procedure for assessing the growth of planar flaws under fluctuating loading (Route 4). It is based on a fracture mechanics analysis, which assumes that a flaw may be idealized as a sharp tipped crack which propagates in accordance with the law relating the crack growth rate, da/dN , and the range of stress intensity factor, ΔK , for the material containing the flaw. The basic steps of the procedure are shown in the flowchart in Figure 7.32. Details of the implementation are given in the subsections below.

Some restrictions on the use of this procedure are as follows: a) it is not appropriate for assessment of short cracks (for many engineering applications a crack is considered short when $a < 1$ mm); guidance on evaluating short cracks is given in section 0.; b) caution is required in applying the approach in the low cycle fatigue range if plastic strain is non-negligible at the location of interest; c) the approach is not valid in the compression-compression range.

7.3.4.1 Step 1: Detected or Postulated Planar Flaw

The flaw type, position and size should be identified. For flaws found in service, this process may require the advice of materials and non-destructive testing experts, particularly for the case of flaws in welds. The flaw detected should be characterised by a suitable bounding profile amenable to analysis. Flaws which are not of simple Mode I type should be resolved into Mode I orientation. Note that it may also be possible later to re-characterise a flaw in the case that the initial assessment leads to an unacceptable result. Advice on flaw characterisation is contained in Annexes D and E.

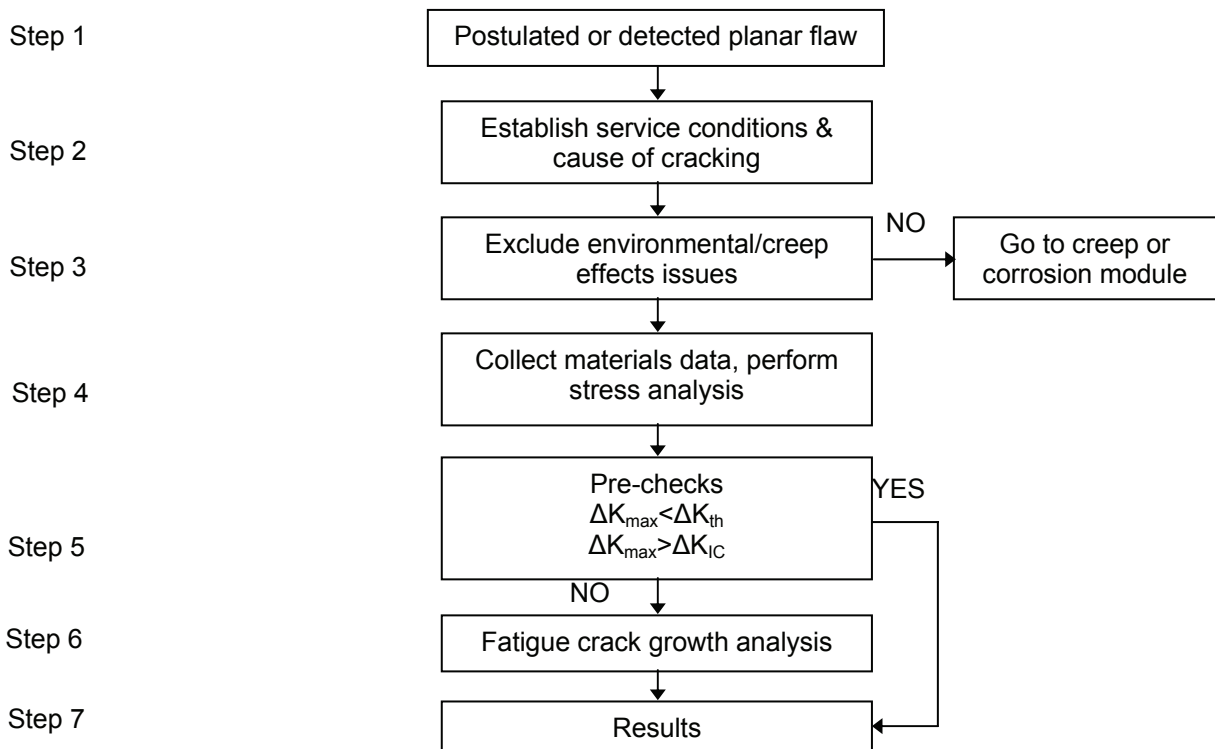


Figure 7.32 - Flowchart for the fatigue crack growth assessment (Route 4)

7.3.4.2 Step 2: Establish Service Conditions and Cause of Cracking

The service life to date and the desired future service life should be defined. For the case of a component that was known to be flaw free at the start of operation, an estimate of the time at which the flaw formed should also be determined. The cause of the cracking should be established to ensure that the fatigue crack growth procedure is applicable.

7.3.4.3 Step 3: Exclude Environmental or Creep Effects

If the flaw is characterised as surface breaking, the effects of the environment on the fracture and fatigue properties should be considered. This requires it to be demonstrated that the environment in question does not influence these properties, or that any effects are accounted for in the materials data used in the analysis. For further guidance the user is referred to the corrosion module (Section 9).

If the temperature in the vicinity of the flaw during operation exceeds $0.4T_m$, where T_m is the melting point of the material in degree Kelvin, time-dependent effects may need to be considered and the user is referred to the creep module (Section 8).

7.3.4.4 Step 4: Collect Materials Data and Perform Stress Analysis

The materials relevant to the feature to be assessed should be defined, including, in the case of weldments, the weld metal and heat-affected zone structures. The material properties data required to follow the steps in the procedure are:

- a) elastic modulus, Poisson ratio and relevant physical constants.
- b) tensile properties (yield strength, ultimate tensile strength and cyclic stress-strain curve, if required)
- c) fracture toughness
- d) constants for the Paris or Forman-Mettu fatigue crack growth laws
- e) fatigue stress intensity threshold

Guidance on obtaining these data is given in Annex N. They should be appropriate to the type of assessment to be performed, the temperature range and the environment. The data should relate to the correct cyclically-conditioned state and the effects of thermal ageing may also need to be considered. Some of these factors may be inter-related, and it is necessary to use consistent material properties data in different steps of the procedure.

Elastic stress analyses of the uncracked feature should be performed for the extremes of the service load cycles identified under Step 2, assuming homogeneous properties. A shakedown assessment of the uncracked feature should then be performed. It should be determined that the feature satisfies strict or global shakedown. If shakedown cannot be demonstrated, it may be necessary to employ inelastic analysis methods. If shakedown is demonstrated, the crack depth should be such that the compliance of the structure is not significantly affected. It is necessary to resolve the load history into cycle types and frequencies of occurrence suitable for analysis. This includes both historical operation and the assumed future service conditions. Advice is contained in section 7.2.1.1. For random loading, unless the order of application of cycles is known, cycles or blocks of cycles should be assumed to occur in the most damaging order. This is not always clear and it may be necessary to perform several calculations to determine the worst case.

The stress intensity factor range should be calculated from the values of the linear elastic stress intensity factor, K , over the loading cycle and which depends on the loading and the crack size and may vary with position around a crack front. Stress intensity factor solutions are provided in Annex A. Alternatively, published solutions, numerical analysis methods or weight function techniques may be used, but the basis of the method and the results should be documented. For partial-thickness surface or embedded flaws, ΔK should be determined at the ends of both the minor and major axes of the elliptical idealization of the flaw. It is also necessary to evaluate the ratio of minimum to maximum stress intensity factor, R . The value of R should be calculated from the shakedown analysis rather than the simple elastic analysis. The shakedown analysis affects only the value of R and not the total stress intensity factor range, as the residual stress is independent of position in the cycle.

7.3.4.5 Step 5: Pre-Checks

Before proceeding with the fatigue crack growth calculation two pre-checks are foreseen:

- (a) Stability of the flaw at the maximum cyclic load

The component should be assessed against fracture initiation under fault or overload conditions at the initial flaw size using the fracture part of this procedure (see section 6). This assessment should use the initial values of any residual stresses, not those in the shakedown state. If failure is conceded at this stage, the assumptions in the analysis should be revisited or remedial action taken. Only if sufficient margins can be justified is it permissible to continue to Step 6 to justify future service life under the fatigue loads.

(b) Stress intensity threshold for crack growth

If the maximum value of ΔK is less than the threshold stress intensity ΔK_0 , the crack growth da/dN is assumed to be zero. This result should be reported in Step 7 below.

7.3.4.6 Step 6: Calculate Crack Growth

The crack size at the end of the assessed period of operation is calculated by integrating the appropriate fatigue crack growth expression. This involves three sub-steps, which are repeated for pre-set cyclic increments: update the stress intensity factor as a function of the current flaw dimensions; compute the increment in crack size from the crack growth rate law, and check its stability at fault or overload load levels using the fracture procedure. The following paragraphs describe these for the Paris Law as implemented in BS7910 [7.15] and for the more sophisticated Forman-Mettu [7.16] equation, used in the ESACRACK [7.17] and NASGRO procedures [7.18]. The latter approach can describe the complete sigmoidal shape of the crack growth vs. stress intensity factor range relationship (Figure 7.33) and includes the effects of stress ratio, mean stress level and other important parameters.

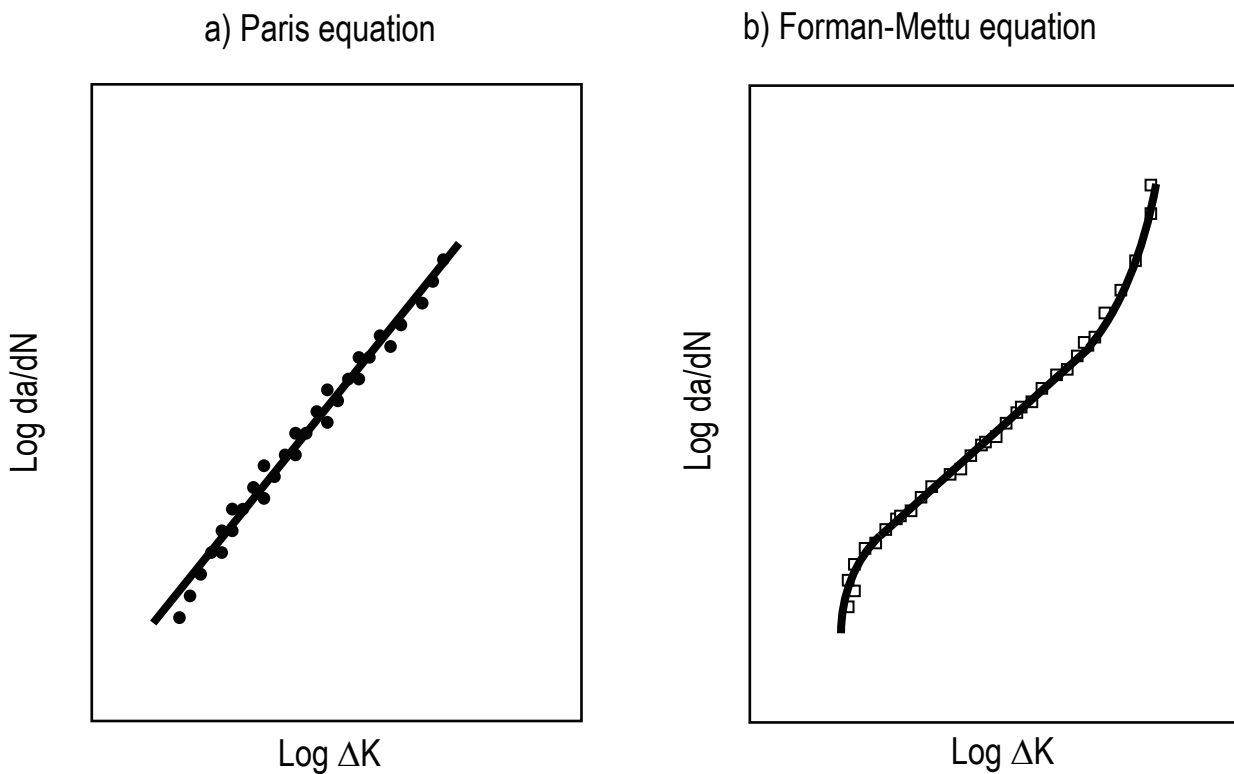


Figure 7.33 - Schematic showing how the fatigue crack growth rate is represented by the Paris or the Forman-Mettu equations.

7.3.4.6.1 Paris Equation

The relevant equation is as follows:

$$da / dN = C(\Delta K)^m \tag{7.38}$$

where A and m are constants which depend on the material and the applied conditions, including environment and cyclic frequency.

For situations in which crack growth near the threshold is significant, a less conservative form of equation (7.38) based on the effective value of ΔK , ΔK_{eff} , may be justified. In these circumstances, the relevant equation is the following:

$$da / dN = C (\Delta K_{eff})^m \quad (7.39)$$

where the default value of ΔK_{eff} is ΔK . At temperatures up to 100°C, advantage can be taken of the proximity to the threshold, ΔK_{th} , such that for $\Delta K < (\Delta K_{th} / R)$

$$\Delta K_{eff} = (\Delta K - \Delta K_{threshold}) / (1 - R) \quad (7.40)$$

where R is the stress ratio (or effective stress ratio for welded joints):

$$R = \frac{S_{min}}{S_{max}} \quad (7.41)$$

where S_{min} and S_{max} are the minimum and maximum values of the stress range respectively. The growth of the crack, Δa , should be estimated for one cycle from the value of ΔK using the crack growth relationship. The flaw dimension, a , should then be increased by Δa . Similarly, the growth, Δc , at the ends of a part wall surface breaking or embedded flaw should be estimated for one cycle from the value of ΔK calculated for those flaw ends. The length of the flaw, $2c$, should be increased by $2\Delta c$.

Taking the peak value of the tensile stress in the stress cycle, the stress intensity factor corresponding to the new size and shape should be estimated using the incremented crack dimension. This should be compared with the limiting value with regard to other failure modes. If acceptable, the next stress cycle should be considered and the procedure repeated. If the specified fatigue design life is reached and the limit to growth is not exceeded, the flaw should be regarded as acceptable. For elliptical and semi-elliptical flaws, the crack front shape changes as a and c increase. This analysis should be continued until one of the following occurs.

a) For embedded flaws: When the crack breaks through to one surface, it should be treated as a surface crack of length $2c$ and, unless failure may be deemed to have occurred, for example by leakage caused by breakthrough, the analysis can be continued for this new geometry.

b) For surface flaws: When the crack breaks through to the far surface it should be treated as a through-thickness crack of length $2c$ and the process of incremental growth can then be continued unless failure may be deemed to have occurred, for example by leakage.

The above procedure entails a cycle-by-cycle calculation of crack growth. In some situations, this is impracticable and an approximate numerical integration method may be preferable. In particular for cases where ΔK is a simple function with the form $\Delta K = Y(\Delta\sigma)\sqrt{\pi a}$ the cyclic life can be obtained directly from the integrated form of equation (7.39):

$$\int_{a_i}^{a_f} \frac{da}{Y^m(\pi a)^{m/2}} = C (\Delta\sigma)^m N \quad (7.42)$$

where Y is a shape function describing the flaw geometry.

7.3.4.6.2 Forman-Mettu Approach

This method follows a similar cycle-by-cycle integration method as discussed above using the sigmoidal crack growth rate relationship:

$$\frac{da}{dN} = C \left[\left(\frac{1-f}{1-R} \right) \Delta K \right]^n \frac{\left(1 - \frac{\Delta K_{th}}{\Delta K} \right)^p}{\left(1 - \frac{K_{max}}{K_c} \right)^q} \quad (7.43)$$

where N is the number of applied fatigue cycles, a is the crack length, and C , n , p , and q are empirically derived constants. Explanations of the crack opening function, f , the threshold stress intensity factor range, ΔK_{th} and the critical stress intensity factor, K_c are presented below.

a) **The crack opening function, f** , for plasticity-induced crack closure is defined as:

$$f = \frac{K_{op}}{K_{max}} = \begin{cases} \max(R, A_0 + A_1R + A_2R^2 + A_3R^3) & R \geq 0 \\ A_0 + A_1R & -2 \leq R < 0 \end{cases} \quad (7.44)$$

where K_{op} is defined as the minimum stress intensity of the cycle required to re-open the crack and the various coefficients are given by:

$$A_0 = (0.825 - 0.34\alpha + 0.05\alpha^2) \left[\cos\left(\frac{\pi}{2} S_{max} / \sigma_0\right) \right]^{1/\alpha} \quad (7.45)$$

$$A_1 = (0.415 - 0.071\alpha) S_{max} / \sigma_0 \quad (7.46)$$

$$A_2 = 1 - A_0 - A_1 - A_3 \quad (7.47)$$

$$A_3 = 2A_0 + A_1 - 1. \quad (7.48)$$

Here α is a plane stress/strain constraint factor, and S_{max} / σ_0 is the ratio of the maximum applied stress to the flow strength. Values of α range from 1, which corresponds to a plane stress condition, to 3, which corresponds to a condition of plane strain. Materials such as high-strength steels, for which the K_{Ic}/σ_Y ratio is fairly low, are assigned relatively high α values (2.5 or higher), while materials with higher K_{Ic}/σ_Y ratios usually have α values ranging from 1.5 to 2.0. In addition, S_{max}/σ_0 , the ratio of the maximum applied stress to the flow strength, is assumed to be constant. For materials that exhibit only a very small stress ratio effect, the eqn.(7.44) may have been fitted without considering the effects of crack closure, so that the R and f terms drop out. In this case, for positive stress ratios the entire ΔK range contributes to crack propagation, whereas for negative stress ratios K_{max} is to be used in place of ΔK .

Note that non-conservative life predictions may be obtained from Forman-Mettu analyses of structures which cycle to a relatively high compressive stress, with a negative stress ratio of the order of $R = -1$ to -2 . In such cases, substituting the absolute value of S_{min} for S_{max} and using this to calculate an appropriate S_{max}/σ_0 value may lead to better results.

For constant amplitude fatigue loading, multiplying ΔK by a crack-closure factor, β_R , produces more accurate crack growth predictions for semi-elliptical surface cracks and quarter-elliptical corner cracks. This β_R factor is applied only at points where the crack front intersects a free surface, and it is a function of the stress ratio (R -ratio). For $R > 0$, β_R is given by:

$$\beta_R = 0.9 + 0.2R^2 - 0.1R^4 \quad (7.49)$$

and for $R \leq 0$, β_R is assumed to have a value of 0.9. As noted in the introduction to this module, the above crack opening function was derived from an analysis of centre-cracked panels, subjected to a constant load amplitude condition, in which the crack front advances through a zone of plastically deformed material. This means that the effect of bending was not included in the analysis and that the crack opening equation accounts for plasticity-induced crack closure, but not necessarily other effects, such as extensive oxide-induced or roughness-induced crack closure.

b) **The threshold stress intensity factor range**, ΔK_{th} , is approximated by the following empirical equation:

$$\Delta K_{th} = \Delta K_0 \left(\frac{a}{a + a_0} \right)^{1/2} / \left(\frac{1 - f}{(1 - A_0)(1 - R)} \right)^{(1 + C_{th}R)} \quad (7.50)$$

where R is the stress ratio, f is the Newman closure function, A_0 is a constant used in f , ΔK_0 is the threshold stress intensity factor range at $R = 0$, C_{th} is an empirical constant, a is the crack length, and a_0 is an intrinsic crack length. The intrinsic crack size a_0 is assigned a fixed value of 0.0381 mm. The parameter R_{cl} is the cut-off stress ratio above which the threshold is assumed constant. In some cases independent values of C_{th} have been used for negative and positive R values to provide extra flexibility in the data fitting process. These are denoted C_{th}^- and C_{th}^+ respectively.

c) **Critical stress intensity factor**, K_{In} : this is a quasi-fracture toughness value used to describe the acceleration of the crack growth rate at high ΔK values. Its value is determined from the calibration procedure for the parameter in the Forman-Mettu crack growth equation. It is possible to apply so-called K_c values, which are a function of thickness, and part-through fracture toughness (K_{Ie}) values in appropriate circumstances. The following relationship is applied to describe the K_c vs. thickness behaviour:

$$K_c / K_{In} = 1 + B_k e^{-\left(A_k / t_0\right)^2} \quad (7.51)$$

where

$$t_0 = 2.5(K_{In} / \sigma_{ys})^2 \quad (7.52)$$

It is noted that in addition to being a function of thickness, the critical stress intensity factor depends on crack length or stress level i.e. the R-curve effect. It should be noted that the K_c -vs.-thickness curve fit for a given material in Annex M currently represents an average of the data points and does not account for the above factors. Therefore, the user is cautioned that a crack growth analysis for high stress, low cycle fatigue conditions could produce un-conservative results at shorter crack lengths.

For part-through crack geometries, K_{In} can be set equal to a constant value of K_{Ie} (see Annex M).

d) **Crack instability criterion**: crack instability is usually assumed to occur if K_{max} exceeds the critical stress intensity factor K_{In} . For most of the part-through crack geometries, K_{max} at both the surface and deepest points can be compared with K_{Ie} . However, for part-through cracks that have free surfaces, K_{max} at the surface tips can be compared with 1.1 times K_{Ie} . Failure is also assumed to occur if the net section stress exceeds the flow strength of the specified material, where the flow strength is defined as the average of the yield and ultimate tensile strengths.

7.3.4.7 Crack Growth under Variable Amplitude Loading

For many structures the fatigue loading is random or variable rather than constant amplitude cycling. This can have a significant influence on the lifetime prediction through effects such as crack growth retardation (following an overload) or crack growth acceleration. Several approaches are available for treating such effects, including the Willenborg model [7.19], the Wheeler model [7.20], and the strip-yield model [7.21]. Their application to a

fatigue crack growth analysis should be supported by an appropriate justification of their suitability to the circumstances under consideration.

7.3.5 Route 5 - Non-Planar Flaw Assessment

Non-planar flaws can be assessed in the same way as planar flaws using Route 4. Since they are not crack-like, this will be conservative. However, it may be the only option if it is necessary to quantify the growth of the flaw under fatigue loading and to ensure the margin against unstable fracture at a specific crack size. Otherwise, Route 1 or Route 2 using S-N curves for welded joints can be applied directly, in cases for which the equivalent fatigue strength is established for the non-planar flaw under consideration. At present, this approach is available only for assessing slag inclusions or porosity in steel or aluminium alloy butt welds. The overall flowchart for Route 5 is shown in Figure 7.34.

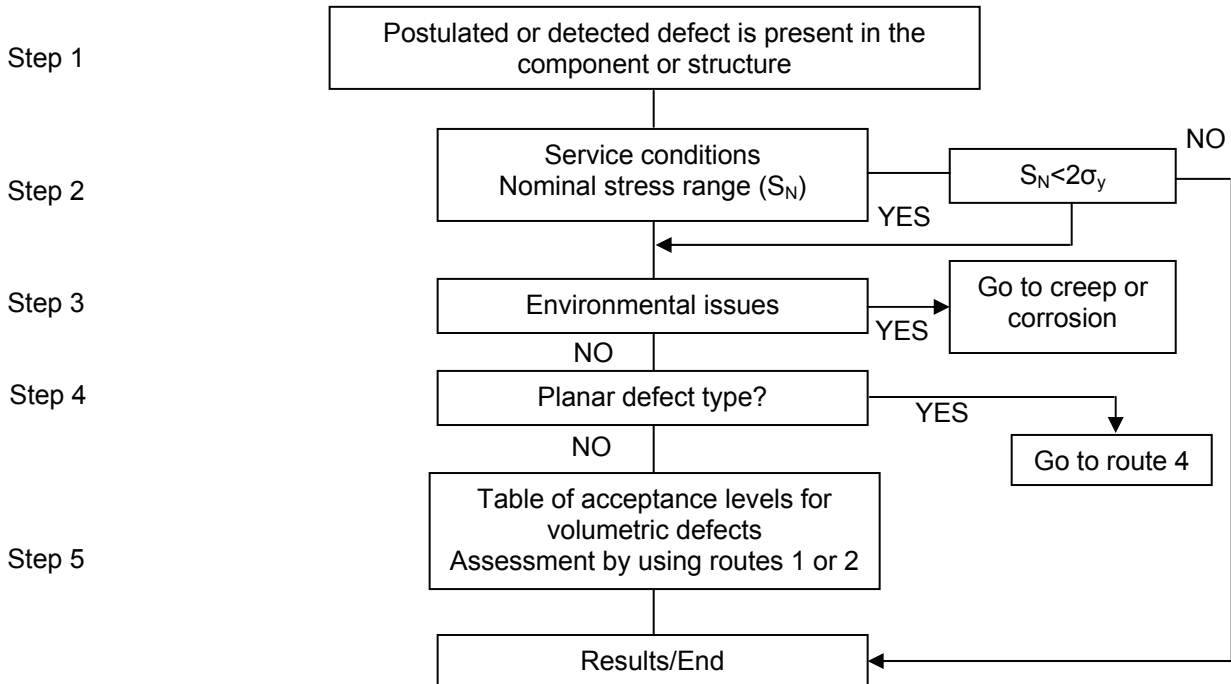


Figure 7.34 - Stepwise flowchart for Route 5

7.3.5.1 Step 1: Postulated or Detected Non Planar Flaw is Present in the Component or Structure

Route 5 assumes that a non planar flaw is postulated or is detected by NDE in the structure or component which is assessed in fatigue. Annex D gives guidelines on NDE detection.

7.3.5.2 Step 2: Service Condition

Fatigue resistance will be calculated in Route 1 by using nominal stress range S_N or Hot spot stress range calculation as defined in Routes 1 and 2.

7.3.5.3 Step 3: Environmental Issues

See section 7.2.2.

7.3.5.4 Step 4: Types of Imperfections

The types of imperfections covered in this document are listed below. Other imperfections, not yet covered, may be assessed by assuming similar imperfections with a comparable notch effect.

A - Imperfect shape : Undercut and

B - Volumetric discontinuities

- Gas pores and cavities of any shape

- Solid inclusions such as isolated slag, slag lines, flux, oxides and metallic inclusions

C - Planar discontinuities

If a volumetric discontinuity is surface breaking or near the surface, or there is any doubt about the type of an embedded discontinuity, it should be assessed like a planar discontinuity.

7.3.5.5 Step 5: Effects and Assessment of Imperfections

At geometrical imperfections, two effects affecting fatigue resistance can be distinguished:

1 - Nominal stress and Local notch effect (Route 1)

Here the interaction with other notches present in the weld joint is decisive. Two cases are to be distinguished:

- Additive notch effect: If the location of the notch due to the weld imperfection coincides with a structural discontinuity associated with the geometry of the weld shape (e.g. weld toe), then the fatigue resistance of the welded joint is decreased by the additive notch effect. This may be the case at shape imperfections.

- Competitive notch effect: If the location of the notch due to the weld imperfection does not coincide with a structural geometry associated with the shape geometry of the weld, the notches are in competition. Both notches are assessed separately. The notch giving the lowest fatigue resistance is governing.

2 - Crack-like imperfection (Route 4)

After inspection and detection of a weld imperfection, the first step of the assessment procedure is to determine the type and the effect of the imperfection as given here.

If the weld imperfection cannot be clearly associated to a type or an effect of imperfection listed here, it is recommended that it is assumed to be crack-like (lack of penetration, lack of fusion, other). In that case, this imperfection has to be assessed by using fracture mechanics (Route 4).

7.3.5.5.1 Undercut

The basis for the assessment of undercut is the ratio u/t , i.e. depth of undercut to plate thickness, as indicated in Table 7.12. Though undercut is an additive notch, it is already considered to a limited extent in the tables of fatigue resistance of classified structural details (Route 1). Undercut does not reduce the fatigue resistance of welds which are only longitudinally loaded.

Table 7.12 - Route 5 Acceptance levels for undercuts

Material/Weld	Fatigue class	Allowable undercut u/t
---------------	---------------	--------------------------

		butt welds	fillet welds
Welds in steel	100	0.025	not applicable
	90	0.05	not applicable
	80	0.075	0.05
	71	0.10	0.075
	63	0.10	0.10
	56 and lower	0.10	0.10
Welds in aluminium	50	0.025	not applicable
	45	0.05	not applicable
	40	0.075	0.05
	36	0.10	0.075
	32	0.10	0.10
	28 and lower	0.10	0.10
Notes:			
1) undercut deeper than 1 mm should be assessed as a crack-like imperfection			
2) values given are applicable only to plate thickness from 10 to 20 mm			

7.3.5.5.2 Porosity and Inclusions

Embedded volumetric discontinuities, such porosity and inclusions, are considered as competitive weld imperfections which can provide alternative sites for fatigue crack initiation than those covered by the fatigue resistance tables of classified structural details (see Annex N). Acceptance levels for various FAT classes are shown in Table 7.13. Before assessing the imperfections with respect to fatigue, it should be verified that the conditions for competitive notches apply, i.e. that the anticipated sites of crack initiation in the fatigue resistance tables do not coincide with the porosity and inclusions to be assessed and no interaction is expected. It is important to ensure that there is no interaction between multiple weld imperfections, be it from the same type or different types. Combined porosity or inclusions should be treated as a single large one. If there is any doubt about the coalescence of porosity or inclusions in the wall thickness direction or about the distance from the surface, the imperfections should be assessed as crack-like (Route 4).

Table 7.13 Route 5 Acceptance levels for porosity and inclusions in welds

Material/Weld	Fatigue class	Max. length of an inclusion in mm		Limits of porosity in % of area * **
		as-welded	stress relieved +	
Steel welds	100	1.5	7.5	3
	90	2.5	19	3
	80	4	58	3
	71	10	no limit	5
	63	35	no limit	5
	56 and lower	no limit	no limit	5
Aluminium welds	40 and higher	1.5		0 +)
	36	2.5		3
	32	4		3
	28	10		5

	25 15 and lower	35 no limit		5 5
<p>* Area of radiograph used is length 2.5of weld affected by porosity multiplied by width of weld</p> <p>** Maximum pore diameter or width of an inclusion less than ¼ plate thickness or 6 mm</p> <p>*** Stress relieved by post weld heat treatment</p> <p>+) single pores up to 1.5 mm allowed</p>				

7.3.5.5.3 Crack-like Imperfections (Route 4)

Planar discontinuities, cracks or crack-like flaws are identified by non-destructive testing and inspection. NDE indications are idealised as elliptical cracks for which the stress intensity factor is calculated according to Route 4. **For embedded flaws:** The shape is idealised by a circumscribing ellipse, which is measure by its two half-axes a and c. The crack parameter "a" (crack depth) is the half axis of the ellipse in the direction of the crack growth to be assessed. The remaining perpendicular half-axis is the half-length of the crack "c". The wall thickness parameter "t" is the distance from the centre of the ellipse to the nearest surface. If the ratio $a/t > 0.75$, the flaw is to be recategorised as a surface flaw (Figure 7.35). **For surface flaws:** They are described in terms of a circumscribing half-ellipse. The wall thickness parameter is "t". If the ratio $a/t > 0.75$, the flaw is regarded as being fully penetrating and is to be re-categorised as a centre or edge crack, whichever is applicable (Figure 7.36)

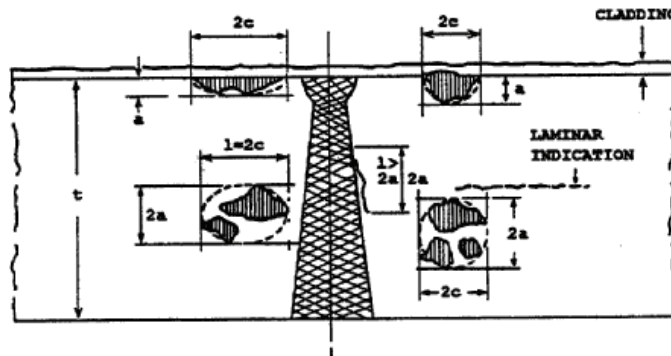


Figure 7.35 - Treatment of NDE indications.

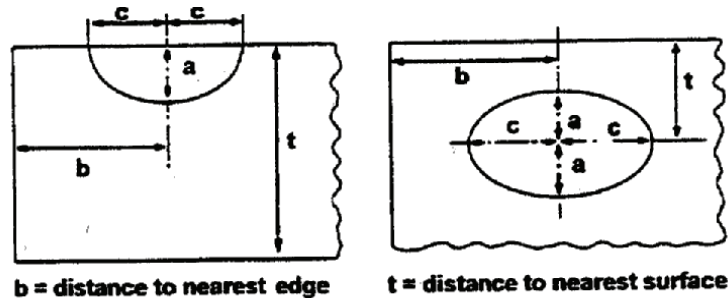


Figure 7.36 - Idealised surface breaking and sub-surface flaws.

7.4 Life Improvement [7.22]

7.4.1 Introduction

Post weld improvement techniques may increase the fatigue strength of welded joints that are likely to fail from cracking from the weld toe. Such techniques rely on two main principles:

a) *Reduction of the severity of the weld toe stress concentration.* The primary objective is to remove or reduce the size of the weld toe flaws and thus extend the crack initiation part of the fatigue life. A secondary objective is to reduce the stress concentration effect of the weld profile by achieving a smooth transition between the plate and the weld face. A variety of techniques belong to this group as shown in Figure 7.37.

b) *Introduction of beneficial compressive residual stress.* In this approach compressive residual stresses are introduced in the weld toe region. These have the effect of keeping the weld toe in a state of compression with the result that an applied tensile stress must first overcome the residual stress before it becomes damaging. Compressive residual stresses are commonly induced by mechanical plastic deformation of the weld toe region. Residual stresses then arise as a result of the restraint imposed by the surrounding elastic material. An overview of techniques in the residual stress group is shown in Figure 7.38.

A third group may be identified as consisting of a combination of a geometry modification technique and a treatment that introduces residual stresses. This may facilitate quality control of the improvement and also contribute to a reduction in scatter in fatigue life. Corrosion may have a particularly harmful effect on smooth surfaces and it is therefore mandatory that a protection system is used when corrosion may affect improved welds. It is noted that corrosion protection systems such as paint or metal plating deposition are not considered as improvement methods per se and are therefore not discussed further in this section.

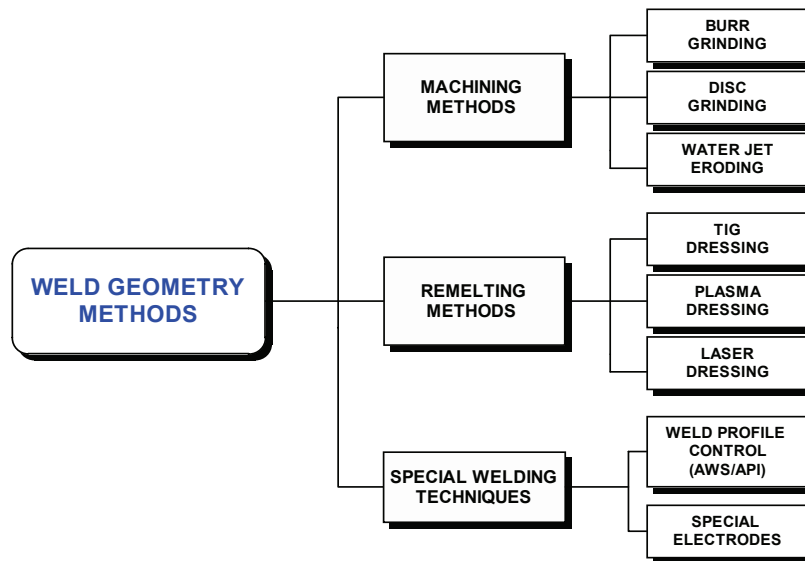


Figure 7.37 - Techniques for reduction of stress concentration factors

The effects of all improvement techniques are sensitive to the method of application and the applied loading, being most effective in the low stress high cycle regime. They may also depend on the material, structural detail and dimensions of the welded joint. Consequently, fatigue tests for the verification of the procedure in the endurance range of interest are recommended.

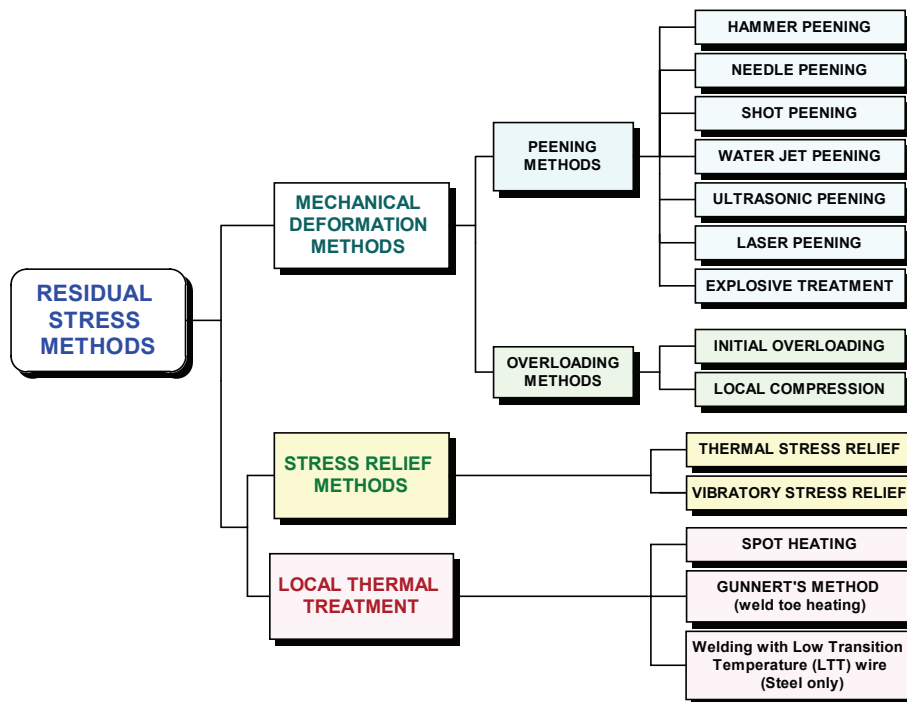


Figure 7.38 - Techniques for modification of residual stress

Recommendations for selected post weld improvement procedures are given below. They may be used under the following circumstances: a) Increasing the fatigue strength of new structures, b) Repair or upgrading of existing structures. The recommendations apply to nominal stress and structural hot spot stress method; they do not apply to effective notch stress and fracture mechanics methods.

7.4.2 Applicability of Improvement Methods

The recommendations apply to all arc welded steel or aluminium components subjected to fluctuating or cyclic stress and designed to fatigue limit state criterion. They are limited to structural steels up to a specified yield strength of 900 MPa and to structural aluminium alloys commonly used in welded structures, primarily of the AA 5000 and AA 6000 series. The recommendations apply to welded joints of plates, of sections built up of plates or similar rolled or extruded shapes, and hollow sections. Unless otherwise specified, the plate thickness range for steel is from 6 to 150 mm, for aluminium from 4 to 50 mm. The application is limited to joints operating at temperatures below the creep range. In general, the recommendations do not apply under low cycle fatigue conditions, so the nominal stress range is limited to. For special improvement procedures, additional restrictions may be given. The improvement procedures described below, apply solely to the weld toe and to cracks starting from this point. All other points of a possible start of fatigue cracks therefore should be carefully considered as e.g. the weld root or weld imperfections. The recommendations do not apply to joints operating under free corrosion.

7.4.3 Procedures for some improvement techniques

Grinding with a rotating file (burr), TIG dressing and hammer and needle peening are commonly used improvement techniques and are described in some detail in the following sections. More information is found in the IIW guidelines for improvement techniques.

7.4.3.1 Burr Grinding

The primary aim of the grinding is to remove, or reduce the size of, the weld toe weld toe flaws from which fatigue cracks propagate. At the same time, it aims to reduce the local stress concentration effect of the weld profile by smoothly blending the transition between the plate and the weld toe.

Equipment: A high speed pneumatic, hydraulic or electric grinder with rotational speed from 15 000 to 40 000 rpm is required. A pressure from 5 to 7 bars for air-driven grinders is recommended. The tool bit is normally a tungsten carbide burr (or rotating file) with a hemispherical end. To avoid a notch effect due to small radius grooves, the burr diameter should be scaled to the plate thickness (t) at the weld toe being ground. The diameter should be in the 10 to 25 mm range for application to welded joints with plate thickness from 10 to 50 mm. The resulting root radius of the groove should be no less than 0.25t.

Safety aspects: The high-speed grinding tool removes material at a high rate and is therefore capable of inflicting serious injuries to the operator or bystanders. The cutting operation itself produces hot, sharp cuttings and some noise. Therefore, heavy protective clothing together with leather gloves, safety glasses and ear protection are mandatory.

Weld preparation: The weld should be de-slugged and cleaned by wire brush before burr grinding.

7.4.3.1.1.1 **Procedure:** The quality of grinding depends on the skill of the operator, and each operator should experiment to find a technique that gives the desired result. Therefore, only general advice is given below. The burr grinding procedure is illustrated in

7.4.3.1.1.1.2 Figure 7.39. The burr is centred over the weld toe. The axis of the tool should be 45-60° to the main plate, and approximately 45° to the direction of travel. The grinder can be either pushed or pulled along the weld. Usually the former is more successful at establishing a straight groove of even depth. Grinding has to be extended to areas well outside the highest stress region at the ends of attachments, as indicated in

Figure 7.39. In general, grinding must extend to a depth of at least 0.5 mm below any visible undercut, see Figure 7.40. For plates up to 40 mm thick, the maximum allowable depth is 7 % of the plate thickness, i.e the maximum depth for a 20 mm plate is 1.4 mm. For thicker plates, the maximum depth of grinding is 3 mm. However, it is clearly preferable to minimise the depth of groove produced and, in general, a maximum of 1mm will be sufficient.

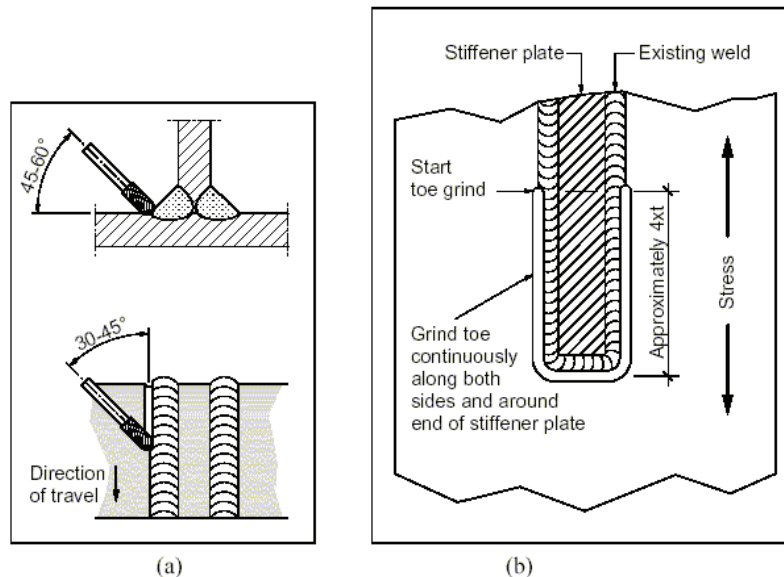


Figure 7.39 - Burr grinding procedure

In large scale planar welded joints with plate thickness of the order of 42 mm and more, the high notch stresses in the toe region extend up on the weld face, and inter-bead toes may become crack initiation sites rather than the weld toe. This applies in particular to welds with low face angles. The treatment must therefore be applied to inter-bead toes within a region extending up the weld face by a distance (w) of at least half the leg length L , as illustrated in Figure 7.40.

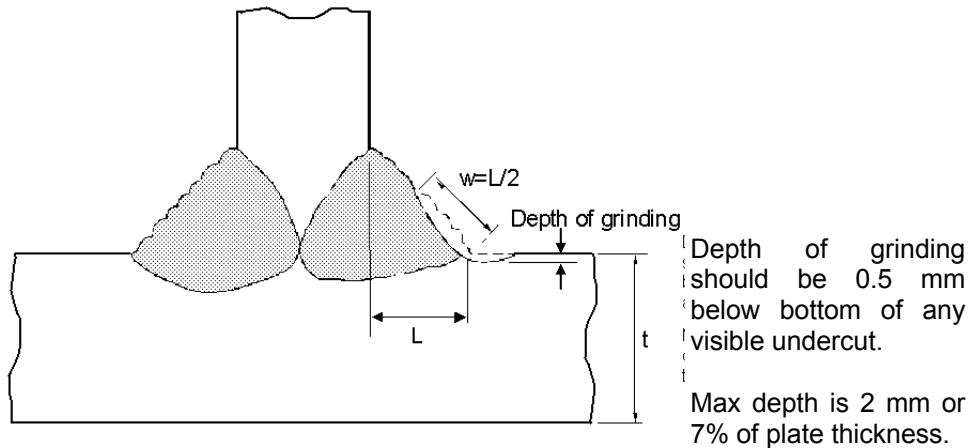


Figure 7.40 - Burr grinding, showing depth and width of groove in stressed plate

A similar situation arises for welds in tubular joints, particularly those with large beta ratios ($\beta = \text{brace diameter/chord diameter}$), where the maximum stress is likely to be located on the weld face. Thus the whole weld face is highly stressed and must be ground as well as both weld toes. The weld toe geometry to be achieved by burr grinding is illustrated in Figure 7.41. Note that the burr radius has to be scaled to the plate thickness and to the grinding depth. An adequate throat thickness must be maintained from a consideration of static strength and to prevent root cracking.

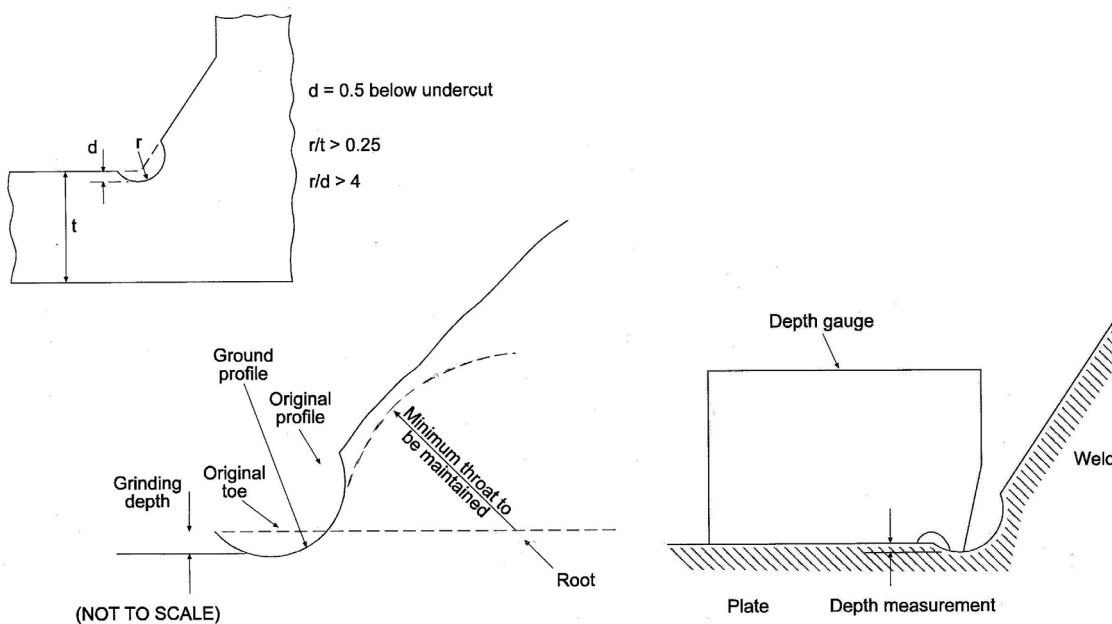


Figure 7.41 – Details of burr ground weld geometry

The grinding rate depends on the weld geometry and material, but will be typically 50 to 100 mm per minute. The finished ground surface should be as smooth as possible, with no visible evidence of the original weld toe and any grinding marks at right angles to the weld toe line.

Inspection and quality control: The inspection procedure must include a check on the weld toe radius, the depth of grinding, and confirmation that the weld toe has been removed completely. A depth gauge similar to the one used for measuring weld toe undercut may be used, although the accuracy is low. Visual examination under a bright light should be made in order to ensure that all traces of the original weld toe have. The ground surface of the groove should be inspected to make sure there are no deep scratches in the length direction, i.e. all grinding marks should be normal to the weld. A low power (approx. x5) magnifying glass is suitable.

7.4.3.2 TIG dressing

Introduction: The aim of TIG dressing is to remove the weld toe flaws by re-melting the material at the weld toe. It also aims to reduce the local stress concentration effect of the local weld toe profile by providing a smooth transition between the plate and the weld face. The present specifications are only applicable to connections with main plate thicknesses of at least 4 mm for aluminium and 6 mm for steel.

Equipment: A standard TIG Welding machine is used. Argon is normally used as shielding gas. The addition of helium is beneficial since this gives a larger pool of melted metal due to a higher heat input.

Weld preparation: TIG dressing is sensitive to most types of common weld contaminants such as mill scale, rust, oil and paint. The weld and adjacent plate should be thoroughly de-slugged, and wire brushed. If necessary, light grinding should be used to obtain a clean surface. Insufficient cleaning tends to result in the formation of gas pores that can have a strong detrimental effect on fatigue performance. The problem of porosity is particularly important in TIG dressed aluminium welds.

Dressing Conditions and procedure

Tungsten electrode: The shape of the arc depends on the shape and condition of the electrode tip. If the tip is contaminated or rounded by wear (oxidation), the arc becomes concentrated with the result that the re-melted zone narrows with an unfavourable effect on the bead shape. It is also difficult to start the arc and to keep it stable. These problems can be avoided by re-grinding the tip or replacing the electrode.

Shielding gas: If the gas flow rate is low or strong draughts disturb the gas shield the arc becomes unstable and defects such as surface pores are formed, or the electrode and bead oxidise. An adequate gas supply rate depends on many factors, including gas cup size, welding conditions and welding location (presence of draughts). An optimum flow rate should therefore be determined by trial dressing. For TIG dressing of duplex stainless steels it is advisable to add 1 to 2% nitrogen to the shielding gas to avoid unfavourable changes to the austenite-ferrite balance.

Dressing parameters: The objective of TIG dressing is to obtain a smooth transition from the plate to the weld bead. Dressing conditions may vary with the welding position, but as a general rule a high heat input should be used since this normally gives a low hardness in the HAZ. Additionally, a high heat input also allows higher dressing speeds. An excessive heat input caused by a combination of high current and a low travel speed usually produces undercut or a poor bead profile.

Position of TIG torch and dressing zone: For an optimum result the re-melted zone has to be positioned carefully with respect to the original weld toe. Normally the best result is obtained when the arc centre is located a small distance away from the weld toe, as indicated in Figure 7.42 a). A slight sideways tilt of the torch from the perpendicular position may help to obtain a favourable bead profile. In addition, a small backward tilt may help to maintain an adequate gas shield. If the arc is positioned too close to the weld bead it may result in the formation of a new toe as shown in Figure 7.42 b) and c). In general the electrode should be directed more towards the parent plate for steeper weld profiles, whereas for flatter beads the electrode should be positioned closer to the weld toe. If bead shapes similar to those shown in Figs. 7.42 b) and c) are obtained, remedial treatment should be considered, see below. A re-melted weld toe as shown in Figure 7.42 (a) represents an optimum shape with respect to fatigue.

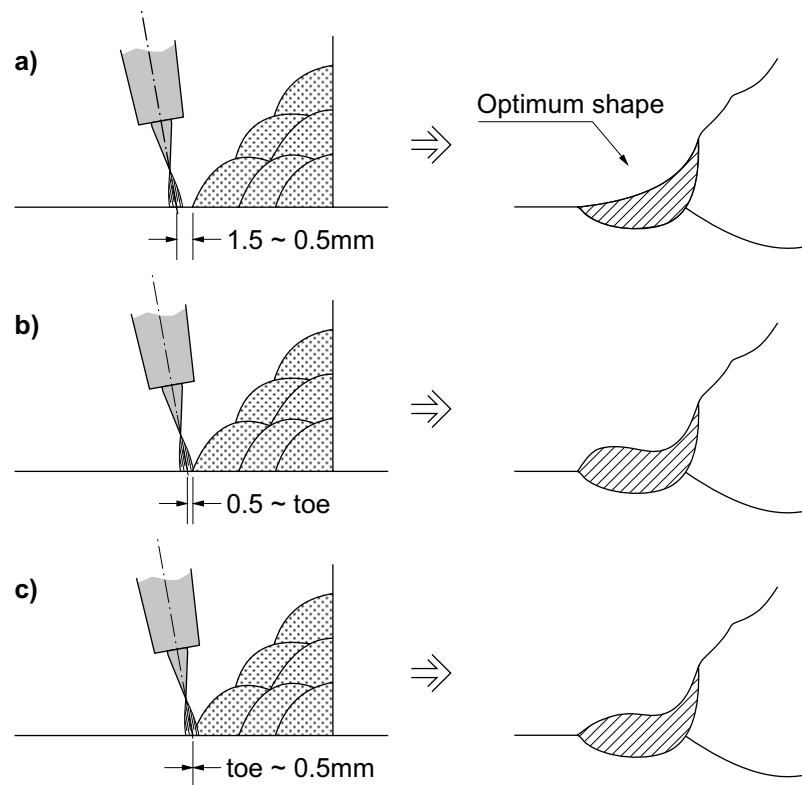


Figure 7.42 – Position of torch and resulting profiles

Operator and inspector training: The quality of TIG dressing depends on an optimum combination of dressing parameters and the manual skills of the operator. The optimum dressing conditions are related to the individual characteristics of the welding equipment. The optimum shape of the dressed profile also depends to some extent on the shape of the initial bead profile. For this reason it is recommended that a trial programme is set up to familiarize the welder with the technique and develop optimum dressing conditions. The trials should include dressing with different. Arc starting and stopping techniques should also be practised with different heat inputs and torch positions. After completion of training, the operator should treat at least 1m of similar weld before starting production treatment. **Remedial dressing:** If the TIG-dressed weld does not satisfy the inspection criterion with respect to weld shape a new dressing run may be performed. If necessary a weaving technique may be tried or filler material could be used. The ease of repeating TIG dressing is one of the advantages of this method. **Inspection:** The dressed weld should have a smooth transition from the plate to the weld face, with a minimum toe radius of 3 mm. The weld should be checked for complete treatment along the entire length of the part treated. **Corrosion protection for ground or TIG dressed welds:** The benefit of burr grinding and TIG dressing is severely reduced if the surface is degraded by corrosion. Therefore, for maximum benefit, the dressed surface must be adequately protected against possible corrosion. The protection may be of a temporary nature, as would be the case for a part of an offshore structure that would eventually be submerged and protected by a cathodic protection system. In other cases permanent protection must be provided by other means, e.g. a paint system.

7.4.3.3 Hammer Peening

Introduction.

In hammer peening, compressive residual stresses are induced by repeatedly striking the weld toe region with a blunt-nosed tool. Heavy peening of thin plates may introduce plate bending and secondary bending stresses. Therefore, the specifications given below are apply only to connections with thickness of the peened plate at least 4 mm for steel and 8 mm for aluminium. The magnitude of the residual stresses introduced by peening methods depends to a large extent on whether the weld to be peened is under tensile or compressive loading during the peening operation. A better result can be expected if the peened component is loaded in such a way

as to give tensile stress in the region to be peened. Conversely, a compressive loading during peening will reduce the effectiveness of the treatment.

Equipment: A pneumatic or hydraulic hammer is commonly used. A suitable pneumatic hammer gun operates at an air pressure of 5 to 7 bars and delivers 25 to 100 blows per second. Impact energy is typically in the range 5 to 15 Joules. The weight of the gun is from about 1 to 3.5 kg. Most research investigations of hammer peening have made use of the above types of hammer gun, both of which are primarily intended for use as chipping hammers. However, riveting guns have recently been found to be better suited for peening because they are lighter and have better vibration dampening. These features will increase operator comfort and ease of use, which in turn should improve control over the peening operation and hence consistency and reliability of the resulting treatment. Hardened steel tool bits with approximately hemispherical tips, diameters between 6 and 18 mm, and length typically 50 to 200 mm are used. Alternatively, elongated or boat shaped bits are used. Such tools are not generally available as standard equipment, but they can be produced relatively simply by grinding the tips of standard chisels.

Operator and inspector training: Hammer peening is carried out manually. Some skill is required, and therefore the operator should receive appropriate training, including a demonstration of successfully treated welds as well as unacceptable treatment. Some trial treatments, over at least 1m of weld, should be carried out before attempting to treat the actual component. **Weld preparation:** The weld cap and adjacent parent material shall be fully de-slugged and wire brushed or ground to remove all traces of oxide, scale, spatter and other foreign material. **Safety aspects:** Hammer peening is a noisy operation and it is essential that the operator and others working in the vicinity should use ear protection. Normal protective clothing for working in a fabrication shop is adequate, but it should include a face-mask or goggles. Vibration from peening equipment may cause discomfort or physical harm, and the operator should not perform the operation for extended periods of time. Vibration damping gloves may help to alleviate this problem. **Procedure:** Effective treatment requires reasonably accurate positioning of the tip of the tool over the weld toe so that metal on each side (both weld metal and parent plate) is deformed. This will normally be achieved by supporting the hammer firmly and keeping the peening tool tip in close contact with the weld toe as it is moved along the weld. Typically hammer is held at about 45° to the plate surface and approximately perpendicular to the direction of travel, as shown in Figure 7.43, although in practice there will be a tendency to slope slightly as the tip of the tool tries to run ahead of the operator.

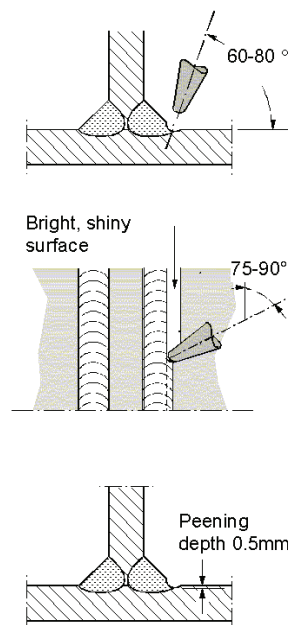


Figure 7.43 – Hammer peening procedure

The resulting groove must be smooth and free from obvious individual indentations. The depth of the groove should be a minimum of 0.3 mm for structural steels with yield stress below 600 MPa. The travel speed will depend to some extent on access and peening position, but also on the equipment used. A hammer gun that is heavy and vibrates will cause the tool to jump along the weld, missing some areas. Repeated peening, usually four passes, is then needed to achieve full coverage and a smooth surface. Lighter, vibration-damped hammer

guns facilitate slower travel speeds, and hence more thorough treatment per pass. A travel speed of 50 to 100 mm/min per pass, similar to typical welding speeds, is normally sufficient to achieve the required depth in two passes, although a lower speed might be necessary for higher strength steels.

The diameter of the tool tip influences the resulting appearance of the hammer peened surface. In general, the smaller the diameter, the greater the likelihood that the actual weld toe itself will be peened and eventually disappear. Peening with a large diameter tool (greater than 12 mm) does not usually reach the weld toe but instead deforms material either side of it. Although in general the desired effect will be achieved with fewer passes using a large diameter tool, the presence of the original weld toe is a disadvantage from the viewpoint of inspection. In particular, it is not obvious that the toe has been correctly treated (i.e. left in a state of compressive residual stress) and remnant traces of weld toe confuse in-service inspection, since it is difficult to distinguish between them and fatigue cracks. Thus, the use of a small diameter tool, or a combination of small and larger diameter tools, with the aim of deforming the actual weld toe offers the best compromise. Inspection would then ensure that all traces of the original weld toe had disappeared.

In circumstances in which the treated weld will be subjected to a high-tensile mean stress in service, hammer peening will offer little or no benefit. When practicable, this problem can be overcome by performing the peening operation while the weld is under tensile load. For maximum benefit, this should be at least as high as the minimum stress to be experienced in service.

Inspection and quality control: In general, it is not possible to verify that hammer peening has been performed correctly by visual inspection alone. Important features like coverage and surface finish can only be described qualitatively, while the extent of plastic deformation, which reflects the level of compressive residual stress induced, is too small for reliable measurement in most practical circumstances. An important step is therefore to establish an acceptable hammer peening procedure and then to ensure that it is followed.

The hammer peening procedure should be established by performing trials on the material to be treated, preferably containing a representative weld, in the same position as the welded joint to be treated. The toe should be peened and examined after each pass. The treatment can be assumed to be complete when there is a uniform indentation along the weld toe with a smooth surface finish, and all traces of the original plate toe have disappeared. As a guide, but not a requirement, the indentation depth below the original plate surface is likely to be of the order of 0.5 mm. The minimum depth is 0.3 mm. The indentation depth will not normally exceed 1 mm. Treatment of the actual weld detail should be verified by visual inspection. This will check hammer peening position, coverage and general uniformity by comparing the hammer peened area with a reference sample or photograph.

7.4.3.4. Needle Peening

Introduction

In the needle peening process the material at the weld toe is plastically deformed by rods with rounded tips in order to introduce beneficial compressive residual stresses. Before peening it is recommended to grind the weld toe lightly in order to remove undercuts and weld toe irregularities, and subsequently to finish with a grinding tool to obtain a dull surface in order to facilitate inspection. In needle peening, compressive residual stresses are induced by repeatedly hammering the weld toe region with a bundle of round-tipped rods. Compared with hammer peening, it is generally more suitable when large areas need to be treated. e.g. welds in tubular joints. As in the case of hammer peening, the following specification is restricted to plate thicknesses of at least 4mm for steel and 8mm for aluminium. The magnitude of the residual stresses introduced by peening methods depends to a large extent on whether the weld to be peened is under tensile or compressive loading during the peening operation. A better result can be expected if the peened component is loaded in such a way as to give tensile stress in the region to be peened. Conversely, a compressive loading will reduce the effectiveness of the peening treatment. **Equipment:** A standard needle gun of the type used for removing slag and scale is suitable for needle peening, Figure 14(a). However, where necessary it is useful to modify the end piece, as shown in Figure 14 (b), to align the steel rods in a rectangular pattern rather than a circular one; this will facilitate the treatment of weld toes. Additionally the ends of the rods should be rounded. **Procedure:** The aim in needle peening is to deform the material plastically at the weld toe to induce beneficial compressive residual stresses. Effective treatment requires reasonably accurate positioning of the needles over the weld toe so that metal on each side (weld metal and parent plate) is deformed. Needle peening can be performed immediately after welding, while the weld is still hot, if required. The toe should be needle peened four times to achieve optimum benefit and adequate coverage. The resulting surface should be bright in appearance and contain a uniform distribution of small indentations. The operation is carried out with the tool held at approximately 45° to the plate surface with the ends of the needles in contact with the weld toe. Sufficient force should be applied to the tool to

prevent unsteady movement and to ensure even treatment. It is not necessary for the operator to exert undue force in this operation, particularly when using a lightweight gun, and therefore operation in the overhead position can be carried out with relative ease. The rate of treatment is approximately 800mm per minute. **Quality control and documentation:** It is important to achieve full coverage of the weld region to be treated. To this end, peening should be continued until the area is free for untreated spots. The time to do this should be noted. It is recommended that 100 % coverage of needle marks is checked visually, using a 5-10 X power magnifying glass. Then the area is treated again for the same length of time, to achieve what is termed 200% coverage. Photographs taken at intervals along the peened area, which should include appropriate identification markers, provide a suitable record of the needle peening treatment. Care is needed to arrange the lighting source in such a way that the photographs show any areas that inadvertently may have been untreated. After prolonged use, the tips of the needles will revert back from the rounded shape introduced by grinding to being flat ended. At this time, the tips should be reground to produce a rounded shape.

7.4.4 Fatigue design data for improved welds

7.4.4.1 Fatigue strength of joints improved by weld toe grinding or TIG dressing

Benefit from weld toe grinding or TIG dressing of steel components can only be claimed for details in design Class FAT 90 or lower in the IIW notation for S-N curves, as shown in Figure 7.44. This limitation is due to the fact that the higher classes include non-welded details, details whose lives are not governed by weld toe failure or the welds that have been already been improved, e.g. by grinding the weld flush with the surface. For steels with specified yield stress higher than 350 MPa the benefit consists of an upgrade by a factor of 1.5 applied to the stress range, corresponding to a factor of 3.4 on life, with a change in slope to $m = 5$ at 2×10^6 cycles, as shown in Figure 15. The highest class which can be claimed is FAT 125. Additionally, in the low endurance regime the S-N curve is limited by the IIW parent material curve, i.e. the FAT 160 curve with a slope parameter of $m = 5$. For lower grade steels, with specified minimum yield strength below 350 MPa, the improvement factor is 1.3, corresponding to a factor of 2.2 on life. The highest class which can be claimed in this case is FAT 100.

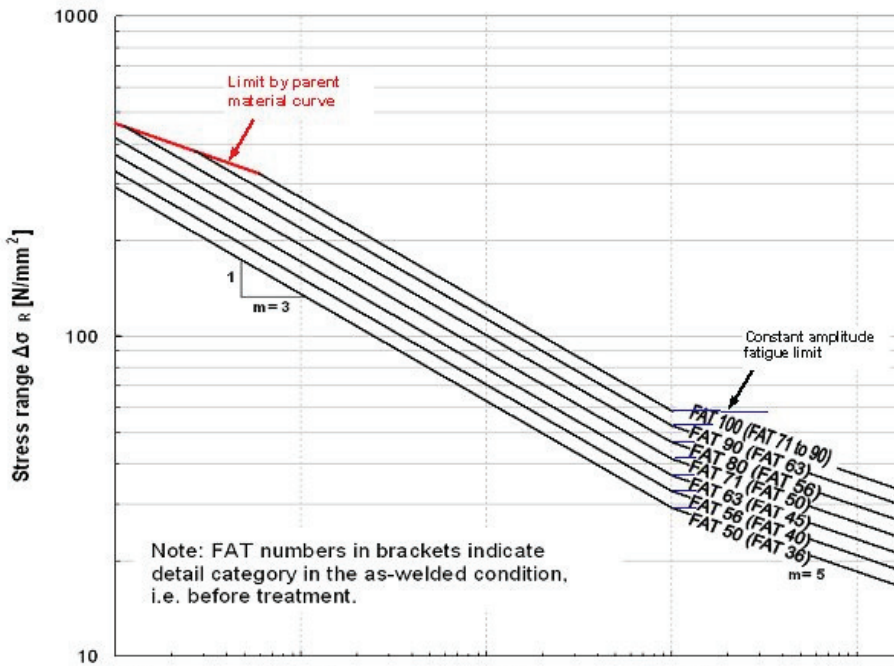


Figure 7.44 – Design S-N curves for toe ground or TIG dressed welds in steel structures

In the low cycle region, all S-N curves are limited by the IIW parent material curve, i.e. the FAT 160 curve with a slope parameter of $m = 5$ [6]. The S-N curves to be used for fatigue design on details improved by grinding or TIG dressing are shown in Figure 7.44.

Thickness effects of joints improved by TIG dressing

TIG dressing reduces the stress concentration factor, and the thickness correction factor $f(t)$ for TIG dressed joints is

$$f(t) = \left(\frac{25}{t_{eff}} \right)^{0.20}$$

where $t_{eff} = 0.5$ for $L/t \leq 2$ and $t_{eff} = t$ for $L/t > 2$ and L is the sum of the attachment plate thickness and the leg lengths.

7.4.4.2 Fatigue strength of joints improved by hammer peening or needle peening

Benefit from hammer peening or needle peening of steel components can only be claimed for details in design Class FAT 90 or lower in the IIW notation for S-N curves, as shown in Figure 7.45. This limitation is due to the fact that the higher classes include non-welded details, details whose lives are not governed by weld toe failure or the welds that have been already been improved, e.g. by grinding the weld flush with the surface. For steels with specified yield stress higher than 350 MPa the benefit consists of an upgrade by a factor of 1.6 applied to the stress range, corresponding to a factor of 4.0 on life. The S-N curve has a change in slope to $m=5$ at 2×10^6 cycles, as shown in Figure 7.45. Additionally, in the low endurance regime the S-N curve is limited by the IIW parent material curve, i.e. the FAT 160 curve with a slope parameter of $m=3$.

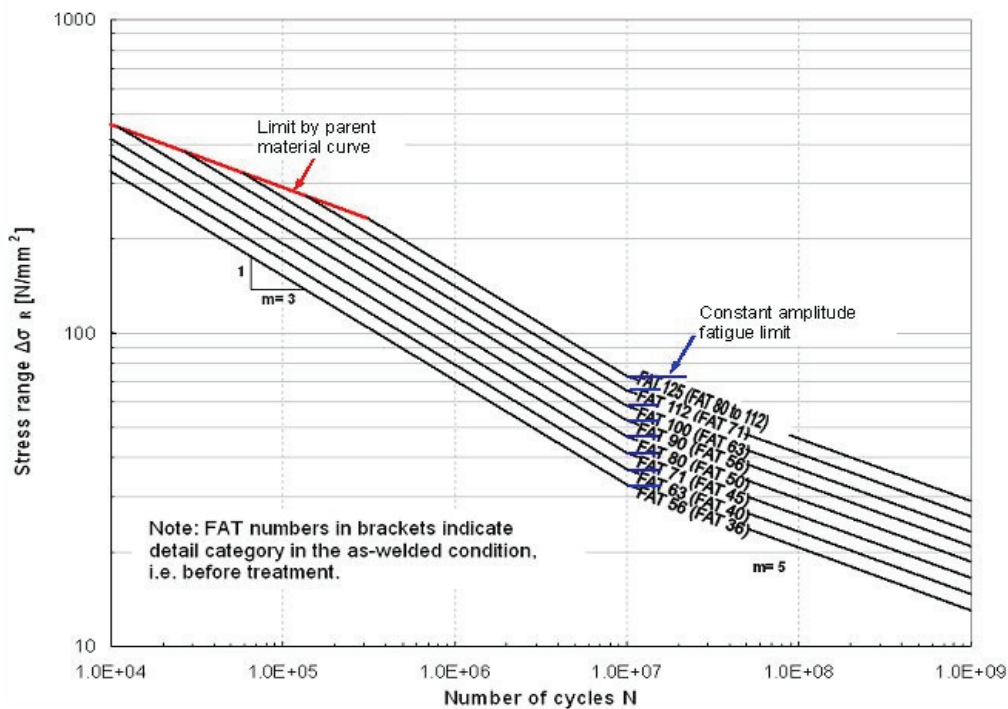


Figure 7.45 – Design curve for hammer peened or needle peened welds in steel structures

For lower grade steels, with specified minimum yield strength below 350 MPa, the improvement factor is 1.3, corresponding to a factor of 2.2 on life. The highest class that can be claimed is in this case FAT 112.

Thickness effects of joints improved by hammer or needle peening

TIG dressing reduces the stress concentration factor, and in accordance with Section 3.5.2 in Ref. 6 the thickness correction factor $f(t)$ for TIG dressed joints is

$$f(t) = \left(\frac{25}{t_{eff}} \right)^{0.25}$$

where $t_{eff} = 0.5$ for $L/t \leq 2$ and $t_{eff} = t$ for $L/t > 2$ and L is the sum of the attachment plate thickness and the leg lengths.

Effects of variable amplitude loading for joints improved by hammer or needle peening

Due to the sensitivity of hammer peened welded joints to applied mean stress, the higher S-N curves can only be used under the following circumstances:

- The maximum nominal compressive stress in the load spectrum is lower than $0.25 \times \sigma_Y$.
- When the applied stress ratio $R < 0$, the S-N curve is used in conjunction with full stress range
- When the applied stress ratio $R \geq 0$ (all stresses in tension) the S-N curve is used in conjunction with the maximum stress instead of the full stress range.

The limitations are illustrated in Figure 7.46.

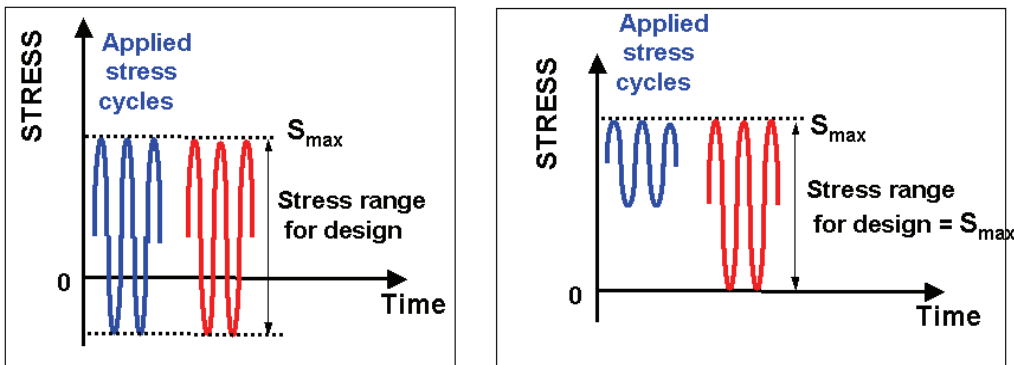


Figure 7.46 – Limitations in allowable stress ranges for hammer peened or needle peened welds in steel and aluminium alloys

7.5 Special Options

7.5.1 Dang Van criterion

7.5.1.1 The macroscopic-microscopic approach

Generally the fatigue criteria are applied at a macroscopic scale. Such an analysis does not take in account the fatigue damage phenomenon which takes place in a grain of the metal at a mesoscopic scale [7.23].

7.5.1.2 Link between macroscopic and mesoscopic scales

At a given point x , the mechanical state in the continuous medium is described by the macroscopic stress tensor, $\Sigma(x)$. Around the point x , an elementary volume, $V(x)$, can be defined. It is assumed homogeneous and isotropic and corresponds to constant stress and strain tensors. In fact, the elementary volume contains numerous metallic grains having different orientations, shapes and internal states. At the mesoscopic scale, the mechanical state of a grain is described by $\sigma(y : x)$ where y is the grain position in the local repère related to $V(x)$. The stress and strain in $V(x)$ are not homogeneous; they are different from those defined in the macroscopic scale:

$$\underline{\underline{\sigma}}(y : x : t) = \underline{\underline{\Sigma}}(x : t) + \underline{\underline{\rho}}(y : x : t) \quad (7.53)$$

Where $\underline{\underline{\rho}} = (y : x : t)$ is the mesoscopic residual stress field, fully balanced in $V(\underline{x})$.

In the high cycle fatigue regime, the elastic shakedown assumption leads to the time independent parameter $\underline{\underline{\rho}}^*$. The determination of this parameter leads to identifying the centre of the smaller circumscribable hypersphere to the macroscopic loading path. The coordinate of this centre, in the stress deviatoric field, defines $\underline{\underline{\rho}}^*$.

7.5.1.3 Failure criterion

Based on the mesoscopic parameters, the Dang Van criterion can be written [7.24] :

$$\forall \underline{n} \forall t \quad \hat{\tau}(n, t) + a \hat{p}(t) \leq b \quad (7.54)$$

Where $\hat{p}(t)$ and $\hat{\tau}(t)$ are respectively the instantaneous hydrostatic pressure and the instantaneous shear stress associated to the macroscopic stress after elastic shakedown,

$$\hat{\underline{\underline{\sigma}}} = (t). \quad (7.55)$$

The criterion can also be written :

$$\max_{\underline{n}} \left\{ \max_{\tau} [\hat{\tau}(\underline{n}, t) + a \hat{p}(t)] \right\} \leq b \quad (7.56)$$

The mesoscopic pressure is equal to the macroscopic pressure at every time and can be written as:

$$\hat{p}(t) = P = tr \left\{ \underline{\underline{\Sigma}}(t) \right\} / 3 \quad (7.57)$$

The maximum mesoscopic shear stress, obtained considering every possible facets (\underline{n}) is given by:

$$\tau(t) = \{ \sigma_I(t) - \sigma_{III}(t) \} / 2 \quad (7.58)$$

The constants **a** and **b** are derived using the endurance limits respectively in alternate bending (f_{-1}) and in alternate torsion t_{-1} :

$$a = \frac{t_{-1} - (f_{-1}/2)}{f_{-1}/3} \quad b = t_{-1} \quad (7.59)$$

The Dang Van criterion can be rewritten as follows

$$\max_t [\tau(t) + aP(t)] \leq b \quad (7.60)$$

Graphically, the loading path is drawn in the Dang Van diagram (P,t). If this loading path is located beneath the “material line”:

$$\tau + aP = b \tag{7.61}$$

crack initiation does not occur Figure 7.47(a) On the contrary, if the loading path crosses the “material line” a fatigue crack will occur at the critical point Fehler! Verweisquelle konnte nicht gefunden werden.(b).

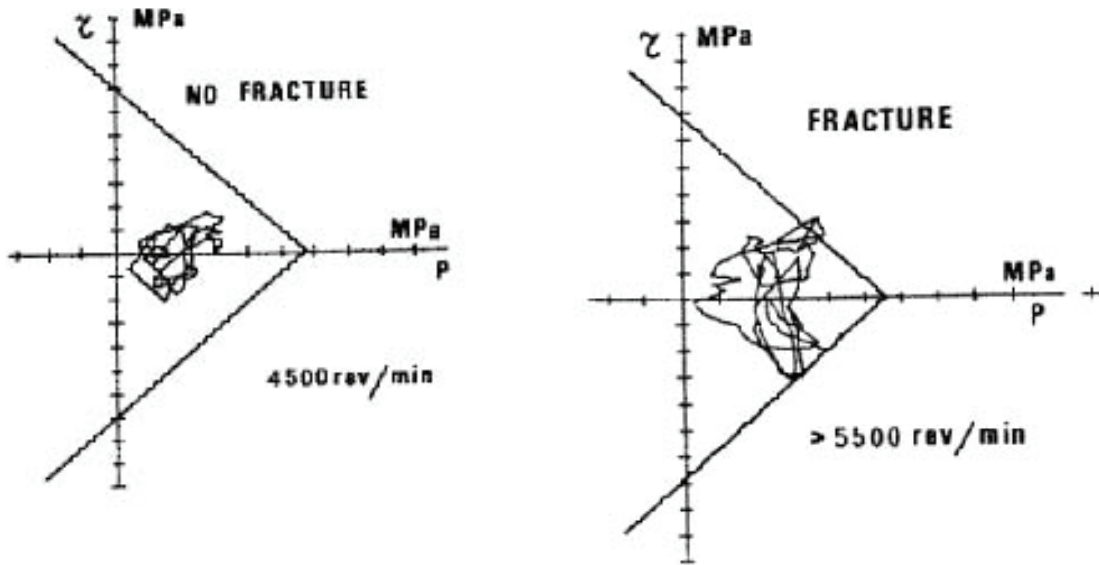


Figure 7.47 a) & b) – Example of loading path for a car engine crank shaft (from ref. [7.25])

7.5.2 Multiaxial analysis

Fatigue assessment methods have been mainly developed for uniaxial stress fields, i.e. constant principal stress direction during cycles, but in numerous cases the stress field is more complex, with rotation of the principal stress direction during the cycles. Examples include a tube submitted to variable axial and torsion loads or a ship double hull bottom knuckle submitted to the longitudinal hull girder and transverse local wave loads (Figure 7.48).

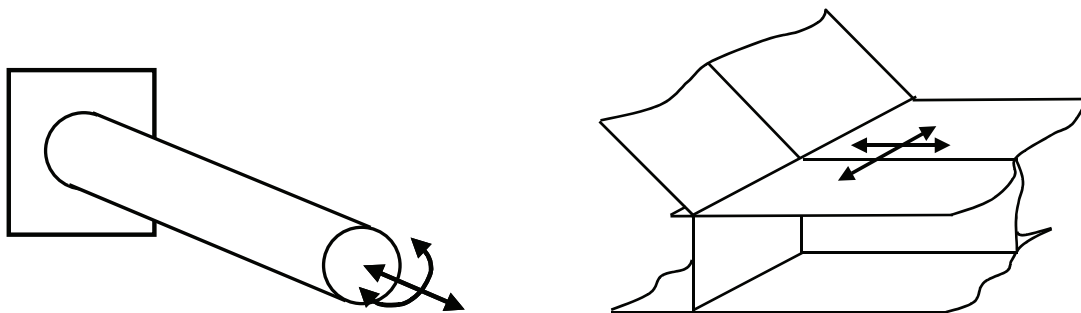


Figure 7.48 – Practical examples of multiaxial loading

Test results show that:

- a) A fatigue crack tends to originate from a weld toe and propagates in the same plane, at least for the majority of the life

- b) in-phase bending (or tension) and bending (or tension) combination seems more damaging than bending (or tension) only
- c) out-of-phase loading is more damaging than in-phase under bending (or tension) with torsion.

Fatigue assessment for multiaxial loading is a subject of on-going R&D. Two possible assessment methods are proposed here:

- use of the shear and hydrostatic pressure as used in the Dan Vang approach (see section 7.5.1)
- use of an effective equivalent stress hypothesis (EESH) [7.26], which is described in the following section 7.5.2.1.

7.5.2.1 Local effective equivalent stress

This section deals with pure bending or/and axial load, and bending or/and axial combined with torsion loads.

7.5.2.1.1 Local stress for fatigue assessment

The local normal and shear stresses on an interference plane θ are given by:

$$\sigma(\theta) = \frac{\sigma_x + \sigma_y}{2} + \frac{\sigma_x - \sigma_y}{2} \cos(2\theta) + \tau_{xy} \sin(2\theta)$$

$$\tau_n(\theta) = \frac{\sigma_x - \sigma_y}{2} \sin(2\theta) - \tau_{xy} \cos(2\theta) \quad (7.62)$$

where the parameters are defined as in Figure 7.49.

The plane angle θ has to be selected as follows:

- ductile material (structural steel): integral value of shear stresses over all planes
- semi-ductile material (wrought aluminum, cast steel): plane of maximum normal / shear stress combination
- low ductility material (cast aluminum, cast iron, sintered steel): plane of maximum normal stress

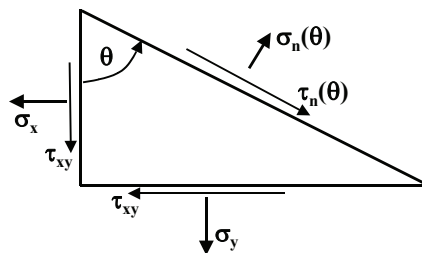


Figure 7.49 – Stress definition for equation (7.62)

7.5.2.1.2 Effective equivalent stress

Two cases are to be considered, in-phase and out-of-phase loadings.

a) In-phase loading

Without torsion, i.e., pure bending or/and axial loading, the equivalent stress is given by:

$$\sigma_{eq}(0) = \sqrt{\sigma_x^2 + \sigma_y^2 - \sigma_x \sigma_y} \quad (7.63)$$

With combined bending or/and axial and torsion loadings, the equivalent stress is given by:

$$\sigma_{eq}(0) = \sqrt{\sigma_x^2 + \sigma_y^2 - \sigma_x \sigma_y + f_s^2 3\tau_{xy}} \quad (7.64)$$

where:

$$f_s \text{ is the ratio of pure axial load stress to pure torsion load stress: } f_s = \frac{\sqrt{\sigma_{x,a}^2 + \sigma_{y,a}^2 - \sigma_{x,a} \sigma_{y,a}}}{\sqrt{3\tau_t^2}}$$

b) Out-of-phase loading

The effective equivalent stress can be determined for a phase angle φ on the basis of the von Mises hypothesis as follows:

$$\sigma_{eq}(\varphi) = \sigma_{eq}(0) \frac{F(\varphi)}{F(0)} \sqrt{\frac{1 + K_{t,x}}{1 + K_{t,\tau}} \exp\left[1 - \left(\frac{\varphi - 90}{90}\right)^2\right]} \quad (7.65)$$

$$\text{where: } F(\varphi) = \frac{1}{\pi} \int_0^\pi f_p(\theta) d\theta \quad (7.66)$$

with $f_p(\theta) = \tau_n(\theta, \varphi)$ for constant amplitude loading

or $f_p(\theta) = \frac{1}{N_S} \sum_{i=1}^{N_S} \tau_n(\theta, \varphi)$ for variable amplitude loading

where N_S is the number of steps of the stair curve loading histogram

$K_{t,x}$ stress concentration factor for normal stress $\sigma_x = K_{t,x} \sigma_{nom}$

$K_{t,\tau}$ stress concentration factor for shear stress $\tau_{xy} = K_{t,\tau} \tau_{nom}$

For ductile material, only shear stress causes damage, however the fatigue life reducing effect of dislocations initiated in different directions is considered by an integration of shear stresses over all planes. The ratio of damage parameter $F(\varphi)$ is:

$$F(\varphi) = \frac{1}{\pi} \int_0^\pi f_p(\theta) d\theta \quad \text{with} \quad f_p(\theta) = \tau_n(\theta, \varphi) \quad \text{or} \quad f_p(\theta) = \frac{1}{L_S} \sum_{i=1}^{L_S} \tau_n(\theta, \varphi)$$

The size factor $\frac{1 + K_{t,x}}{1 + K_{t,\tau}}$ represents the influence of stress gradients on the equivalent stress in interaction with

changing phase angles or principal stress directions. However, the size factor and consequently the root-term in eqn. (7.67) is only valid for seam welded thick plates with low stress concentrations. In this cases, the defect population addressed by rotating principal stresses is much higher than for welded thin sheets with sharp weld roots (high stress concentration). Since, therefore, the probability of crack initiation from a defect in a thick weld

is much higher, the root-term is applied. But this is not necessary for thin joints with plate thickness less than or equal to 3 mm, i.e. the root-term is skipped. It should be noted that Von Mises is a special case of this hypothesis used for uniaxial as well as in-phase loading.

7.5.2.2 Failure Criteria

When using the shear and hydrostatic pressure, the failure criteria to be used for the fatigue assessment is the Dang Van criterion defined in 7.5.1. When using the effective equivalent stress, the S-N curve and the failure criteria to be used for the fatigue assessment are the same as for uniaxial normal stress [9, 10]. The number of cycles results from the number of cycles of the equivalent stress for uni-axial loading.

7.5.3 Rolling contact fatigue

7.5.3.1 Introduction

Rolling contact fatigue may lead to initiation of fatigue cracks at a depth quite far beneath the running surface and propagate downwards in the rolling direction until fatigue damage. Modelling crack initiation in rolling contact fatigue necessitates overcoming two main difficulties:

- i. The evaluation of the thermo mechanical quantities induced by repeated rolling contact; because of the small size of the contact area, the stresses are beyond the elastic limit, so, it is necessary to take in account of the plastic deformation and residual stresses resulting from the sequence of repeated rolling. Therefore different limit states may be obtained depending on the intensity of the applied load, the friction coefficient and the material properties: elastic state, elastic shakedown state (the limit cycle is elastic, but early plastic deformation induces a fixed residual stress pattern), plastic shakedown and ratchetting.
- ii. The prediction of damage (this latter is closely linked to the mechanical limit state). This necessitates the use of multi-axial fatigue criteria able to deal with complex multi-axial loading situations.

To solve problem (i) the calculation must be capable of determining the stabilized state of any kind of inelastic structures subjected to repeated moving loads, directly or by following the evolution pass-by-pass [7.29, 7.30, 7.31]. For problem (ii) in the case of high-cycle fatigue, the multi-axial fatigue criterion proposed by Dang Van is used (see 7.5.1). Its main attribute is that it can be easily identified by classical fatigue uniaxial laboratory tests like repeated tension or torsion. This criterion is essentially based on elastic shakedown hypothesis. The Manson-Coffin law is considered in the case of low-cycle fatigue, especially for the prediction of shelling initiation.

7.5.3.2 Analytic determination of the limit thermo-mechanical state for fatigue assessment

The determination of the thermo mechanical fields induced by repeated rolling/sliding contact is the first step for the understanding and the prediction of fatigue damage phenomena which may occur in the parts in contact. However, this task presents many difficulties due to load level which induced plastic deformation. The simulation of such processes by using classical existing finite element software necessitates incremental translations of the loading. This way of calculating is time-consuming and cumbersome. Therefore the method used and proposed [7.29], valid for 2-D and 3-D problems, relies on the steady-state assumption in the moving contact reference. It leads to the two following numerical procedures for the calculations of stresses and strains either for an arbitrary number of loading passes or directly for the stabilized state (elastic shakedown, plastic shakedown or ratchetting): (i) the pass-by-pass stationary method (PPSM) for a single load pass; (ii) the direct stationary method (DSM) for a repeated moving load, this method goes straight to the steady-state for the calculation of a single pass. Computing the successive passes by the PPSM method, allows determination of the stabilized state and its characteristics (number of cycles before reaching the stabilized state, residual stresses, plastic deformations etc.). This stabilized state can, of course, be ratchetting. In such a case, the ratchetting rate is immediately deduced as the increment of surface displacement or plastic strains caused by a pass. The DSM method is used for the direct determination of the stabilized state, in the case of shakedown (elastic or plastic).

7.5.3.3 Numerical methods for treatment of fatigue

Two kinds of fatigue criteria can be used to predict crack initiation in the parts in contact. When these part suffer cyclic plasticity (plastic shakedown) or ratchetting, low-cycle fatigue is likely to occur. For this kind of fatigue, the Manson-Coffin law is used to predict the number of cycles to crack initiation. In the case of elastic shakedown or elastic behaviour of the rail, high-cycle fatigue is likely to occur and Dang Van criterion [7.32, 7.33, 7.34, 7.35] is used. The Dang Van multi-axial high-axial high-cycle fatigue criterion is based on a multi-scale approach which assumes that elastic shakedown happens before crack initiation. Thanks to the shakedown assumption at the local scale, it is possible to estimate the local stress cycle from the macroscopic stress cycle. The criterion is then expressed as an inequality related to the mesoscopic stresses at all instants t of the cycle, so that damaging load can be precisely characterized. The criterion used is expressed as:

$$\max \{ \tau(t) + ap(t) \} \leq b \quad (7.67)$$

Where $\tau(t)$ and $p(t)$ are the instantaneous mesoscopic shear stress and hydrostatic stress, a and b are material constants, which can be determined by two different classical fatigue tests. For instance, they are related to classical experimental fatigue strengths f_{-1} (in alternate bending) and t_{-1} (in alternate twisting) by:

$$a = \frac{t_{-1} - (f_{-1}/2)}{(f_{-1}/3)}$$

$$b = t_{-1} \quad (7.68)$$

Practically, the fatigue resistance of a structure is checked point-by-point, using two ways :

- The first one is the representation of the loading path ($p(t)$, $\tau(t)$) at each point in the (p , τ) diagram. In this diagram, two constants, a and b define a safety domain (no fatigue cracks) which is the region below the line ($\tau + ap = b$). If the loading path at each point is entirely in the safety domain, there is no fatigue crack, otherwise fatigue damage occurs.
- The second one is the evaluation at each point of the quantity :

$$\alpha = \max_i \{ (\tau(t) + ap(t) - b) / b \} \quad (7.69)$$

A positive value of α means occurrence of fatigue crack.

7.5.3.4 Example of application to analysis of rail damage

The 2-D calculations are performed to evaluate the stabilized state and the residual stress pattern at different depths in a rail. By that way we obtained the local stress cycle for different conditions of traffic. Application of the adequate fatigue criterion allows predict the locus of the crack initiation in relation with the load parameters. The methodology was presented in [7.30]. The results obtained are summarized in the fatigue map presented as shown in Figure 7.50. This type of fatigue corresponds to the region (1) of the map: initiation in depth, high cycle fatigue in the elastic domain and elastic shakedown zones. Region (2) corresponds to surface damage. When the plastic shakedown occurs (plastic deformation cycles), this regime leads to shelling which is relevant to low cycle fatigue. In the case of high friction (braking zone) surface plastic flow may be severe, so that wear phenomena are predominant. This methodology is now applied in the 3-D case. The moving load is characterized by $a = 10$ mm and $Po/Ke = 4.25$. The fatigue limits of the rail steel are: $f_{-1} = 460$ MPa and $t_{-1} = 270$ MPa. The stabilized mechanical state is an elastic shakedown. Figure 7.51 shows the result of the application of the Dang Van multi-axial fatigue criterion: the most critical point is in depth, which is typical of kidney-shape crack initiation.

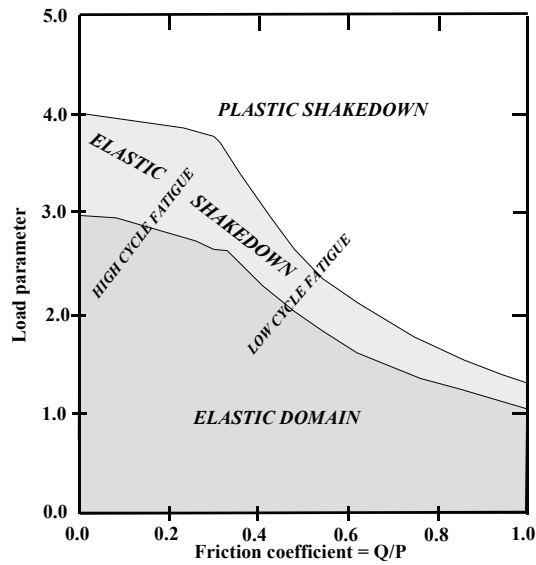


Figure 7.50 - Shakedown and fatigue map for line contact and full sliding [7.30]

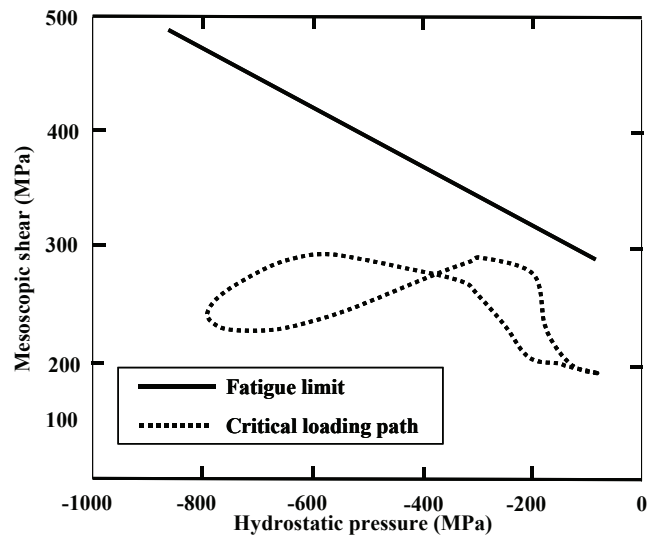


Figure 7.51 - Example of the Dang Van criterion and loading path at the most critical point [7.30]

7.5.4 Fatigue – creep

Fatigue Creep assessment is described in chapter 8.8.3 of the procedure.

7.5.5 Fatigue – corrosion

Fatigue corrosion assessment is described in chapter 9.2.6 of the procedure.

7.5.6 Growth of Short Cracks

The fatigue life of components with short cracks in the length scale of 1 mm or below may also be assessed by a fracture mechanics based approach. Generally, the load amplitudes are high. As a consequence, elastic plastic fracture mechanics has to be used. This, however, depends on the availability of solutions for the cyclic J-integral, ΔJ , the extension of which to fatigue is described in [7.36].

For the common case of a semicircular surface crack, the use of an approximation formula published by Dowling [7.37] is recommended

$$J = \left(1.24 \frac{\sigma^2}{E} + \frac{1.02}{\sqrt{n'}} \sigma \varepsilon_{pl} \right) a \quad (7.70)$$

where a is the radius of the circle and n' is taken from the stabilised cyclic-stress-strain curve, eq. In the present section 0, stresses σ and strains ε , including plastic strains ε_{pl} , are local stresses and strains at the location under investigation in the absence of the crack. They are identical to the stresses and strains used under Route 3, Section 7.3.3, of this procedure. The use of closure-free, i.e. effective, ranges of the cyclic J-integral is recommended, ΔJ_{eff} .

$$\Delta J_{eff} = \left(1.24 \frac{\Delta \sigma_{eff}^2}{E} + \frac{1.02}{\sqrt{n'}} \Delta \sigma_{eff} \Delta \varepsilon_{pl,eff} \right) a \quad (7.71)$$

For cracks in notched regions, less conservative J-solutions are given in [7.38].

Use crack growth law

$$\frac{da}{dn} = C_J \Delta J_{eff}^{m_J}; \quad \Delta J_{eff} > \Delta J_{eff,th,SC} \quad (7.72)$$

for calculation of crack growth. C_J and m_J values may be taken from long crack growth data which have to be expressed in terms of ΔJ_{eff}

Constant amplitude crack opening stress, $\sigma_{op,ca}$, may be taken from equation (7.44) to (7.48) replacing $\frac{K_{op}}{K_{max}}$

by $\frac{\sigma_{op,ca}}{\sigma_{max}}$. A corresponding crack opening strain $\varepsilon_{op,ca}$ has to be calculated using the stress-strain relation of the ascending hysteresis loop branch. Generally, short cracks may be assumed to open and close at the same strain values rather than the same stress values.

$$\varepsilon_{op} = \varepsilon_{cl} \quad (7.73)$$

Therefore, the short crack closure stress, σ_{cl} , has to be calculated using the descending hysteresis loop branch together with ε_{cl} . The effective stress range as inserted in equation (7.74) then reads

$$\Delta \sigma_{eff} = \sigma_{max} - \sigma_{cl} \quad (7.74)$$

Effective strain ranges are

$$\Delta \varepsilon_{eff} = \varepsilon_{max} - \varepsilon_{cl} \quad (7.75)$$

and

$$\Delta \varepsilon_{pl,eff} = \Delta \varepsilon_{eff} - \frac{\Delta \sigma_{eff}}{E} \quad (7.76)$$

For the flaw-free material state an initial virtual flaw size, $a_{0,virt}$, can be calculated by backward integrating equation for a number of cycles, N , using the known crack length for which the initiation of the technical crack, a_{tcinit} , has been defined. This latter crack length, a_{tcinit} , corresponds to the known number of cycles, N , as described by equation. Choose amplitudes for this backward integration which result in approx. $N \approx 1000$. The short crack growth calculation has to start at the larger of two values: measured, $a_{0,meas}$, or calculated, $a_{0,virt}$. Endurance limits in terms of stress, $\Delta\sigma_E$, and strain, $\Delta\varepsilon_E$, should be taken from material test results for $R=-1$. Especially, as $a_{0,virt}$ does not take into account all short crack effects, an endurance limit is not supposed to be accurately predicted when using $a_{0,virt}$ together with long crack threshold data,

$$\Delta K_{eff,th,LC} = \sqrt{E\Delta J_{eff,th,LC}} \quad (7.77)$$

Therefore, an intrinsic crack length, a^* , is defined via

$$a^* = \frac{\Delta K_{eff,th,LC}^2}{E \left(1.24 \frac{\Delta\sigma_{E,eff}^2}{E} + \frac{1.02}{\sqrt{n'}} \Delta\sigma_{E,eff} \Delta\varepsilon_{E,pl,eff} \right)} - a_{0,virt} \geq 0 \quad (7.78)$$

A reduced, crack length dependent short crack threshold is introduced via

$$\Delta J_{eff,th,SC} = \Delta J_{eff,th,LC} \frac{a}{a + a^*} \leq \Delta J_{eff,h,LC} \quad (7.79)$$

For variable amplitude loading the sequence of closed hysteresis loops (cycles) has to be calculated according to Route 3, Section 7.3.3. For each loop the following calculations have to be performed in the sequence of their occurrence.

- Calculate its constant amplitude crack opening strain $\varepsilon_{op,ca}$. Compare it to the crack opening strain which the previous cycle has left $\varepsilon_{op,old}$.
- For the following cases
 - a) $\varepsilon_{op,ca} \geq \varepsilon_{op,old}$
 - b) $\varepsilon_{max} \leq \varepsilon_{op,old}$
 - c) $\varepsilon_{op,ca} < \varepsilon_{op,old}$ and at the same time $\sigma_a < 0.4\sigma_Y$

define the actual crack opening strain by

$$\varepsilon_{op,act} = \varepsilon_{op,old} \quad (7.80)$$

- Calculate the effective ranges as described above for constant amplitude loading but replacing $\varepsilon_{op,ca}$ by $\varepsilon_{op,act}$

The crack growth increment alters $\varepsilon_{op,act}$. Calculate the new value, $\varepsilon_{op,new}$,

$$\varepsilon_{op,new} = \varepsilon_{op,ca} + (\varepsilon_{op,act} - \varepsilon_{op,ca}) \frac{\exp\left(-0.103 \frac{mm}{N} \frac{\sigma_{UTS}}{MPa} a\right)}{\exp\left(-0.103 \frac{mm}{N} \frac{\sigma_{UTS}}{MPa} (a - \Delta a)\right)} \quad (7.81)$$

$\varepsilon_{op,new}$ should be stored in variable $\varepsilon_{op,old}$ to serve as old value for the next hysteresis loop. σ_{UTS} is the ultimate tensile strength of the material.

- For the cases $\varepsilon_{op,ca} \leq \varepsilon_{op,old}$ and at the same time $\sigma_a \geq 0.4 \cdot \sigma_Y$ the actual crack opening strain is set to $\varepsilon_{op,ca}$ (7.82)

Calculate the effective ranges as described above for constant amplitude loading but replacing $\varepsilon_{op,ca}$ by

$\varepsilon_{op,act}$.

- Calculate the crack growth increment, Δa , cycle by cycle using equation .

For more details on the sequence dependent crack opening strains see [7.38] and [7.39].

7.6 Additional information

7.6.1 Variable amplitude loading

Fatigue design assessment under variable amplitude loading is performed applying the linear damage summation or crack propagation approaches. However when dealing with variable amplitude testing, the way to represent the obtained results is rather complex. The present chapter provides guidance on how to handle variable amplitude fatigue test results and to determine a fatigue strength curve.

7.6.1.1 Loading description

Three different ways can be used to describe a variable amplitude history.

7.6.1.1.1 Time history sequences description

A variable amplitude loading (Figure 7.52) can be grouped into discontinuous or partially continuous random processes. A long term history requires a representation by a series of short term sequences, each of them being continuous. The long term history is obtained by joining the short term sequences in the correct order.



Figure 7.52 – Variable random stress time history

7.6.1.1.2 Histogram description

The loading history can be represented by a series or number of cycle ranges. In such a case the order of the cycles is lost. The original loading time history is processed through a cycle counting procedure which is

intended to summarize the original signal by defining cycle ranges and number of cycles for each range. There are several different cycle counting methods. All are based on the partition of the whole load range (between the lowest minimum and the highest maximum) into levels or classes. The most commonly used are:

- level crossing counting ;
- peak counting ;
- simple range counting ;
- range pair counting ;
- "rainflow" counting.

This procedure allows for the definition of a number of cycles to failure of the component in the same way as for constant amplitude loading conditions. When the original loading history is processed with the relevant counting method, one of the two following routes is followed:

- cumulative frequency diagram and building constant range blocks (b) ;
- transition matrix and reconstruction of the loading history by random draw in the transition matrix.

7.6.1.1.3 Power or energy density spectrum description

When the short term time history can be considered statistically stationary and ergodic, which is generally the case for a loading induced by natural phenomena, the loading history can be represented by a power spectrum or energy density spectrum. The energy density spectrum is obtained by computing the Fourier integral of the time signal correlation function or by using a spectral analysis process. In such a case the order and the range of the cycles are lost. The cumulative frequency diagram can be computed from the energy density spectrum. To do so, a short term statistical distribution of the maxima of the time history must be assumed. For a narrow band signal, the distribution of the maxima is a Rayleigh distribution.

7.6.1.2 Data reduction

Although the reconstructed control signal is a simplified modelling of the true original signal, it remains usually a very complex signal that may lead to a very long and heavy fatigue assessment process. In many cases the lowest cycles are neglected providing a threshold load level. This operation consists of filtering either the original signal or the reconstructed one or both. This threshold level is selected as to assume that load cycles below the threshold are really non-damaging ones and can hence be neglected. Since the so-called non-damaging smaller cycles are the most numerous ones (low amplitude vibrations), this kind of filtering leads to an even simpler control signal and hence to an easier fatigue testing procedure. However, filtering may be dangerous if performed in a wrong way: the higher the threshold, the simpler is the resulting control signal but the higher is the risk of neglecting actually damaging cycles leading to an overestimation of the fatigue life of the specimen.

7.6.1.3 Presentation of results

For variable amplitude, the load or stress range to be associated with the number of cycles at failure of a sample is not directly defined. Various possibilities exist to provide the variable amplitude life time test results:

- Miner sum (linear damage sum)
- Equivalent load or stress range
- Gassner-line.

In each case the S-N curve of the tested material or welded joint under constant amplitude has to be known.

7.6.1.3.1 Miner sum

The Miner sum is calculated from the cumulative frequency diagram (stress range $\Delta\sigma$ versus number of cycles N) and an S-N curve. It is given by the following formula:

$$D = \frac{N_t}{C} \int_0^{\infty} \Delta\sigma^m f(\Delta\sigma) d\Delta\sigma \quad (7.83)$$

where:

N_t : total number of cycles of the cumulative frequency diagram

C : constant of the S-N or Wöhler curve expressed by: $(\Delta\sigma)^m N = C$

$f(\Delta\sigma)$: probability density function of $\Delta\sigma$, derived cumulative frequency diagram function

When the cumulative frequency diagram is given as a stair curve (number of cycles n_i versus stress range $\Delta\sigma_i$), the Miner sum is given by the following formula (Figure 7.53):

$$D = \sum_i \frac{n_i}{N_i} \quad (7.84)$$

The life time can be expressed by Miner sums D_i versus loading histories (i) described following a method as given in 7.6.1.1.

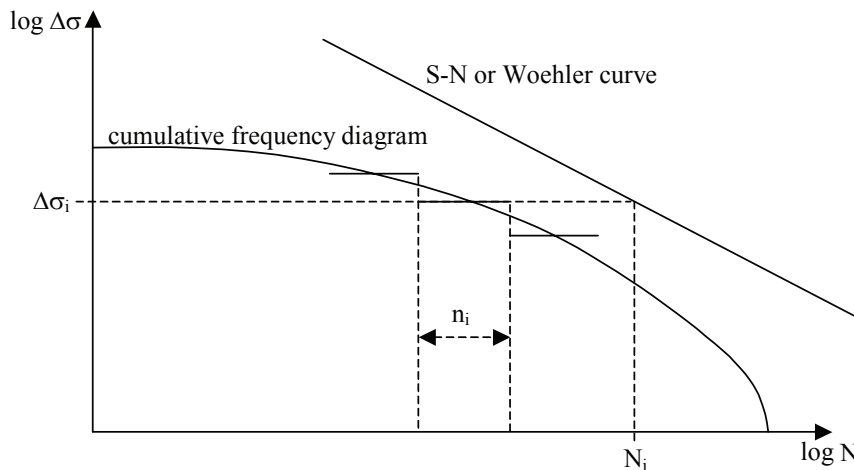


Figure 7.53 – Miner sum principle

7.6.1.3.2 Equivalent stress range

From a cumulative frequency stair diagram (see Figure 7.53), the equivalent stress range is defined as:

$$\Delta\sigma_{eq} = \left[\frac{\sum_i n_i (\Delta\sigma_i)^m}{N_{ref}} \right]^{1/m} \quad (7.85)$$

where:

m : power parameter of the S-N curve expressed by $(\Delta\sigma)^m N = C$

N_{ref} : reference number of cycles to determine the stress range level at failure on the S-N curve.

Often N_{ref} is taken equal to the total number of cycles N_t of the cumulative frequency diagram. The life time can be expressed by a curve, equivalent stress range $\Delta\sigma_{eq,i}$, reference number of cycles $N_{ref,i}$, versus loading histories (i) described following a method as given in 7.6.1.1.

7.6.1.3.3 Gassner curve

A point of the Gassner curve represents the number of cycles associated to the maximum stress range level of a given short term cumulative frequency diagram obtained by repetition of this diagram until failure (Figure 7.54). The life time is expressed by a curve, maximum stress range $\Delta\sigma_{\max,i}$ number of cycles at failure N_i , versus loading histories (i) described following a method as given in 7.6.1.1.

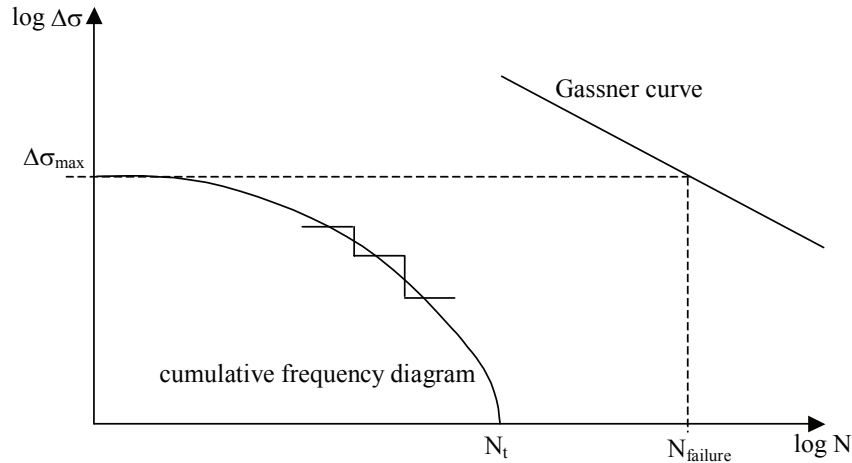


Figure 7.54 – Gassner curve determination principle

7.7 Bibliography

- [7.1] A. Hobbacher, Recommendations for fatigue design of welded joints and components, IIW document XIII-1965-03/XV-1127-03, February 2004
- [7.2] IIW Structural Hot-Spot stress approach to fatigue analysis of welded components –doc XIII-1819-00
- [7.3] Bureau Veritas rules for steel ships classification – Fatigue check of structural details – Part B, Chapter 7, Section 4 – Edition May 2003
- [7.4] Forman, R.G. and Mettu, S.R., 1992. Behaviour of surface and corner cracks subjected to tensile and bending loads in a Ti-6Al-4V alloy. In: Ernst, H.A., Saxena, A. and McDowell, D.L. Editors, 1992. Fracture Mechanics 22th Symposium 1 American Society for Testing and Materials, Philadelphia, pp. 519–646, ASTP STP 1131.
- [7.5] A. Brand, J.F. Flavenot, R.Gregoire, C.Tournier, Données technologiques sur la fatigue, Doc. CETIM, 1999
- [7.6] A. Brand, R. Sutterlin, Calcul des pieces à la fatigue, méthode du Gradient, Doc CETIM, 1980
- [7.7] VDI 2226, Empfehlung für die Festigkeitsberechnung metallischer Bauteile, 1965
- [7.8] DIN 4768 1990-5, Ermittlung der Rauigkeitskenngrößen Ra, Rz, Rmax mit elektrischen Tastschnittgeräten; Begriffe, Meßbedingungen. Beuth-Verlag, Berlin
- [7.9] E. Haibach, FKM-Guideline Analytical Strength Assessment of Components in Mechanical Engineering. 5th revised edition, 2003, VDMA Verlag, Lyoner Str. 18, D-60528 Frankfurt. ISBN 3-8163-0425-7

- [7.10] H. Neuber, Trans. ASME Ser E., J. Appl. Mech. Vol. 28, pp 544-550, 1961
- [7.11] G. Glinka - Calculation of Inelastic Notch-Tip Stress-Strain Histories Under Cyclic Loading, Engineering Fracture Mechanics, 22, (5), pp. 839-854 (1986).
- [7.12] K. Dang Van, M.H. Maitournam – Steady-state flow in classical elastoplasticity: application to repeated rolling and sliding contact Journal Mech. Phys. Solides, 41 (11), 1993, p. 1691-1710
- [7.13] H.P. Lieurade, M. Truchon, J.F. Flavenot – La prévision de l'amorçage des fissures de fatigue à partir d'entailles, Revue Française de Mécanique, 1992, n°1
- [7.14] R.N. Smith. P. Watson & T.H. Topper, A stress-strain parameter for the fatigue of metals, Journal of Materials, 1970, 5, pp. 767-778
- [7.15] British Standard BS 7910: 'Guide to Methods for Assessing the Acceptability of Flaws in Metallic Structures', 2005.
- [7.16] Forman, R.G. and Mettu, S.R., Behaviour of surface and corner cracks subjected to tensile and bending loads in a Ti-6Al-4V alloy, in Ernst, H.A., Saxena, A. and McDowell, D.L. (Ed.), 1992. Fracture Mechanics 22th Symposium, ASTM, Philadelphia, pp. 519–646 ASTP STP 1131.
- [7.17] NASA, Fatigue Crack Growth Program “NASGO” version 3.0 – reference manual JSC-22267B, NASA Lyndon B. Johnson space Centre, 2000
- [7.18] ESACRACK User's Manual, Version 4.0, TOS-MCS/2000/41/In, Issue 1, May 2000, ESTEC, Noordwijk, The Netherlands
- [7.19] J.D. Willenborg et al, A Crack Growth Retardation Model using the Effective Stress Concept, Air Force Flight Dynamics Laboratory, Report AFFDL-TM-71-1-FBR, 1971
- [7.20] O.E. Wheeler, J. Basic. Eng. Trans ASME Series D, Vol. 94, 1972, pp 181-186
- [7.21] Ten Hoeve, H.J.a.d.K., A.U., Implementation of the Improved Strip Yield Model into NASGRO Software - Architecture and Detailed Design Document. National Aerospace Laboratory (NLR) Report: NLR CR 95312L, 1995.
- [7.22] IIW Weld recommendation on post weld improvement of steel and aluminium structures, doc XIII - 1815-00, rev 7, July 2005
- [7.23] K. Dang Van, Introduction to Fatigue Analysis in Mechanical Design by the Multiscale Approach, CISM Courses and Lectures N° 392, Springer Verlag Wien, New York, 1999.
- [7.24] K.Dang Van et al, Criterion for High Cycle Fatigue Failure under Multiaxial Loading, Proc. Int. Conf. on Multiaxial Fatigue, Sheffield 1986.
- [7.25] K. Dang Van, A.Le Douaon, H.P. Lieurade, Multiaxial fatigue limit: a new approach, in “Advances in Fracture Research”, Proc. 6th Int. Conf. on Fracture, Pergamon Press, 1984, p. 1879–1885.
- [7.26] C.M. Sonsino - Multiaxial Fatigue of Welded Joints under In-Phase and Out-of-Phase Local Strains and Stresses, Int. Journal of Fatigue 17 (1995) No. 1, pp. 55-70
- [7.27] C.M. Sonsino, M. Kueppers, M. Eibl, G. Zhang - Multiaxial Fatigue Behaviour of Laser Beam Welded Thin Steel Joints, IIW-IIS doc XIII-2008-04 (2004)
- [7.28] C.M. Sonsino, M. Wallmichrath, M. Kueppers, - Assessment of Multiaxial Ftigue Test Results on Welded joints by Application of the IIW-Formula and Modfiations, IIW-IIS doc XIII-2046-06 (2005) [7.29] K. Dang Van, M.H. Maitournam, Steady-state flow in classical elastoplasticity : application to repeated rolling and sliding contact, J.Mech, Phys.Solids 41 (11) (1993) 1691-1710.
- [7.30] K. Dang Van et al, Elastoplastic analysis of repeated moving contact : application to railways damage phenomena, Wear 196 (1996) 77-81.

- [7.31] K. Dang Van, M.H. Maitournam, Thermomechanical state near rolling contact area, in D. Dowson et al.(Ed.). Proc. 20th Leeds-Lyon Symposium, Dissipative Processes in Tribology. Elsevier, Amsterdam, 1994, pp. 423-428
- [7.32] K.Dang Van, Introduction to fatigue analysis in mechanical design by the multi-scale approach, in : K. Dang Van, I Papadoupoulos (Eds.), High-Cycle Metal Fatigue in the Context of Mechanical Design, CISM Courses and Lectures No, 392, Springer, Berlin, 1999, pp. 169-187.
- [7.33] K.Dang Van, macro-micro approach in high cycle multi-axial fatigue, ASTM STP 1191 (1993) 120-130.
- [7.34] K.Dang Van, On structural integrity assessment for multi-axial loading paths, in C.J Beevers & A.F Blom (Eds), Theoretical and Concepts and Numerical Analysis of Fatigue, EMAS Ltd., U.K, 1993, pp. 343-357.
- [7.35] P. Ballard et al, High cycle fatigue and a finite element analysis, Fatigue Fract. Eng.Mater.Struct. 18 (3) (1995), pp. 397-411.
- [7.36] C. Wüthrich: The extension of the J-intergral concept to fatigue. Int. J. of Fracture, 20, pp. R35-R37, 1981
- [7.37] N.E. Dowling: J-integral estimates for cracks in infinite bodies. Eng. Frac. Mech., 26(3), pp. 333-348, 1987
- [7.38] M. Dankert, S. Greuling, T. Seeger: A Unified Elastic-Plastic Model for Fatigue Crack Growth at Notches Including Crack Closure Effects. Symposium on Advances in Fatigue Crack Closure Measurement and Analysis, San Diego, Calif., 1997, ASTM, 1999, STP 1343, pp.480ff
- [7.39] M. Vormwald, T. Seeger: The Consequences of Short Crack Closure on Fatigue Crack Growth Under Variable Amplitude Loading. Journal of Fatigue and Fracture of Engineering Materials and Structures, 1991, 14(2/3), pp. 205-225.